# Combination of Chemotherapy and Antiangiogenic Therapies: A Mathematical Modelling Approach

by

Colin Phipps

A thesis
presented to the University of Waterloo
in fulfillment of the
thesis requirement for the degree of
Master of Mathematics
in
Applied Mathematics

Waterloo, Ontario, Canada, 2009

I hereby declare that I am the sole author of this thesis. This is a true copy of the thesis, including any required final revisions, as accepted by my examiners.

I understand that my thesis may be made electronically available to the public.

**Abstract**

A brief introduction to cancer biology and treatment is presented with a focus on current clinical advances in the delivery of chemotherapy and antiangiogenic therapies. Mathematical oncology is then surveyed with summaries of various models of tumor growth, tumor angiogenesis and other relevant biological entities such as angiogenic growth factors. Both strictly time-dependent ordinary differential equation (ODE)-based and spatial partial differential equation (PDE)-based models are considered. These biological models are first developed into an ODE model where various treatment options can be compared including different combinations of drugs and dosage schedules. This model gives way to a PDE model that includes the spatially heterogeneous blood vessel distribution found in tumors, as well as angiogenic growth factor imbalances. This model is similarly analyzed and implications are summarized. Finally, including the effects of interstitial fluid pressure into an angiogenic activity model is performed. This model displays the importance of factor convection on the angiogenic behaviour of tumours.

**Acknowledgements**

I would like to thank my supervisor Mohammad Kohandel for his wealth of ideas and insight; and Gibin Powathil for his collaboration and many useful discussions.

# Contents

# List of Tables

# List of Figures

# Chapter 1

# Biological and Medical Background

## 1.1 Cancer

Cancer is a disease that occurs as a result of genetic mutations in cells due to any number of causes. It is the culmination of these mutations being passed on through the generations of a cell's progeny that leads to tumour formation. A cell population is referred to as being cancerous when these mutations lead to their uncontrolled proliferation and intrusion on nearby tissues. These cancer cells interfere with the normal functioning of cells and are detrimental to the organism's survival. While some forms of cancer do not form a solid mass (such as leukemia), the most common quality associated with cancer is the ability to form an aggressive tumour; the culmination of mutations that usually give the cells all of the following capabilities:

1. Apoptosis avoidance: the ability to escape the natural cell death trigger.
2. Self-sufficient growth signalling: increased production of progrowth factors or heightened sensitivity to them.

3. Antigrowth signal insensitivity: avoidance of differentiation or quiescent state.

4. Angiogenesis promotion: upregulation of proangiogenic factors and insensitivity to antiangiogenic factors, leading to tumour vasculature (see Section 1.2).

5. Senescence prevention: unlimited replicative potential.

6. Invasion: can move to surrounding tissues.

7. Metastasis: can travel through vasculature to colonize other regions of the organism.

This partial list of prevalent cancer traits are based on 'The Hallmarks of Cancer' laid out by D. Hanahan and R. A. Weinberg in the paper of the same name [1]. They make the observation that while most cancers exhibit all these qualities to a degree, these traits can be acquired in practically any order. They also make it clear that cancer cells should not be considered as separate entities from their environment since "mutant cancer cells have conscripted and subverted normal cell types to serve as active collaborators in their neoplastic agenda." They are referring to the many cell types that play a role in cancer cell survival including normal parenchymal cells of the host tissue, endothelial cells that comprise blood vessels, fibroblasts of connective tissue along with many others.

The distinction between a cancerous and a benign tumour is somewhat of a grey area, but the most common classification is that benign tumours are those non-invasive and non-metastatic growths that are typically non-life threatening (although benign tumours that develop in some parts of the body can be fatal). So-called benign tumours may develop into cancerous tumours if they acquire additional mutations that make them dangerous to their host.

The unlimited replicative potential of cancer cell lines is most commonly endowed by increased levels of telomerase [2], an enzyme responsible for maintaining the telomers. Apoptosis is often triggered by the shortening of these telomers, a

process that occurs naturally when a cell divides. However, since the telomers of cancer cells shorten negligibly, they can now evade death, allowing them to divide indefinitely; this is referred to as 'immortalization'.

The invasive nature of cancer cells is a result of decreased cell-cell adhesion due to disruption of the normal production of integrins that tether cells to the extracellular matrix (ECM). In addition, they can often degrade the surrounding ECM in order to facilitate their movement within the tissue. The invasiveness of cancer cells poses a threat to the viability of normal cell populations as they become crowded and react naturally by triggering their own death or those of surrounding normal cells. The normal cells are also deprived of oxygen and nutrients as these invaders use their resources to fuel their movements and proliferation. This invasion is often not limited to those tissues that are directly adjacent to the tumour. Tumour cells often metastasize, making their way into blood vessels or the lymphatic system, using them for transportation to other parts of the body. This process is very complex and includes the original event of entering the vasculature, the process of eventually extravasating into a new tissue, adapting to this new microenvironment and finally the development of another cancer cell colony that could lead to a secondary tumour. While many pioneering attempts by cancer cells from the original tumour will most likely fail, the ones that do succeed will themselves have the potential to further colonize other parts of the body.

Each of these cancer cell traits must be taken into consideration when attempting to treat a tumour. Their ability to avoid apoptosis and senescence implies that natural cell death is relatively rare and must therefore be triggered (directly or indirectly) by an agent. Their upregulated proliferation can be exploited by using drugs that target rapidly dividing cells. The promotion of angiogenesis can be countered by antiangiogenic agents and will be described in detail later. The invasive nature of cancer implies that in many tissues, the surrounding area must also be treated in case cancer cells have migrated to these areas. While metastasis continues to be the most consistent indicator of negative prognosis, this is countered primarily by

expedient treatment and early detection efforts.

## 1.2 Tumour Angiogenesis

Ever since the extremely important connection between angiogenesis and tumour growth was established in [3], the field of oncology has been revitalized by antiangiogenic treatments. These agents will be discussed in the next section; for now the process they are targeting will be discussed: the formation of tumour vasculature. When a tumour begins to form, its existence and growth depend on the diffusion of oxygen and nutrients in its immediate vicinity. However, tumour growth is diffusion-limited, that is, after it reaches a certain size, approximately 2-3mm in diameter, the center of this cell cluster can no longer be sustained by the amount of oxygen attainable via simple diffusion. In response to this, the effected cells begin to release hypoxia-induced factors (HIFs). These HIFs are then responsible for triggering the release of proangiogenic factors in nearby cells, most prominently (and heavily-studied) among them being vascular endothelial growth factor (VEGF).

While this signalling cascade will begin the process of tumour vascularization, it is also the case in many types of cancer that certain genes are upregulated causing high levels of VEGF production or various other modifications of the balance between angiogenic inducers and inhibitors [4].

These processes compound and are very effective in causing blood vessels to sprout from nearby existing vasculature, however, unlike the normal process of angiogenesis, this process is hasty and unregulated. Tumour vasculature is most often highly tortuous and inefficiently structured leading to spatially and temporally heterogeneous blood flow. In addition they have large fenestrations leading to leaky vessels and highly compromised nutrient delivery. The cancer cells that originally triggered the angiogenic switch rarely see the benefit of their efforts since these incoming vessels usually penetrate only the tumour rim, leaving the bulk of the tumour lacking any consistent oxygen supply. As a result, the center of a tumour often

develops into a necrotic core and the hypoxic cells that surround this core maintain constant angiogenic signalling. As the tumour grows the very dense blood vessels and tumour cells become compacted leading to collapsed blood vessels, restricted blood flow and high interstitial fluid pressure.

## 1.3 Cancer Treatment

Prior to the seminal work of Folkman [3], and the subsequent initiation of antiangiogenic therapy, the focus had always been on surgical techniques and cytotoxic agents aimed at directly removing or killing cancer cells. The three central categories that traditional treatments fell into were: surgery, chemotherapy and radiotherapy.

### 1.3.1 Surgery and Radiotherapy

Surgery to remove cancerous tumours has been performed for almost two thousand years, however, cancer was generally considered to be incurable by medical practitioners. After a tumour was surgically removed, it was often observed to recur. Surgery did not become a standard form of treatment until the 19th century with the advent of anesthesia. While surgical techniques have come a long way since then, it still remains likely that the cancer will recur, even after 'successful' surgery. This is due to the fact that even the most precise surgical techniques often leave cells behind because the cancer has already metastasized or they were left undetected in the surrounding normal tissues. Due to this, surrounding normal tissue is often purposefully removed during surgery but in most cases, specifically in the brain or other vital organs, the desire to minimize normal tissue damage is paramount. This is the motivation behind many of the current and novel treatment strategies that are considered in this thesis along with traditional radiation therapy and chemotherapy.

The main limitation of radiotherapy is that it kills surrounding normal cells. Despite the fact that the ionizing radiation is directed at the tumour, all cells which

are exposed are damaged to some extent (and can even themselves be mutated). Many forms of accurate radiotherapy techniques have been developed and it is still a very popular form of treatment.

Both of these therapies have been refined over the years, but since they will not be the subject of the mathematical models to follow, no further detail will be given about surgery or radiotherapy techniques.

### 1.3.2 Chemotherapy

Chemotherapy involves the administration of drugs that kill cancer cells directly. Unfortunately, this cytotoxicity is rarely specific to tumour cells alone leading to the death of many normal cells. This results in a wide array of side effects that limit both the size of the dosage and the minimum time interval between successive administrations. In addition, there is a negative impact on the patient's physical and psychological well-being over the course of treatment. Initially, chemotherapy agents were used primarily on those tumours that were beyond the physical limitations of the surgical and radiotherapy techniques of the time.

The combination of different treatments presented a major leap forward, starting with adjuvant therapy, the administration of chemotherapy agents after surgery to kill the remaining cells. The next step was combination chemotherapy which employed different cytotoxic agents administered concurrently. These were met with success in certain forms of leukemia and lymphoma and these types of drug cocktails are still researched extensively today.

Most often, these drugs damage the DNA or inhibit microtubule formation which kills rapidly dividing cells. One of the most popular chemotherapy agents is doxorubicin that induces apoptosis by essentially wedging itself between the two DNA strands (intercalation) inhibiting transcription and replication.

One of the main current concerns in chemotherapy is the preferential targeting of cancer cells over normal cells. This will be described later when drug delivery

vehicles are introduced.

### 1.3.3 Antiangiogenic Agents

In recent years the focus of cancer treatments has shifted dramatically. Up until the past 10 to 15 years, the central concern was killing the cells which comprised the tumour bulk. However, with the realization that angiogenesis was a crucial part of sustained tumour growth, much energy and effort has been expended on the development of antiangiogenic drugs. Originally the rationale was that destroying all tumour vasculature would lead to the tumour being starved of essential nutrients and oxygen leading to tumour cell death. When endothelial cell killing drugs such as combretastatin were first injected into a tumour, the antiangiogenic effects were deemed to be significant and fast-acting [5], yet the majority of tumour cells remained unaffected. This is due to a number of factors but most importantly, many forms of cancer can survive under hypoxic conditions. Not only does the tumour survive, it also implies that a source of angiogenic signalling remains. Moreover, with no vasculature in the tumour, it is then impossible to deliver chemotherapy drugs to the interior of the tumour. An alternative to this approach, called vascular normalization [6], involves applying enough antiangiogenic drugs to prune underdeveloped and unnecessary vessels which would theoretically lead to a more regular blood vessel structure. While this would likely improve the delivery of oxygen and nutrients to the tumour, it would also provide a means of effectively delivering chemotherapy drugs in a more homogeneous fashion to the tumour. Some successes have been documented, the main limitation being that this state of normalized vasculature lasts for a very brief period of time, referred to as the normalization window, followed by either a return to an irregular, dense system or an overkill of the endothelial cells.

While the efficacy of different treatment strategies remains far from established, there have been a number of different angiogenic mechanisms successfully exploited for antiangiogenic treatments. There are many types of drugs which target endothe-

lial cell proliferation in various ways, some similar to regular chemotherapy drugs, others with differing levels of specificity. While not specifically antiangiogenic, standard chemotherapy agents have been shown to have antiangiogenic effects even before they begin to kill tumour cells [7]. There are a few that do attack endothelial cells directly such as combretastatin, angiostatin and endostatin. Combretastatin disrupts the cytoskeletal structure of the endothelial cells causing them to change into a balloon-shape resulting in vasculature breakdown [8]. Others inhibit the migration or adhesion of endothelial cells. The other key area of antiangiogenic therapy are those that indirectly target the endothelial cells by instead targeting various signalling integrins and factors.

Naturally, due to its large role in tumour angiogenesis, VEGF is a prime target of antiangiogenic therapy. The two most common ways to inhibit the action of VEGF are by receptor-blocking or factor inhibition. In the former case, a small molecule which blocks tyrosine kinase receptors is taken (most commonly an oral administration), preventing the binding of VEGF. Two of these drugs are now commercially available, sunitinib (Sutent) and sorafenib (Nexavar) while there are a handful more in clinical trials. Sunitinib is commonly prescribed for the treatment of gastrointestinal stromal cancer while sorafenib treats some liver cancers; both are effective in treating kidney cancer. The side effects of these treatments are rarely serious but due to their differing nonspecific receptor targeting there is an extremely wide array of possible side effects. Factor inhibiting agents were the first type of anti-VEGF drug developed and the monoclonal antibody bevacizumab was the first anti-angiogenesis drug approved by the FDA mostly due to its successful combination with chemotherapy in a Phase III trial outlined in [9]. Bevacizumab recognizes all of the VEGF isoforms and has widespread clinical applications. Shrouded in some controversy due to questionable approvals for some types of cancer, it also remains one of the most expensive drugs to manufacture. The most serious side effects include the impairment of wound healing and the suspension of the body's natural blood vessel maintenance which has made the research focus turn to drug localization. Large fenestrations in the tumour vasculature lead to some natural

targeting of the areas around the tumour but nanoparticle and nanocell delivery vehicles are currently a very hot area of cancer research. Both forms of anti-VEGF treatments are now primarily used in combination with chemotherapy drugs or radiotherapy.

Not mentioned in the previous discussion, it should be noted that destroying tumour vasculature also has a double-edged sword effect on the likelihood of metastasis. On one hand, destroying tumour vasculature eliminates the avenues to other areas of the body. On the other hand if too much vasculature is destroyed, hypoxia levels increase which has been shown to induce invasion [10] and promote metastasis [11] in tumour cells.

Other forms of antiangiogenic treatment have been proposed, some the result of mathematical models which show a specific mechanism to be a worthwhile target. For instance, the blockade of the coupling between VEGFR-2 and its co-receptor NRP1 was shown to be a good strategy in [12] yet such an inhibitor has not been developed.

### 1.3.4 Other Treatments

While the most popular forms of treatment have been outlined, there are many others which will not be included in the mathematical models to follow but those with potential for significant clinical benefits should be considered in future modelling attempts. Various hormonal therapies have gained prominence across genders since breast and prostate cancers rely heavily on specific hormones for tumour growth. In the case of prostate cancer, the paramount concern is the prevention of tumour cells from obtaining dihydrotestosterone (DHT) by preventing its production or blocking its activity. For breast cancer, the actions of the female sex hormones progesterone and estrogen are inhibited.

Immunotherapy is a treatment that relies on the patient's immune system to fight the cancer. This can be achieved by giving monoclonal antibodies that can

identify antigens specific to the tumour cells. In fact, the antiangiogenic drug bevacizumab can be thought of as a form of immunotherapy against tumour vasculature. The developing field of radioimmunotherapy which uses radioactively conjugated antibodies to target tumour antigens holds promise in treating radio-sensitive tumours (such as lymphomas [13]).

For the past couple of decades, a plethora of reports have gained widespread media attention for touting various foods as cancer-preventing or cancer-causing. While there have been many misinterpretations of studies, there is scientific evidence for the benefits of many agents that can be obtained through diet. While these primarily serve as preventative measures, the treatment of cancer without the use of 'drugs' has gained prominence in naturopathic circles. Those which have been well-studied and found to be advantageous are usually encouraged by oncologists to be used as complementary treatments to their conventional therapy regimes.

## 1.4 Treatment Strategies

### 1.4.1 Maximum Total Dosage

The maximum total dosage (MTD) method has traditionally been the most popular treatment schedule among oncologists. Since the vast majority of chemotherapy drugs have serious side effects and are toxic to normally functioning cells as well as cancer cells, there is an upper limit on how much of the drug can be administered to an individual in a single administration. This amount is referred to as the MTD and anything above this amount would cause the side effects of treatment to be potentially lethal. Taking the MTD requires there to be a break of weeks between each administration allowing the patient to recover from the treatment and healthy cells that were effected to repair. The serious side effects incurred with this strategy are detrimental to the patient on both a physical and emotional level. In addition, research efforts have been forced to focus on drugs which counter side effects of these

strenuous treatments rather than those which would cure the cancer. While this method has fallen out of favour, the MTD is still often explored during experiments, clinical trials and at certain critical points during a patient's treatment.

### 1.4.2 Metronomic

The metronomic technique, coined in [14], is different from MTD in both the scheduling and dosage of treatments. Dosages much lower than the MTD are used and thus less recovery time is needed between treatments. These treatments are applied more frequently, even daily and have been shown to cause less side effects and improved tumour response. This technique has been shown to provide increased antiangiogenic effects (reviewed in [15]) since the tumour vasculature does not have time to repair during breaks in treatment [16]. It is surmised that this antiangiogenic effect is achieved since metronomic scheduling can prevent the action of circulating endothelial progenitor cells (EPCs) which are key components of the vasculature repair [17].

### 1.4.3 Cancer Control vs. Cancer Cure

The predominant mindset for cancer treatment has always been to eradicate the tumour, curing the disease. This goal has been met with varying success, most of the time subjecting the cancer patient to the rigours of cytotoxic chemotherapy or radiotherapy with their array of negative side effects and the subsequent palliative care for these symptoms. In cases that are beyond cure, the clinical prerogative is changed to extending life. This means that the tumour is no longer aggressively attacked and instead only the drugs necessary to prevent patient death are applied until the inevitable occurs. Perhaps this mindset shift is unnecessary; instead the goal could always be control of the tumour, whether that be successful eradication or not, this would be a more realistic yardstick for treatment success. As suggested recently in [18], by controlling the tumour, specifically by preventing metastasis and

its consequences, it may be possible in many cases to extend patient life beyond that afforded by traditional rigourous treatment regimes.

## 1.5 Drug Delivery Vehicles

Encapsulating drugs in liposomal or polymer-based nanoparticles is a promising field of recent medical experimentation, for a detailed review see [19]. By administering drugs in these delivery vehicles, many advantages over direct administrations as free agents have been observed. Improved tumour cell specificity can be achieved by employing natural and engineered targeting and longer circulation times are obtained by immune system avoidance leading to sustained drug release. The natural targeting is enjoyed by most nanoparticles of an appropriate size (usually larger than 100nm). The typical pore size in normal blood vessels is approximately 50nm while the size of tumour vasculature pores can be upwards of 500nm. Due to their size, the nanoparticles cannot escape the tight gap junctions of the normal blood vessels leading to their extravasation primarily in the tumour vicinity. Once they exit the blood vessel, they are now essentially trapped in the tumour tissue. This leads to an increased efficiency of the contained agents and decreased side effects in the normal tissue. This natural targeting process is referred to as the enhanced permeability and retention (EPR) effect and was coined in [20].

### 1.5.1 Phospholipid-based Nanoparticles

Micelles are single-layered spheres of phospholipids, good for carrying hydrophobic agents and are relatively easy to create. However, they have relatively short release times since after injection they are rapidly dissolved to below the minimum micelle concentration. Active areas of micelle research center around improved stability, likely by incorporating polymers into their structure.

Double-layered phospholipid carriers are called liposomes and have the advantage of being able to carry both hydrophobic and hydrophilic drug in a single

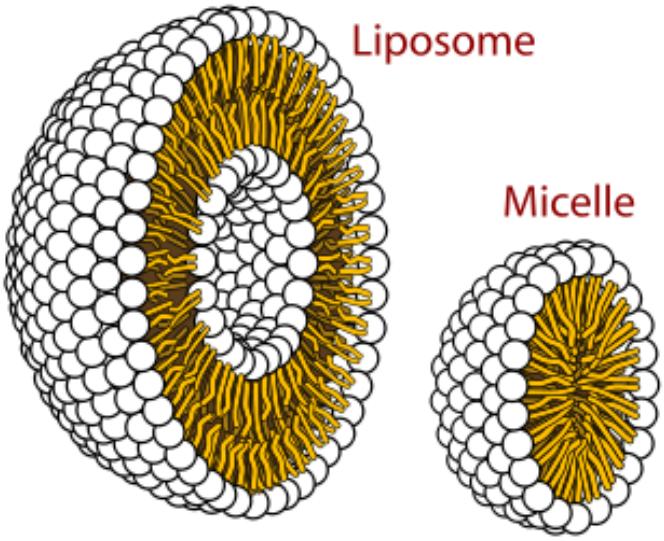


Figure 1.1: Crossections of the two classes of phospholipid-based nanoparticles commonly used in cancer treatment. Source: Wikipedia.

delivery vehicle. Longer circulation times can be achieved due to increased stability of the structure. These also have the advantage of being able to fuse with other lipid bilayers such as the cell membrane. Crossections of these two delivery vehicles, which both have many applications outside the field of drug delivery, can be seen in Figure 1.1. The main disadvantage of lipid-based vehicles is that their surfaces are not easily modifiable for targeting or immune system avoidance.

### 1.5.2 Polymer-based Nanoparticles

There are a couple broad categories of polymer-based nanoparticles with varying levels of effectiveness that will be described.

#### Dendrimers

Dendrimers are manmade, branched polymers that have the ability to bind to various different molecules on their many terminal ends. Since the exact structure is known, they can be loaded precisely. They gained prominence in medical research

when their drug-trapping capabilities were first uncovered, but they remained relatively unpopular in the field due to their increased toxicity over lipid-based and other polymer-based nanoparticles. With the advent of various non-toxic structures, they are often used as drug-loading devices that are then encapsulated in another of the liposomal or polymer-based nanoparticles about to be described.

### Nanospheres

Polymer-based nanoparticles, usually forming a nanocapsule or nanosphere, are typically upwards of 100nm in diameter and hence able to take advantage of the natural targeting granted by the large fenestrations in tumour vasculature via the EPR. While methods are being improved, there is still a relatively large variance in size compared to that of phospholipid-based nanoparticles (there is negligible variance in dendrimer size), leading to the necessity to filter out those which are too small or too large to be effective for the desired clinical purpose.

The major advantage of polymer-based nanoparticles is that their stable surface allows for surface modifications. As a result, in addition to this natural targeting, these nanoparticles also enable bioengineered attempts at increasing cancer cell targeting capabilities. Most commonly, a ligand is attached to the nanoparticle surface whose corresponding receptor is overexpressed on the cancer cell membrane. The prime example of this technique is folate targeting since folate receptors are overexpressed on the cell membrane of many different cancers. Due to the comparatively low concentration of folate receptors on most types of healthy cells, this was identified as a possible marker that could be targeted, see Figure 1.2. By attaching folic acid to both liposomal [23] and polymer nanoparticle surfaces, these nanoparticles would be preferentially taken up by the tumour cells, leaving normal cells mostly unaffected [24]. Folate-targeting has also been shown to be a good method for overcoming multi-drug resistance in some cancer cell lines [25].

Many other cell surface receptors have been exploited for cancer treatment targeting. Tumour vasculature has also been targeted, commonly using the $\alpha_v\beta_3$ inte-

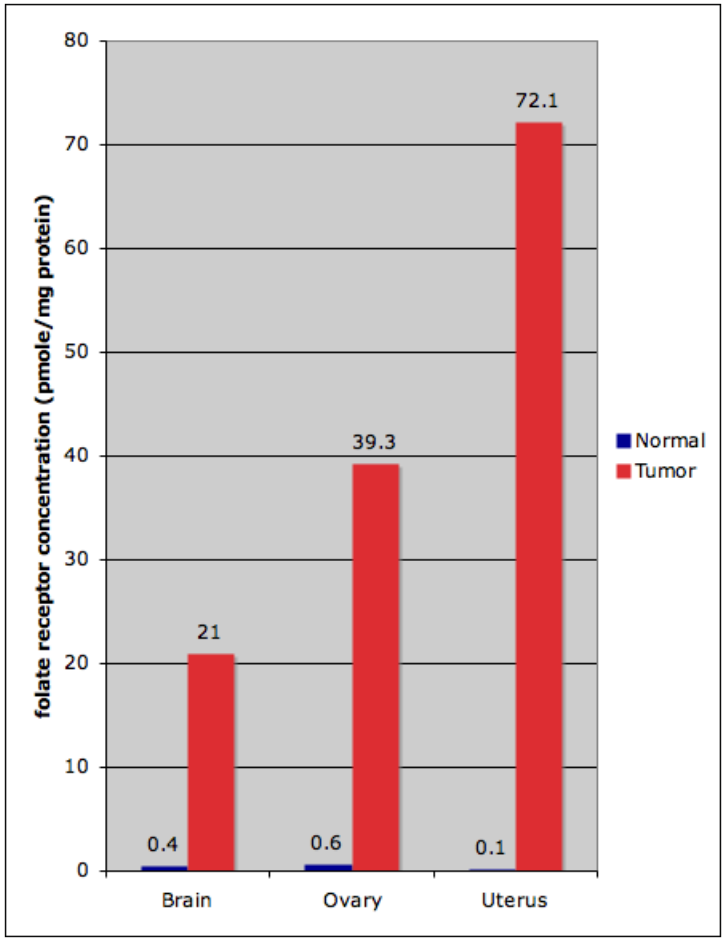


Figure 1.2: Comparing the levels of folate receptors on the cell membrane of normal tissues with medium or high grade tumours. Recreated from [21] using data from [22].

grin as a target for antiangiogenic therapies [26]. Recently, targeted nanoparticles were not loaded with a specifically antiangiogenic drug, instead the chemotherapy drug doxorubicin was used to kill the endothelial cells of the tumour vasculature and some of the surrounding cancer cells. Effects of this treatment on vasculature is shown in Figure 1.3.

The immune system is a large obstacle to overcome for successful drug delivery. As soon as a foreign substance is detected in our bloodstream, our immune system tags them for removal (opsinization) and then macrophages remove them.

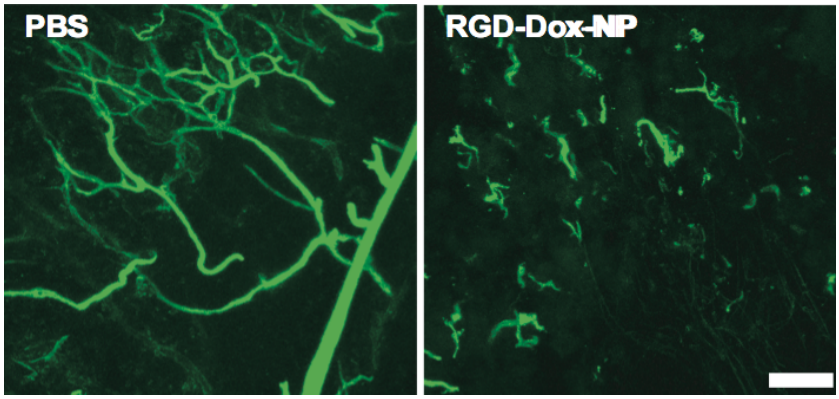


Figure 1.3: Control case using phosphate buffer solution (PBS) and the effect of RGD (integrin-targeting peptide)-Dox(doxorubicin)-NPs. Image from [26].

Therefore, the drug delivery system must attempt to avoid this natural process. By attaching certain polymers to the surface of the nanoparticle envelope, the tagging proteins are prevented from binding to the nanoparticle. A concern that must be kept in mind is that in order to successfully target cancer cells via receptor-ligand binding, the density of these polymers cannot be so high as to interfere with this process.

A very promising area is the apparent ability of nanoparticles to smuggle genetic material into the cell. Typically, cells employ various mechanisms to prevent this from happening, degrading those nucleic acids which are fortunate enough to pass through the cell membrane. However, using nanoparticles, treatments can be developed that directly influence gene expression. Figure 1.4 shows a confocal fluorescence microscopy of gold nanoparticles loaded with oligonucleotides that can effect genes targeting a HeLa cell (immortal cell line from the cervical cancer of Henrietta Lacks).

### Nanocells

Pioneered by Shiladitya Sengupta at the labs of MIT, the nanocell is the term attached to delivery vehicles that have the ability to trap different agents in separate

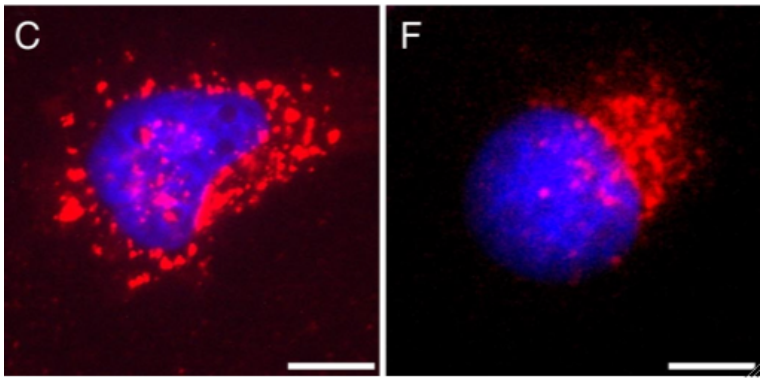


Figure 1.4: Gold nanoparticles of diameter 13-nm (left) and 5-nm (right) targeting HeLa cells. Image from [27].

layers of lipids and polymers. They attempted to achieve the same goals in targeting and immune system avoidance as was done with nanoparticles. These nanocells are approximately 150nm in diameter, allowing them to take advantage of the EPR effect. Initial trials were reported in [28] and used a nanoparticle core (nanocore) loaded with doxorubicin (chemotherapy) inside of a lipid envelope containing the antiangiogenic drug combrestatin. The nanoparticles were heterogeneous in size, so only those between 80-120nm were covered in lipids to form nanocells; see Figure 1.5 for the comparative size of the nanoparticle and the complete nanocell. This delivery vehicle enables the controlled temporal release of two separate drugs in a single administration. First, the outer lipid-bound antiangiogenic agents are released and destroy or prune the surrounding vasculature. The chemotherapy nanoparticles are now captured inside the tumour, liberating cytotoxic agents as they erode. This proces is described in Figure 1.6.

This is an active area of research with recent attempts at improving folate-targeted nanocells reported in [29]. A subsidiary goal in this thesis was to create the nanocell out of cheaper materials, specifically chitosin. Unfortunately, this goal was considered a failure but future research should attempt to provide an alternative to the expensive polyethylene glycol (PEG)-disteroyl phosphatidylethanolamine (DSPE).

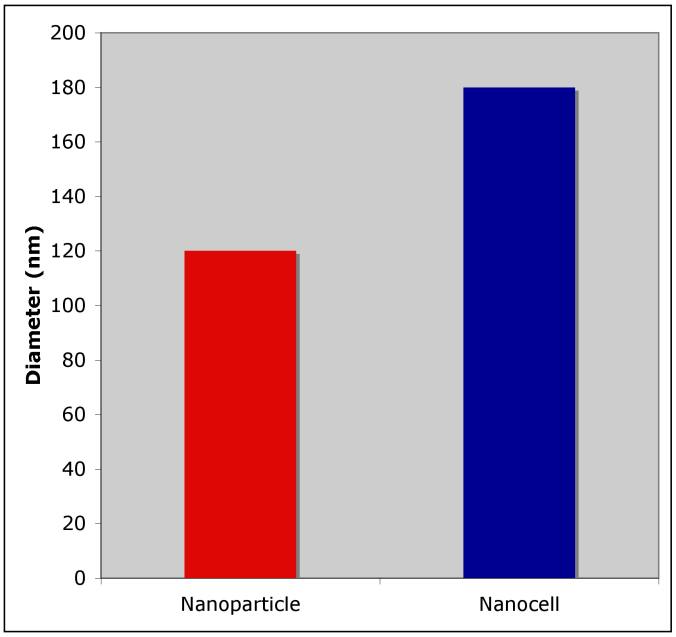


Figure 1.5: Approximate sizes of nanocell and nanoparticle core. Recreated from [28].

In summary, while both liposomes and polymer nanoparticles have these distinct advantages over free agents, each has their own unique disadvantages. Polymer-based nanospheres have limitless potential for surface modification but there is typically a large variance in their size. Before administration, it is necessary to remove those that are too small or too large. Man-made branched polymers (dendrimers) are an ongoing area of research; favourable because of their precise branched structure that could attach many different molecules but risky since they usually are highly toxic. Phospholipid-based micelles are single-layered entities which have shown limited usefulness as nanoparticles due to their relative instability while double-layered liposomes have displayed much longer release times. Both nanocapsules and liposomes seem to be the most widely used although advances in drug-loading due to dendrimers and potential release mechanisms such as an electric or sonar pulse for micelles could make these nanoparticles more popular. In the future, it seems likely that the precise release of more than one agent by nanocells will become the standard for cancer treatment regimes.

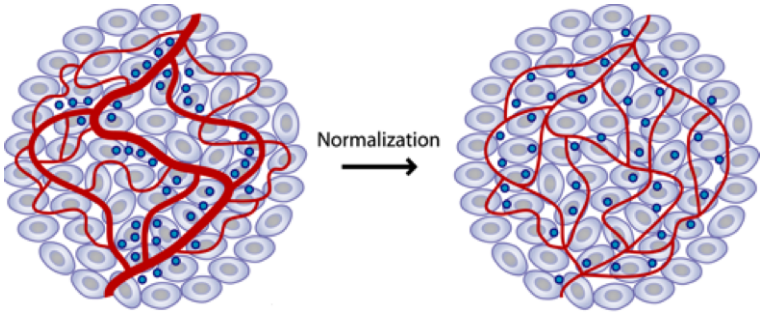


Figure 1.6: The antiangiogenic agent in nanocells leads to tumour vasculature normalization and the trapping of chemotherapy agents in the tumour.

## 1.6 Summary

The understanding of cancer biology has expanded exponentially over the past couple of decades; historically one of the largest threats to life with no known cure, advanced treatment techniques greatly improve chances of survival. The discovery of the important role of tumour angiogenesis led to the development of antiangiogenic treatments which in combination with traditional chemotherapy agents have improved clinical outcomes. Improved targeting and increased circulation time are achieved due to the creation of drug delivery vehicles such as liposomes and polymer nanoparticles. The surface of nanoparticles can be manipulated to target specific cancer cell receptors and to degrade in a controlled way. The recent advent of nanocells that have the aforementioned advantage along with the ability to carry multiple agents could be the next leap forward for efficient delivery and tumour eradication.

Our attention will now turn to modelling the processes of tumour growth and angiogenesis. These will be reviewed with the end goal of predicting the outcome of various combinations of treatments in drug delivery vehicles.

# Chapter 2

# Mathematical Oncology

The search for a mathematical model that accurately predicts tumour growth has been an ongoing field of research for over fifty years. The first models were simple growth functions fitted to clinical data. These led to ordinary differential equation (ODE) models usually borrowed from ecology. While this line of modelling has been supplanted to a large extent by more advanced models that consider spatial effects, recent ODE models have considered the tumours interactions with its microenvironment along with the effects of treatments including chemotherapy, surgery and radiotherapy.

Spatio-temporal models, typically using partial differential equations (PDEs), have enabled modellers to discard the commonly used tumour homogeneity and symmetry assumptions. Incorporating heterogeneity by adding tumour vasculature, growth factors, and hence more accurate drug distribution profiles have been achieved in simulations using these various methodologies. Efforts continue to develop spatial models that include accurate tumour vasculature and dosages of various treatment types; these will be the focus of my modelling attempts.

Some of the predominant mathematical oncology models will be presented along with those that have guided my work.

## 2.1 ODE Models

A number of the classical, strictly time-dependent models will be briefly explained and their solutions presented.

### 2.1.1 Tumour Growth

Tumour growth has been traditionally modelled using ODEs, where a function for their growth rate is formulated based on the qualities that the modeller observes the tumour to exhibit. In other words, a function $f$ is sought so that the tumour cell population (or volume) $n$ is described by

$$\frac{dn}{dt} = f(n), \qquad n(0) = n_0 (> 0). \tag{2.1}$$

The simplest form for this function $f$ assumes that the growth rate is proportional to the present population only, giving $f(n) = rn$ where $r > 0$ is the proliferation rate. This leads to exponential growth where $n(t) = n_0 \exp(rt)$. However, this assumption holds only for a limited time since this growth describes cell populations with a constant division time, abundant resources and unlimited replicative potential. While the latter applies to tumours to a greater extent than normal tissues, tumours still do not have an unlimited growth potential and are often subject to insufficient resources and most likely restricted in size due to spatial constraints and other biological restrictions. In order to account for this, instead of taking a constant proliferation rate, the proliferation rate $k$ is taken to be a decreasing function of $n$. That is, $f(n) = k(n)n$ where $k'(n) < 0$. Most commonly, a static 'carrying capacity' $n_\infty$ is imposed on the tumour cells, so that $k(n) \to 0$ as $n \to n_\infty$ causing $n(t)$ to approach a finite limit corresponding to the maximum tumour size independent of $n_0$. A classical form for $k(n)$ would be $r(1 - n/n_\infty)$ where $r > 0$ corresponding to logistic growth (first proposed by Pierre-Francois Verhulst in ecology), giving

$$f(n) = rn\left(1 - \frac{n}{n_\infty}\right). \tag{2.2}$$

Intuitively this represents a growth rate that is proportional to the current population and the amount of available resources where this resource competition is the population-limiting factor. The solution of this equation is the logistic equation,

$$n(t) = \frac{n_0 n_\infty}{n_0 + e^{-rt}(n_\infty - n_0)}. \tag{2.3}$$

This is the most well-known sigmoid (S-shaped) function where if $n_0 < n_\infty$, the solution increases to $n_\infty$, while if $n_0 > n_\infty$, the solution decreases to this value. If $n_0 = n_\infty$, the constant solution $n(t) = n_0$ arises.

This equation can be generalized to

$$f(n) = \frac{rn}{\nu}\left(1 - \left(\frac{n}{n_\infty}\right)^\nu\right) \tag{2.4}$$

where $\nu > 0$ ($\nu = 1$ is the usual logistic case). This leads to the Richards differential equation which can be solved to find

$$n(t) = \frac{n_0 n_\infty}{(n_0^\nu + e^{-rt}(n_\infty^\nu - n_0^\nu))^{1/\nu}}. \tag{2.5}$$

The solution has an inflection point at $t^* = \frac{1}{r}\ln\left(\frac{n_\infty^\nu - n_0^\nu}{\nu n_0^\nu}\right)$, which corresponds to $n(t^*) = n_\infty/(\nu+1)^{1/\nu}$. This is the point where the growth rate hits a maximum and begins to decrease.

Taking the limit of (2.4) as $\nu \to 0^+$ yields the Gompertz function

$$f(n) = rn\ln\left(\frac{n_\infty}{n}\right).$$

While originally and independently formulated as a law for mortality [30], the above relation with generalized logistic growth was first observed by Richards in [31]. This can be seen by noting that

$$\lim_{\nu\to 0}\frac{1}{\nu}(1 - x^\nu) = \ln(x).$$

A very simple proof of this can be obtained by noting that this limit is equivalent to the definition of the derivative of the function $f(y) = x^y$ at $y = 0$. The solution of this ODE is

$$n(t) = n_\infty\left(\frac{n_0}{n_\infty}\right)^{e^{-rt}}, \tag{2.6}$$

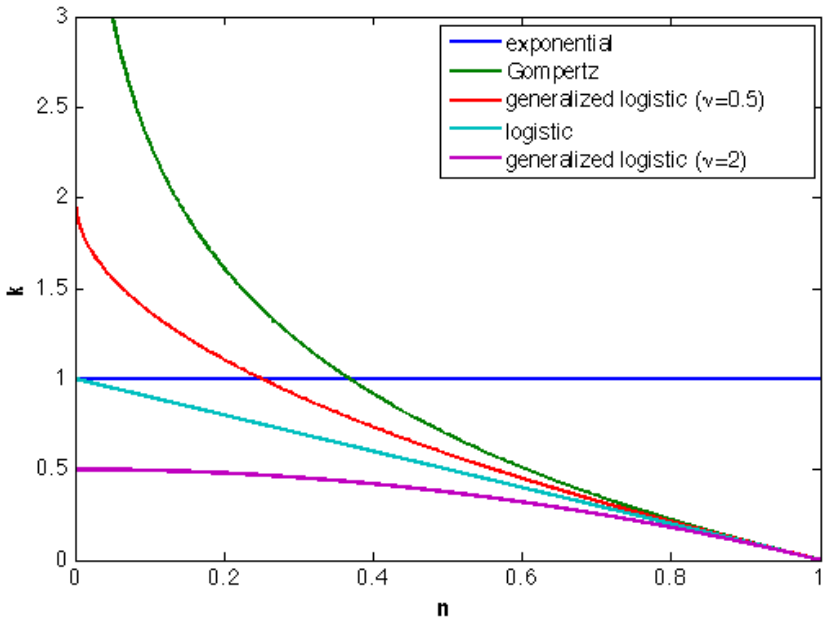


Figure 2.1: Analyzing the proliferation rate of tumour cells as a function of $n$ in various models gives insight into the tumour behaviour.

with an inflection point at $t^* = \ln(\ln n_\infty - \ln n_0)/r$, when $n(t^*) = n_\infty/e$. A criticism of the Gompertz model is that the proliferation rate for small cell populations is unbounded. That is, the proliferation rate limit

$$\lim_{n\to 0^+} k(n) = \lim_{n\to 0^+} r \ln\left(\frac{n_\infty}{n}\right) = \infty,$$

whereas in the generalized logistic case there is a finite limit for this proliferation rate given by $k(0) = r/\nu < \infty$. This is a more reasonable situation since the proliferation rate of small populations is bounded by the rate of cell division. In addition, it has been noted in [32] that the role of the body's immune system is precluded in any model where $k(0)$ is unbounded. Comparing the growth rates of these models occurs in Figure 2.1 and displays the finite limits at $n = 0$ of the other models. It should be noted though that the Gompertz model still does accurately fit many sets of tumour data. The actual growth curves given in Equations 2.3, 2.5 and 2.6 are displayed non-dimensionally in Figure 2.2. For a brief summary of the nondimensionalization of these ODEs see A.1.

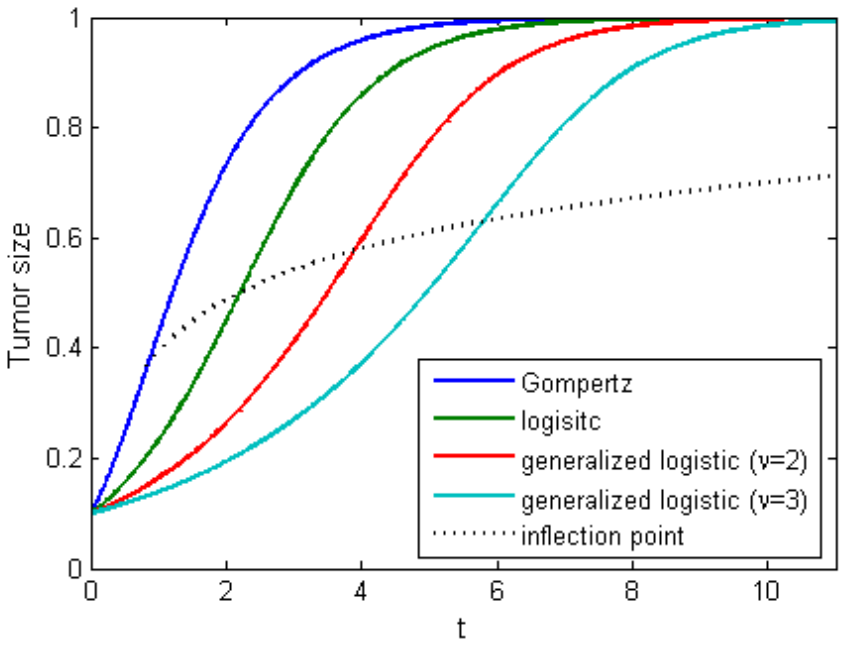


Figure 2.2: Comparison of the classical tumour growth models (non-dimensionalized) showing the inflection point when growth begins to slow.

There are many other variations, generalizations and combinations of the above forms, attempting to more accurately represent tumour growth. However, the one feature they have in common is their s-shaped sigmoid function behaviour. One commonly used combination is the Gomp-ex model proposed in [33] which assumes the tumour is initially experiencing exponential growth since its growth is not yet limited by a lack of resources but at some point competition is introduced leading to Gompertz growth (this eliminates issues with the unbounded growth rate). By taking

$$f(n) = n \max\left(r_1, r_2 ln\left(\frac{n_\infty}{n}\right)\right)$$

the aforementioned transition would occur at

$$n_c = n_\infty e^{-r_1/r_2}.$$

### 2.1.2 The Effect of Chemotherapy

From an intuitive standpoint, it is expected that chemotherapy will have a negative population-dependent effect on the growth rate, and hence we add a term $-g(n)$ to (2.1). For $g$ there are several viable forms. Denoting the known time-dependent chemotherapy dosage by $c(t)$, $g$ is often considered to be proportional to $c(t)n$ (the log-kill model). This model assumes that a given dosage kills a fixed fraction of the tumour cells, not a fixed number of cells and was first applied successfully to leukemia cell populations [34].

While the assumption of a fixed fraction cell-kill is adequate for most applications, it has been observed that this fraction likely reaches a maximum and then begins to decline to some fixed value (usually zero) as treatment progresses. This is due to the fact that many cancer types have the ability to gain drug resistance properties or possibly some subpopulations of the original cancer were always unaffected by the drug. A simple way to incorporate this would be to make $g$ proportional to $c(t)f(n)$: the Norton Simon (NS) model [35]. In this case, the tumour equation would simplify to

$$\frac{dn}{dt} = f(n)(1 - c(t)).$$

### 2.1.3 Angiogenesis and the Effect of Antiangiogenic Therapy

Our understanding of tumour growth will now be augmented by expanding our notion of a carrying capacity. Instead of having a static maximum size, the work of Hahnfeldt et al. [36] is followed where they take this carry capacity to be a function of $t$, that is proportional to the amount of vasculature $m$, present in the tumour. The evolution of $m$ is described by a function $h$ giving a second ODE

$$\frac{dm}{dt} = h(m, n, t).$$

The function $m$ will now reflect the largest size of tumour that is sustainable given the current amount of vasculature present in the tumour. Clearly, if $n = m$, then

the size of the vasculature is just adequate to support the tumour, if $n < m$ then the tumour has the ability to grow and if $n > m$, the tumour must regress.

It is assumed that the process of angiogenesis depends on four key factors: (i) the intrinsic or spontaneous loss rate of vasculature, (ii) proangiogenic factors from the tumour cells, (iii) antiangiogenic factors and (iv) administered antiangiogenic therapies. These are represented respectively in a proposed form for $h$ given by

$$h(m, n, t) = -km + bS(m, n) - dI(m, n) - Ama(t)$$

where $k$ is the spontaneous loss rate, $b$, $c$ and $A$ are constants, the functions $S$ and $I$ correspond to the effects of proangiogenic (stimulation) and antiangiogenic (inhibition) factors respectively and $a(t)$ is the concentration of administered anti-angiogenic agents. Formulating a diffusion-consumption equation for the concentration $f$ of stimulator or inhibitor inside and outside the tumour gives

$$\frac{\partial f}{\partial t} = D\nabla^2 f - k_f f + g, \tag{2.7}$$

where $g = 0$ outside the tumour and $g = g_0$ inside the tumour. Along with the assumptions that the tumour is in a quasi-steady state (setting $\partial f/\partial t = 0$) and radially symmetric, the form of $I$ is found to be $cmn^{2/3}$. Hahnfeldt et. al go on to show that the inhibitor term should grow $m^{p_m} n^{p_n}$ times faster than the stimulation term, where $p_m + p_n = 2/3$. Choosing $p_m = 1$ and $p_n = -1/3$ gives

$$\frac{dm}{dt} = -km + bn - dmn^{2/3} - Ama(t). \tag{2.8}$$

It should be noted that in their analysis $k$ was set to 0, assuming that the natural endothelial cell loss is a neglible effect.

For $b > k$, a unique steady state exists:

$$n_\infty = m_\infty = \left(\frac{b-k}{d}\right)^{2/3}. \tag{2.9}$$

In [37], the optimal combination of radiotherapy and angiogenic inhibitors was treated as as an optimal control problem using a modification of (2.8) where they

replace $n$ by $m$ but retain the results of Hanhfeldt's spatial analysis, so that

$$\frac{dm}{dt} = bm^p - dm^{p+2/3}.$$

It should be noted that for all values of $p$, the steady-state solution of this equation along with any of the possible forms of generalized logistic growth is the same as that for the original equation (2.8), given by (2.9). While taking $p = 1$ would be equivalent to simply replacing $m$ by $n$, they sought to retain the behaviour of the original system and found $p = 2/3$ to be more suitable for this giving the equation

$$\frac{dm}{dt} = bm^{2/3} - dm^{4/3}.$$

In [38] the dependence on the tumour size was retained in the equation for the carrying capacity, it was simply suggested that the function $S(m, n)$ be taken to be $m$ instead of $n$. This is an intuitive switch to make since this implies that the vasculature growth is proportional to the present amount of blood vessels rather than the tumour size. This by itself says that endothelial cell populations will rise exponentially, but once again, when the inhibitor is taken into consideration a saturating state is reached. By antiangiogenic therapy alone, an eradication condition was derived, specifically eradication was achieved for a periodic treatment of period $T$ if and only if

$$\frac{A}{T}\int_0^T a(t)\,dt \geq b - k.$$

## 2.2 Spatial Models

An outline of some previous spatial modelling attempts, some based on the above work, will be overviewed and additional biological features such as blood vessel network structure will be included in our discussion. First growth factors modelling will be outlined, leading to vasculature modelling before showing how these can be incorporated into a tumour model.

### 2.2.1 Modelling Growth Factor Activity

Following [39] for the preliminary modelling, let $f_j^e$ denote the concentration of factor $j$ where the factor can either be considered to be proangiogenic ($p$) or antiangiogenic ($a$) in behaviour, in an environment $e$, where the environment can be malignant ($m$) inside the tumour or host ($h$) outside the tumour. Assuming these factors are produced at a constant rate $g_j^e$, degrade exponentially at a rate $k_j^e$ and diffuse with diffusion constant $D_j^e$, all of which differ inside and outside the tumour and for anti- and proangiogenic factors, the PDE

$$\frac{\partial f_j^e}{\partial t} = D_j^e \nabla^2 f_j^e - k_j^e f_j^e + g_j^e \tag{2.10}$$

is obtained giving a more generalized version of equation (2.7). However, now instead of incorporating this into an equation for vasculature, this equation is now explicitly retained for the growth factors. Now by making a similar pseudo steady-state assumption, it is assumed that local changes in factor concentration are very small: $\partial f_j^e/\partial t = 0$. Further assuming radial symmetry with a tumour of radius $R$, solutions of the moving boundary problem governed by the equation

$$D_j^e \frac{1}{r^2}\frac{\partial}{\partial r}\left(r^2 \frac{\partial f_j^e}{\partial r}\right) - k_j^e f_j^e + g_j^e = 0 \tag{2.11}$$

with suitable boundary conditions can be derived. Since the assumption of radial symmetry will not be used, these solutions are omitted; further details are given in Appendix A.2.

#### Angiogenic Activity

The balance between the proangiogenic and antiangiogenic factors is the determinant of whether or not angiogenesis will be suppressed or initiated. This was represented in [39] by the parameter $\alpha_{\mathrm{GF}}$ and is defined by

$$\alpha_{\mathrm{GF}} = \frac{f_p}{f_a} - 1 \tag{2.12}$$

where $\alpha_{\mathrm{GF}} > 0$ corresponds to angiogenesis being initiated, $\alpha_{\mathrm{GF}} = 0$ when angiogenesis is just suppressed and $\alpha_{\mathrm{GF}} < 0$ implies no angiogenesis is taking place and

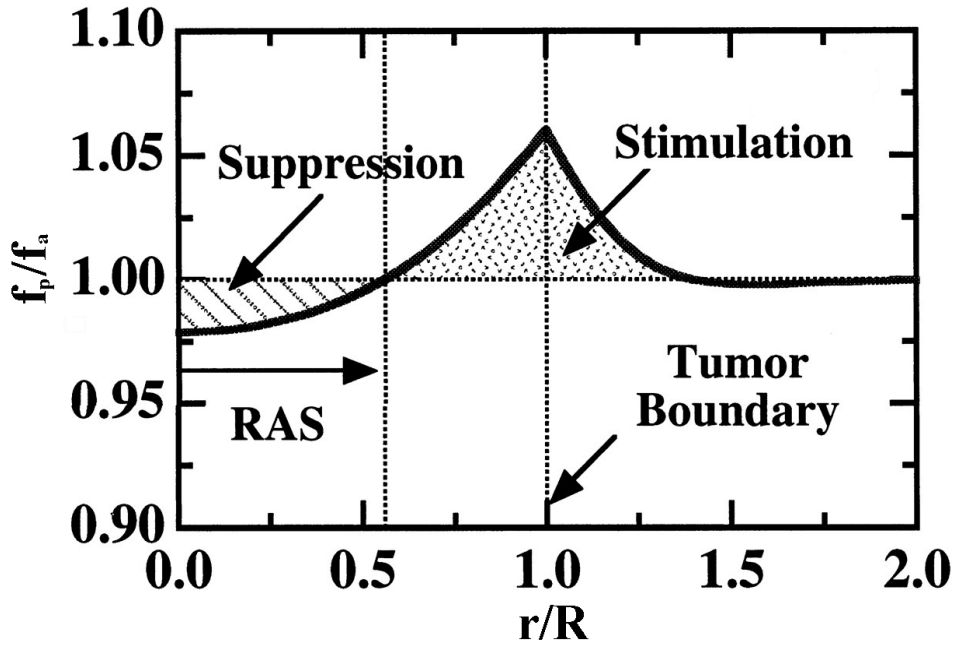


Figure 2.3: Areas of angiogenic suppression and stimulation based on the balance of angiogenic factors. Image from [39].

vessels are degrading. This measure of angiogenic activity could be incorporated into blood vessel development models based on the previous observations. A typical scenario of an angiogenic activity radial profile displaying angiogenic repression at the tumour core and angiogenic stimulation around the rim is shown in Figure 2.3.

### Angiogenesis and Vasculogenesis

In [40], the measure of angiogenic activity $\alpha_{\mathrm{GF}}$ (2.12) is included in a model for endothelial cell growth. Letting $m$ denote the concentration of endothelial cells, they formulated the empirical relation (based on tissue perfusion data from [41]),

$$m = m_0 e^{k_1 \alpha_{\mathrm{GF}}}, \tag{2.13}$$

where $m_0$ is the vascular density of normal tissue and $k_1 > 0$.

As discussed, angiogenesis, the development of blood vessels from pre-existing vasculature, plays a large role in tumour growth and development. Vasculogenesis,

the formation of new blood vessels where there were none before, was believed to only occur during embryonic blood vessel development (embryogenesis) when endothelial cells arise from endothelial progenitor cells (EPCs). However, it has been observed to play a role in tumour vascularization as well [42]. Along with equation (2.13), they include the contribution of vasculogenesis by formulating a PDE for the concentration of EPCs $m_{\text{EPC}}$ in the system,

$$\frac{\partial m_{\text{EPC}}}{\partial t} = k_2 m_{\text{EPC}} \left(1 - \frac{m_{\text{EPC}}}{m_\infty}\right) + \begin{cases} k_3 m\, q\, \alpha_{\text{GF}} & \text{if } \alpha_{\text{GF}} > 0, \\ 0 & \text{if } \alpha_{\text{GF}} \leq 0, \end{cases} \tag{2.14}$$

where the first term represents the logistic growth of EPCs and the second term describes the rate of adhesion of EPCs to tumour vasculature. This adhesion is proportional to the product of EC density $m$, the flux of EPCs $q$ and the level of angiogenic activity $\alpha_{\text{GF}}$. They then use a formula for symmetric tumour growth with a growth rate dependent on $m_{\text{T}} = m_{\text{EPC}} + m$.

Endothelial progenitor cells have been touted in the literature (for example in [43]) as a potential target for antiangiogenic therapy. As such, further modelling attempts should attempt to include them; however, for our purposes their effect on the system is considered to be negligible.

### 2.2.2 Modelling Tumour Vasculature

There are an abundance of different mathematical methods for simulating vasculature networks in the literature. A few general techniques that have inspired the models to follow will be presented here.

#### Continuous Models

Instead of incorporating the exact structure of the blood vessel network into a model, continuous models could be used instead that uses a more coarse-grain concentration of endothelial cells on some domain.

A model of tumour-induced angiogenesis was given in [44] where Anderson and Chaplain developed a mathematical model that incorporated a number of different forms of cell movement in response to various environmental factors. In their model they consider endothelial cell density, proangiogenic factor concentration (they called these tumour angiogenesis factors (TAFs) in their model) and the ECM-bound ligand fibronectin. Fibronectin is primarily responsible for the adhesion of cells, including endothelial cells to the ECM. Using just these three biological entities they were able to consider endothelial cells moving due to three separate phenomena: (i) random motion modelled using simple diffusion, (ii) chemotaxis induced by the proangiogenic factors and (iii) haptotaxis in response to the ligand fibronectin. This leads to the equation for endothelial cell density,

$$\frac{\partial m}{\partial t} = D_m \nabla^2 m - \nabla \cdot (\chi(f_p) m \nabla f_p) - \nabla \cdot (\rho_0 m \nabla l), \tag{2.15}$$

where $D_m$ is the random-motility (diffusion) coefficient, $\chi(f_p)$ is the chemotactic function, and $\rho_0$ is the haptotactic coefficient. The chemotactic function was typically taken to be a constant in previous models but here they use the function $\chi(f_p) = \chi_0 k_1/(k_1 + f_p)$ where $\chi_0$ is the chemotactic coefficient and $k_1 > 0$ in order to achieve decreased chemotactic sensitivity as the proangiogenic factor concentration increases. Given some initial amount of angiogenic factors produced by the tumour cells (note that they are not included in this model), they then assume these factors satisfy the equation

$$\frac{\partial f_p}{\partial t} = D_p \nabla^2 f_p - k_p f_p,$$

where $D_p$ is the diffusion coefficient and $k_p$ is the natural decay rate. Using the steady state of this equation as the initial condition, they then evolve the factor concentration by

$$\frac{\partial f_p}{\partial t} = -\mu_p m f_p, \tag{2.16}$$

representing the binding of these factors to endothelial cells. Fibronectin is considered to be produced by endothelial cells only and the binding of fibronectin to

endothelial cells will once again be modelled using a simple uptake term giving

$$\frac{\partial l}{\partial t} = \omega m - \mu_l m l, \tag{2.17}$$

where the production rate $\omega$ and the uptake rate $\mu_l$ are both positive constants.

Performing simulations of the above system, this model shows a wide array of potential behaviours. Considering haptotaxis, their inclusion or exclusion effects the migration pattern of endothelial cells toward a tumor. Without haptotaxis, endothelial cells migrate directly to the tumour while when it is included, the migration is slower and there is notable lateral movement of the cell clusters as they move through the ECM. The chemotactic term influences the behaviour as certain parameters can be chosen in the chemotactic function that can lead to endothelial cells never connecting with the tumour that they are moving toward.

There has also been a continuous model developed that simply identifies areas as vascularized or non-vascularized. This PDE formulation was given in [45] where $m$ denotes average blood vessel distribution and

$$\frac{\partial m}{\partial t} = D_m \nabla^2 m + g(m),$$

where the appropriate choice of $g(m)$ ensures the development of vascular and non-vascular domains within the tumour as follows. Taking this function to be $g(m) = \alpha m + \beta m^2 + \gamma m^3$ enables us to have three fixed points (when $\alpha < 0$, $\beta > 0$ and $\gamma < 0$). By taking $\alpha = -Z$, $\beta = 3Z$ and $\gamma = -2Z$ (where $Z > 0$) there are two stable fixed points at 0 and 1, along with an unstable equilibrium at 1/2. This corresponds biologically to immature vessels either maturing or regressing, they do not remain in an in-between state normally. Starting from a random initial condition of values between 0 and 1, this system evolves into distinct areas that are absent of blood vessels ($m = 0$) or fully vascularized ($m = 1$). Taking $Z = 1$ gives the model they used

$$\frac{\partial m}{\partial t} = D_m \nabla^2 m + m(-1 + 3m - 2m^2). \tag{2.18}$$

With the growth term being fixed, the remaining parameter $D_m$ describes the speed at which endothelial cells spread out. As can be seen in Figure 2.4, this parameter

effects the spatial vascularization pattern although in the infinite time limit any $D_m > 0$ will result in a fully vascularized region.

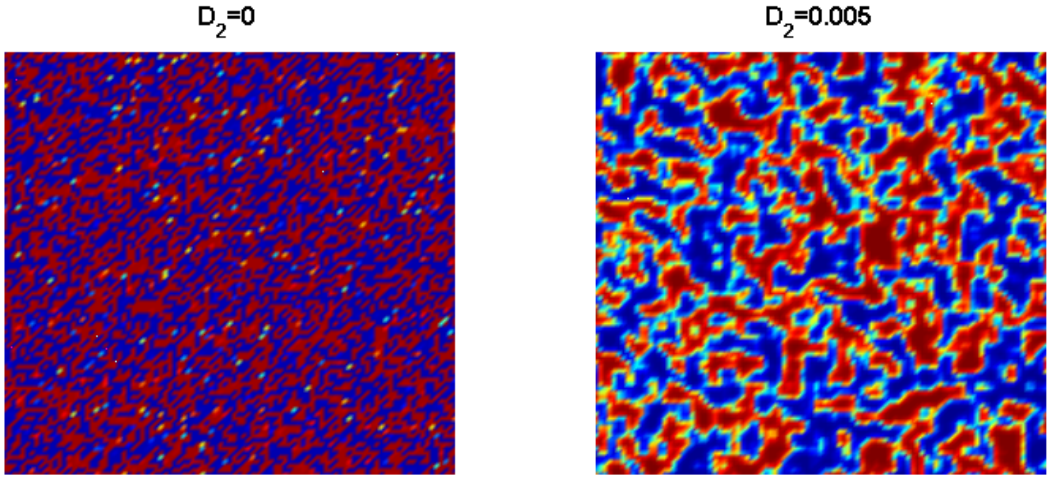


Figure 2.4: Increasing $D_m$ leads to larger areas of vascularization. Images shown are at day 50. Dark blue corresponds to $m = 0$, dark red to $m = 1$.

This vasculature model was coupled with a PDE for tumour growth along with oxygen concentration to study the effects of combination chemotherapy and antiangiogenic therapies. These antiangiogenic therapies were assumed to perform a log-kill of the endothelial cells in the system.

### Discrete Models

To generate an initial distribution of microvessels, Torquato et al. created an algorithm [46] to approximate the microvascular network of the brain. This model could be considered as a random analog of the Krogh cylinder model, a model that was shown to be a poor approximation for vessels in the brain in [47] since it assumes that the vessels are straight, parallel and uniformly spaced while in reality the structure is much more complex. For the model, they assumed the vasculature exists on a triangular lattice that is overlaid on a more complex random lattice that corresponds to individual cells with nonuniform shapes and sizes. None of our tumour models will use automation cells or discrete cell units in general, so the

details of their tumour model and its interaction with the blood vessel model are omitted. To simulate their network the following steps were taken:

1. A random node on the lattice is chosen.
2. A random angle (from the six possibilities) is chosen.
3. The vessel extends at this angle from the original node until one of the following occurs
   (a) The vessel reaches the boundary of the grid.
   (b) The vessel penetrates within a radius of one lattice unit about an existing vessel oriented at the same angle.
   (c) The vessel would cause the intersection of three blood vessels at a single node. If this occurs the vessel is truncated at its last intersection with another vessel.
4. If the vessel does not vascularize at least one unvascularized cell, it is discarded, otherwise, it is incorporated into the network. Repeat.

The above steps are taken in the interest of preserving some of the optimal design characteristics of normal vasculature. It should be noted that while five- and six-way intersections are prevented, the unnatural four-way intersection is still permitted. An example of one of their microvessel network simulations is shown in Figure 2.5.

Random walk techniques have been widely employed to model angiogenesis, in fact the model outlined above by Anderson and Chaplain has a discrete analog that they also outlined in [44]. Probabilities of moving in specific directions are assigned based on the stimuli of factors and fibronectin in their environment. This has the effect of producing vessels that develop according to a directed random walk from a parent vessel in the direction of the tumour mass. This model was successful at reproducing the 'brush border' of dense blood vessels at the tumour

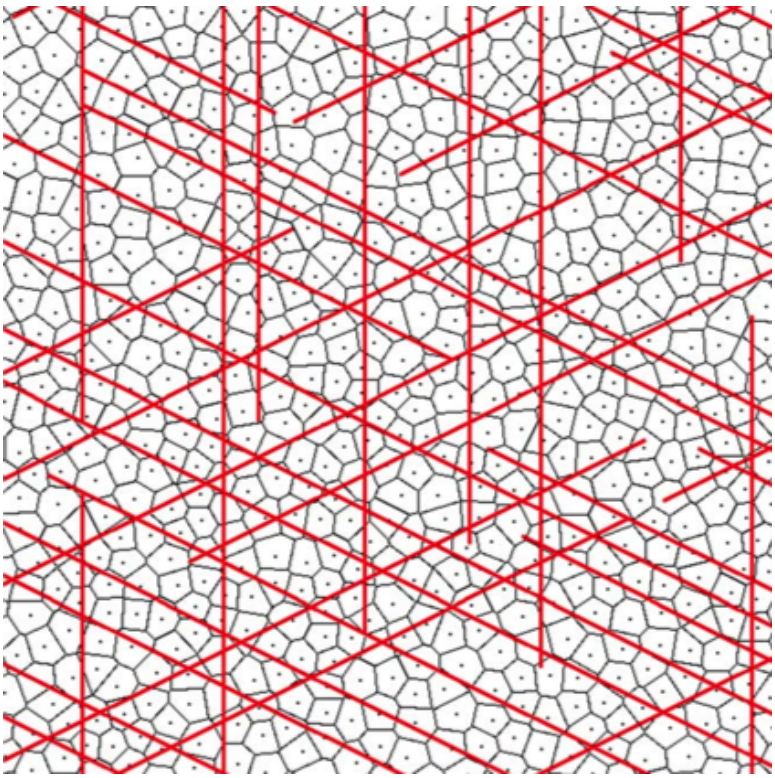

Figure 2.5: A sample simulation of the Torquato et al. microvessel algorithm (showing underlying cell lattice). Image from [46].

periphery. In addition, branching and anastosmosis (blood vessel connections) were observed for some parameter values. This model from [44] has been expanded in many different ways, but perhaps most importantly, the flow through the network and chemotherapy schedules have been considered [48]. The flow was originally found after generating a hollow blood vessel network but has been improved to have this flow effect the network development, leading to the so-called dynamic adaptive tumour-induced angiogenesis (DATIA) model [49] which has been used to test treatments and suggest treatment targets.

In a recent paper [50], random walk vasculature implemented in 3D has been used to study the effect on blood perfusion when tumour vasculature normalization is initiated by antiangiogenic therapy.

Invasion percolation, a technique successfully applied in previous papers in other areas, was applied to tumour vasculature in [51] and works as follows. First, each grid point is assigned a random value, usually uniformly distributed although other distributions could (and probably should) be used. Starting from some point on the grid (conventionally the bottom left corner) the adjacent point with the lowest random value assigned to it is chosen. This process is continued until the desired grid occupancy is reached. The network is formed by connecting all adjacent points that have been chosen. Flow can be added to the model by assuming that the source of blood is the bottom left corner while fluid can exit the grid via the top right corner. Those vessels which have nonzero flow are referred to as the backbone while the rest are assumed to be non-perfused and are pruned from the system when considering the vasculature of healthy tissue. It has been suggested that the fractal dimension of the vasculature structure could be an important quality in judging the validity of vasculature models. Various vasculature network generating schemes can be evaluated in this matter including the invasion percolation method which seems to correspond well with the fractal dimension of tumour vasculature. The fractal dimension of the vasculature structure $d_m$ is calculated using the box-counting method which is calculated by finding

$$d_m := \lim_{l \to 0} \frac{\ln N_m(l)}{\ln(1/l)},$$

where $N_m$ is the number of boxes with side length $l$ needed to cover all the vessels in the vasculature network. This implies that $N_m \propto l^{-d_m}$.

Using a hexagonal lattice as the basis for vascular development was proposed in [53] and developed in [52] has been applied to tumour vasculature in [54] and more recently in [55]. An underlying triangular lattice was added in order to incorporate tumour cells at these sites. The basis for the vasculature is a tripod consisting of three tubes of length $l$ separated by 120°. A difference in [55] compared to [52] is the first step in creating the initial vessel structure. In [52] the entire network was created by randomly attaching tripods to the terminal points of pre-existing tripods. The initial condition was three source tripods equally spaced on the periphery of

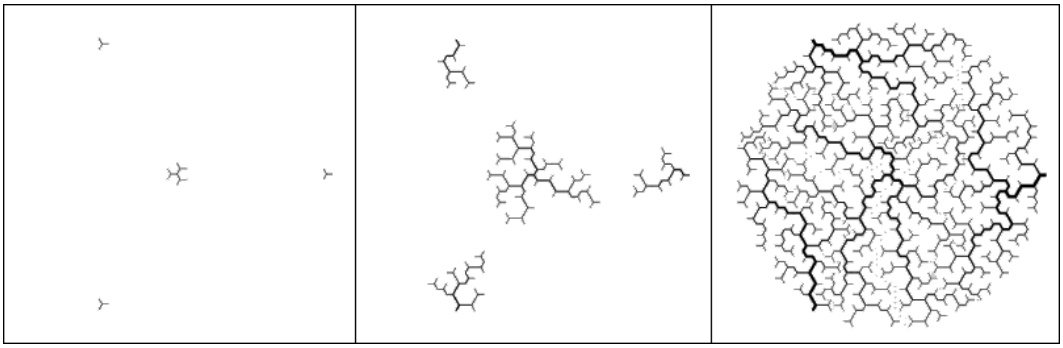

Figure 2.6: The development of blood vessel networks on a hexagonal lattice. Image reproduced from [52].

the roughly circular domain with three sink tripods placed in the center of the domain. See Figure 2.6 to see the development of this 2D network. In [55] there are a handful of initial vessels simulated first with directed random walks that are taken to be either sources or sinks. Tripods are then randomly attached to points on these vessels or to tripods which have already been placed. Tripods continue to be randomly placed until no permissible location remains. With arteries and veins corresponding to sources and sinks respectively, the tripod networks of the disconnected veins or arteries are connected with single tubes which are considered to be capillaries. These vessels have different diameters based on 'Murray's Law' [56] that relates the parent vessel radius $r_0$ to the radii of its two branches $r_1$ and $r_2$ by the equation

$$r_0^\alpha = r_1^\alpha + r_2^\alpha,$$

where $\alpha > 0$ is called the diameter (or bifurcation) exponent. Originally shown by Murray that $\alpha = 3$ minimizes the energy required for blood transport [56], observations have suggested a lower value and it was found in fact that $\alpha = 2.7$ minimizes the amount of vascular wall material needed [57]. By fixing the radii of the tips of these trees, the radii of a vessel can be found recursively once all its descendants' radii have been found. These networks are then remodelled due to pressure or shear force dependent processes and further development of this model depends on both the oxygen concentration provided by the vasculature and the

concentration of growth factors being excreted by tumour cells. See Figure 2.7 for a couple simulations of their algorithm with different initial conditions.

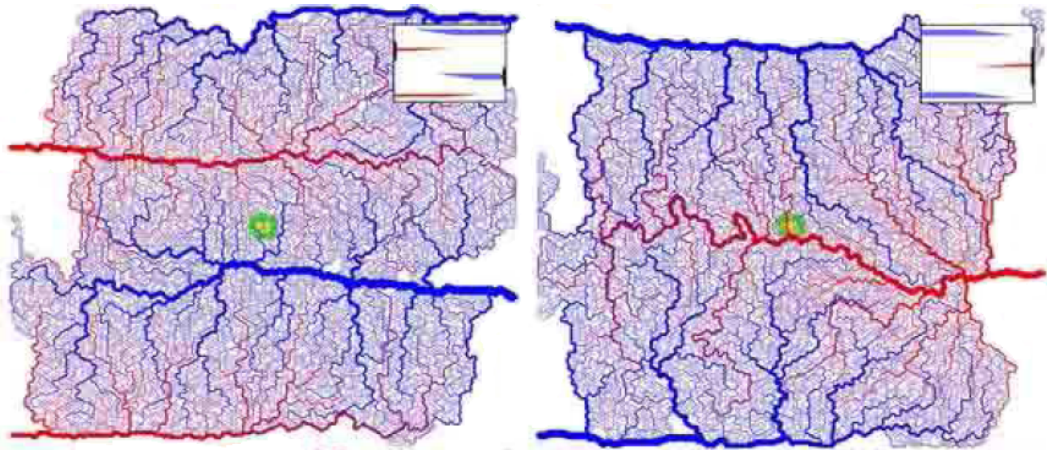

Figure 2.7: Sample simulations from initial conditions given in top right corner of images. Images from [55].

The main reason vasculature was originally included in tumour growth models was to better predict tumour growth and gain an understanding of the dynamics of their interaction. For a more detailed review of tumour-induced angiogenesis see [58]. The other added benefit of including blood vessels is the ability to calculate an accurate drug distribution. To this end, drug delivery models dependent on the blood vessel network will be outlined.

## 2.3 Pressure and Drug Delivery

In [59] Jain reviews a model that describes, "the transport of molecules across tumour vasculature". The mathematical formulation appears to be important in describing the distributions of various agents in the tumour. In [60], it is shown using a mathematical model that the heterogeneous (and hence, unfavourable) distribution of monoclonal antibodies (MAbs) is primarily due to interstitial fluid pressure (IFP). They even show that in a tumour, despite the homogenizing effects of high vascular permeability and interstitial transport coefficients, the heterogeneous

antigen distribution and blood perfusion along with hindered interstitium diffusion and extravascular MAb binding are not sufficient to describe this heterogeneous MAb distribution. This model was further developed and analyzed in [61]. Their formulation will be outlined here for incorporating IFP into a drug distribution model. This will be needed later to formulate the PDE for other macromolecules (specifically nanoparticles and angiogenic factors).

Assuming a radially symmetric tumour mass, the radially outward fluid velocity at the tumour periphery, $u_R$, can be found by dividing the fluid loss by the total tumour surface area:

$$u_R = \rho V Q_{IF}/A = \rho R Q_{IF}/3,$$

where $\rho$ is the tumour density (g/mL), $Q_{IF}$ is the net fluid loss from the tumour periphery and $R$, $A$ and $V$ are the tumour radius, surface area and volume (cm, $cm^2$, $cm^3$) respectively. Values for $Q_{IF}$ have been obtained in a number of studies [62, 63, 64] with values around 0.14-0.22 mL/h/g-tissue, much larger than the typical lymphatic drainage in normal tissues (0.002-0.07 mL/h/g).

From Starling's Law, the net fluid loss from a single vessel, $J_f$ (mL/s), is given by

$$J_f = L_p S[p_v - p_i - \sigma_T(\pi_v - \pi_i),] \tag{2.19}$$

where $L_p$ is the hydraulic conductivity of the vascular wall (cm/mmHg-s), $S$ is the total exchange area of the vessel ($cm^2$), $p_{v(i)}$ is the vascular (interstitial) pressure (mmHg), $\pi_{v(i)}$ is the plasma (interstitial) osmotic pressure and $\sigma_T$ is the osmotic reflection coefficient of plasma proteins (the fraction of solute filtered through a membrane if there is zero concentration difference with high filtration rate). In normal tissues, the excess fluid $J_f$ would be removed by the lymphatic system; in tumours the fluid can either leak toward the core of the tumour, or toward the periphery. Inward flow would lead to increased IFP until an effective pressure, $p_e = p_v - \sigma_T(\pi_v - \pi_i)$, is reached at which point $J_f = 0$. Outward flow would lead to excess fluid entering the interstitium. The interstitial velocity of this fluid, $u_i$, is

related to the IFP by Darcy's Law:

$$u_i = -K\frac{dp_i}{dr}, \tag{2.20}$$

where $K$ is the hydraulic conductivity of the interstitium and $r$ is the distance from the tumour core.

Considering the conservation of mass between the fluid filtered from the vessels with the fluid moving toward the periphery gives

$$\frac{1}{r^2}\frac{d(r^2u_i)}{dr} = \frac{J_f}{V}. \tag{2.21}$$

Substituting equations (2.19) and (2.20) into (2.21) yields

$$\frac{1}{r^2}\frac{d}{dr}\left(r^2\frac{dp_i}{dr}\right) = -\frac{L_p}{K}\frac{S}{V}(p_v - p_i - \sigma_T(\pi_v - \pi_i)). \tag{2.22}$$

The transport of solute molecules $J_s$ due to extravasation from blood vessels, described by the membrane pore model, can be written as a sum of its diffusive and convective parts, where diffusion is proportional to the difference between the plasma concentration $c_p$ and the interstitial concentration $c_i$ and convection is proportional to the fluid leakage $J_f$ in (2.19) giving

$$J_s = PS(c_p - c_i)\mathrm{Pe}/(e^{\mathrm{Pe}} - 1) + J_f(1-\sigma)c_p, \tag{2.23}$$

where Pe is the Peclet number defined by

$$\mathrm{Pe} = \frac{J_f(1-\sigma_f)}{PS},$$

$P$ is the vascular permeability coefficient and $\sigma_f$ is the osmotic reflection coefficient for the solute. For most molecules the first term can be ignored since they do not diffuse very much, instead their primary means of movement is convection.

Once the macromolecule leaves the blood vessel and enters the interstitial space, diffusion may become a more important factor in its movement. Its diffusion is proportional to $dc_i/dr$ while the convection is proportional to interstitial fluid velocity $u_i$ given in (2.20). This gives the interstitial flux

$$I = r_f u_i c_i - D\frac{dc_i}{dr}, \tag{2.24}$$

where $D$ is the constant interstitial diffusion coefficient and $r_f$ is the retardation factor (the ratio of solute velocity to fluid velocity). Now, balancing the solute extravasation from blood vessels in (2.23) with the solute moving in the interstitial space gives a convection-diffusion equation for solute concentration in the interstitium

$$\frac{\partial c_i}{\partial t} = \frac{D}{r^2}\frac{\partial}{\partial r}\left(r^2\frac{\partial c_i}{\partial r}\right) - r_f\frac{1}{r^2}\frac{\partial}{\partial r}(r^2 u_i c_i) + \frac{J_s}{V}.$$

The above equation can be useful when considering the extravasation of drug delivery vehicles from tumour vasculature and the release of the agents contained therein and could be easily expanded to a non-radially symmetric case.

Drug delivery models have now been reviewed, specifically the extravasation from blood vessels and its spread through tissue. However, the actual interactions between the agent and the targeted tumour cell have not been considered. To this end, models for the binding between ligands present on delivery vehicles and the cell membrane receptors will be evaluated now.

## 2.4 Receptor-Ligand Binding Models

When a cell receptor and a nanoparticle conjugated with ligands are brought close to each other due to non-specific interactions (Brownian motion, van der Waals forces, etc.), receptor-ligand binding may occur. It will be suggested here that a model developed by Bell [65] to describe binding events between two cells could be potentially extended to this situation.

### 2.4.1 Bell's Deterministic Model

Letting $N_1$ be the density of total available receptor, $N_2$ the density of total available ligand, $N_{iu}$ the density of unbound receptor/ligand respectively for $i = 1, 2$ and $N_b$ the density of bound receptor-ligand, they satisfy

$$N_i = N_{iu} + N_b, \qquad i = 1, 2. \tag{2.25}$$

Assuming bond formation is governed by the simple kinetic equation

$$\frac{dN_b}{dt} = k^+ N_{1u} N_{2u} - k^- N_b, \tag{2.26}$$

where $k^{+/-}$ is the forwards/backwards (association/disassociation) kinetic rate constant. Using (2.25), (2.26) becomes

$$\frac{dN_b}{dt} = k^+ (N_1 - N_b)(N_2 - N_b) - k^- N_b. \tag{2.27}$$

If it is further assumed that $N_1 \gg N_b$, then (2.27) simplifies to

$$\frac{dN_b}{dt} = k^+ N_1 (N_2 - N_b) - k^- N_b, \tag{2.28}$$

and at equilibrium,

$$N_\infty = K N_1 N_2 / (1 + K N_1), \tag{2.29}$$

where $K = k^+/k^-$ and is referred to as the association constant.

Binding is assumed to be a (conceptually separated) two-step reaction, where at first they diffuse into sufficiently close proximity to permit the second reaction step (as in [66]). Denoting the so-called "encounter complex" where receptor and ligand are within some critical radius $C$ by $R \circ L$ and the bound receptor-ligand by $RL$, this concept can be represented as the chemical reaction

$$R + L \underset{d_-}{\overset{d^+}{\rightleftharpoons}} R \circ L \underset{r_-}{\overset{r^+}{\rightleftharpoons}} RL$$

where $d, r^{+/-}$ are the appropriate directional reaction rates.

In many cases, since the concentration of the encounter complex is low compared to receptor or ligand concentration, it is assumed that the rate of change of the encounter complex is negligible, i.e. $d[R \circ L]/dt = 0$. Thus, the kinetic rate constants can be approximated by

$$k^+ = d^+ r^+ / d^- + r^+ \text{ and } k^- = d^- r^- / d^- + r^+.$$

If it is further assumed that $r^+ \gg d^-$, i.e. the encounter complex is much more likely to react than to dissociate, which is true in a viscous membrane, then $k^+ = d^+$ and $k^- = d^- r^- / r^+$.

Determining the strength of bonding between a ligand-conjugated nanoparticle and a receptor-rich cell is important so now the force necessary to separate the cell-particle bond is calculated. From kinetic theory for the strength of solids (see [67]), the lifetime $\tau$ of one of these bonds is given by

$$\tau = \tau_0 e^{(E_0 - \gamma f)/k_B T}, \tag{2.30}$$

where $\tau_0$ is the reciprocal of a natural frequency of oscillation of atoms in solids ($\approx 10^{-13}$s), $E_0$ is the bond energy, $f$ is the applied force per bond, $\gamma$ is an empirically determined parameter to account for structure and imperfections (reactive compliance), $k_B$ is the Boltzmann constant ($\approx 8.617 \times 10^{-5}$eV/K) and $T$ is temperature.

It is natural to identify $\tau(f = 0)$ with the inverse reverse rate constant $(k^-)^{-1}$. Suppose a force $F$ is attempting to separate the cells where each bond is equally stressed, so the force per bond is $F/N_b$. Then the reverse reaction rate $k^-$ in (2.28) should be modified to

$$k^- = k_0^- e^{\gamma F/k_B T N_b}, \tag{2.31}$$

where $k_0^-$ is the unstressed rate of disassociation. The revised ODE is given by

$$\frac{dN_b}{dt} = k^+ N_1 (N_2 - N_b) - N_b k_0^- e^{\gamma F/k_B T N_b}. \tag{2.32}$$

If the force is zero before $t = 0$, there is initially an equilibrium given by (2.29). After a while, a new equilibrium will be reached where $N_\infty$ is given by (2.29) except $K = k^+/k_0^-$ and is multiplied by $e^{-\gamma F/k_B T N_b}$.

To find the critical force $F_C$, which is just strong enough to detach the ligand and receptor, the two terms on the RHS of (2.32) are considered. Refer to Figure 2.8 to see that for $F = F_C$, the two terms are equal at their point of tangency, i.e. when their slopes are equal. Thus, the critical force per potential bond, $f_C$, is

$$f_c = \frac{F_C}{N_1} = \frac{k_B T \alpha_c}{\gamma}, \tag{2.33}$$

where $\alpha_c$ is the solution of $\alpha_c e^{\alpha_c + 1} = K N_2$.

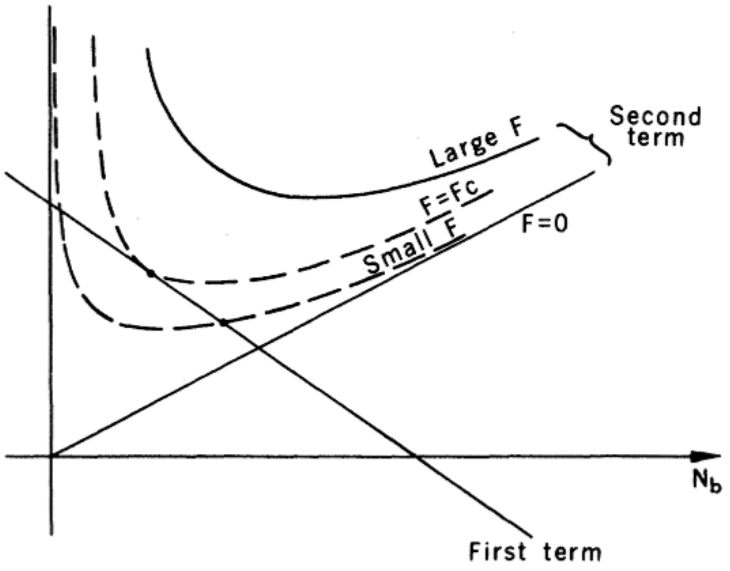


Figure 2.8: Equilibrium solutions of (2.32) correspond to equality of the first and second terms. Observe that for the critical force, the curves are tangent. Figure from [65].

### 2.4.2 A Stochastic Model

This stochastic formulation is based upon the deterministic equation derived by Bell and was derived in [68]. Letting $X_t$ denote the concentration of bound ligand-receptors at time $t$ and $A = \gamma/k_BT$, the assumption $N_1 \gg X_t$ is used but now $X_t$ at any given time is a probability distribution of bonds, not a particular value. Our focus is limited to one square unit of area (to ensure $X_t$ is discrete).

Letting $X_{\Delta t} = X_{t+\Delta t} - X_t$, for $1 \leq X_t \leq N_2 - 1$,

$$P\{X_{\Delta t} = i | X_t\} = \begin{cases} k^+ N_1(N_2 - X_t)\Delta t + o(\Delta t) & \text{if } i = 1 \\ k^- e^{\frac{AF}{X_t}} X_t \Delta t + o(\Delta t) & \text{if } i = -1. \end{cases} \tag{2.34}$$

Making adjustments for $X_t = 0$ and $X_t = N_2$, a system of PDEs can be formu-

lated for the discrete probabilities $p_i(t) = P\{X_t = i\}$,

$$\begin{aligned}
\frac{\partial p_0(t)}{\partial t} =& k^- e^{AF} p_1(t) - k^+ N_1 N_2 p_0(t), \\
\frac{\partial p_i(t)}{\partial t} =& k^+ N_1 (N_2 - (i-1)) p_{i-1}(t) + (i+1) k^- e^{AF/(i+1)} p_{i+1}(t), \\
& - (k^+ N_1 (N_2 - i) + i k^- e^{AF/i}) p_i(t) \qquad \text{for } 0 < i < N_2, \\
\frac{\partial p_{N_2}(t)}{\partial t} =& k^+ N_1 p_{N_2 - 1}(t) - N_2 k^- e^{AF/N_2} p_{N_2}(t).
\end{aligned} \tag{2.35}$$

Since $\sum p_i = 1$, the distribution of $X_\infty$ is found by solving the steady-state solution of (2.35):

$$\begin{aligned}
p_i(\infty) &= \frac{N_2!}{(N_2 - i)!} \frac{(KN_1)^i p_0(\infty)}{\prod_{1 \le j \le i} j e^{AF/j}}, \\
p_0(\infty) &= \left( 1 + \sum_{i=1}^{N_2} \frac{N_2!}{(N_2 - i)!} \frac{(KN_1)^i}{\prod_{1 \le j \le i} j e^{AF/j}} \right)^{-1}.
\end{aligned} \tag{2.36}$$

In the case where there is no separating force, the probability-generating function (PGF) $P(\theta) = \sum p_i \theta^i$ is found to be the Taylor expansion of $g(\theta) = (1 + KN_1)^{-N_2} (1 + KN_1 \theta)^{N_2}$, i.e.

$$P(\theta) = \sum_{i=0}^{N_2} \frac{g^{(i)}(0)}{i!} \theta^i. \tag{2.37}$$

The mean is $P'(1) = KN_1N_2/(1+KN_1)$ which agrees with the previous model's equilibrium solution in (2.29).

Turning our attention again to the force necessary to separate all bonds, it is necessary to focus on $p_0(\infty)$, the probability that there are no bonds formed. If $F = F_C$, then $p_0 = 1$ to many decimal places, but even when $F = F_C/2$, $p_0 > 0.99$, a stark contrast with the predictions from the deterministic model.

### 2.4.3 Cell Adhesion with Two Receptors

The model in [69] will be followed in order to consider the situation where a large number of adhesion molecules are randomly placed on both the surface of the sphere (nanoparticle) and the plane wall (cell membrane). In their paper they considered the binding of leukocytes to the vascular endothelium. However, some of the methods outlined below could prove useful. Receptor-ligand pairs are randomly tested for bond formation according to deviation length-dependent binding kinetics. A bond formation is thought of as a spring with fixed (with respect to the appropriate surface) endpoints. The force and torque exerted by a bond on the sphere and its probability of bond breakage are dependent on the length and orientation of the spring. Summing external forces and torques determines the translational and rotational velocities of a sphere under flow.

The kinetics of a single bond are described using Bell's model, specifically Equation 2.31, which relates the rate of dissociation with the applied force $F$. Now using the Boltzmann distribution of affinity (see [70]),

$$\frac{k^+}{k^-} = \frac{k_0^+}{k_0^-} \exp\left(\frac{-\sigma|\mathbf{x}_b - \lambda|^2}{2k_BT}\right), \tag{2.38}$$

where $\sigma$ is Hooke's Law spring constant, $|x_b - \lambda|$ is the deviation bond length and $k_0^+$ is the unstressed association rate (has not been experimentally measured), we find

$$k^+ = k_0^+ \exp(\sigma|\mathbf{x}_b - \lambda|(\gamma - \tfrac{1}{2}|\mathbf{x}_b - \lambda|)/k_BT).$$

A short-range repulsive force between the surfaces has the form

$$F_{\text{rep}} = F_0 \frac{\delta e^{-\delta\epsilon}}{1 - e^{-\delta\epsilon}},$$

where $1/\delta$ is the length scale (on the order of angstroms) and $\epsilon$ is the separation between the surfaces. The direction of this force is normal to the plane or in interactions between two particles, along the line which connects their centers. The roughness of the cell and the particle is assumed to be caused by 'bumps'; these bumps are dense enough to support the particle but spread out enough that

they do not substantially effect the flow of the objects. The adhesion or repulsion between these surfaces is assumed to take place between the tips of these bumps. Gravitational force is also added since most particles of interest are more dense than the liquid that they are in.

For small particles, the particle's inertia can be neglected and we need only look at the motion of the fluid which is given by the Stokes and continuity equations

$$-\nabla p + \mu \nabla^2 \mathbf{u} = 0, \qquad \nabla \cdot \mathbf{u} = 0.$$

where $p$ is the pressure, $\mathbf{u}$ is velocity and $\mu$ is the fluid viscosity.

So-called no-slip conditions are imposed at the cell surface:

$$\mathbf{u} = \mathbf{U}_\alpha + \omega_\alpha \times (\mathbf{x} - \mathbf{x}_\alpha), \qquad \mathbf{x} \in S_\alpha$$

where $\mathbf{U}_\alpha$ and $\omega_\alpha$ are the translational and rotational velocities of the particle $\alpha$, $\mathbf{x}_\alpha$ is its center of mass and $S_\alpha$ is its surface.

## 2.5 Summary

The classical tumour growth models along with the effects of chemotherapy form the simplest class of tumour-treatment models. The addition of angiogenesis as an effect on the tumour carrying capacity improved the validity of non-spatial models. In Chapter 3 an extension of this model was considered that includes both chemotherapy agents and antiangiogenic agents. These ODE models have the distinct advantage of intuitive and computational simplicity while those that include spatial effects have more detailed and accurate heterogeneities.

The many spatial models of angiogenesis presented here represent a very small fraction of those that exist in the literature but serve as a brief survey of important classes of models. Along with angiogenic factor concentrations, it is believed that a continuous formulation for endothelial cell density can be useful in tumour growth models and will be used to predict treatment outcomes in Chapter 4.

Incorporating the effects of convection and interstitial fluid pressure on the extravasation of molecules from blood vessels will make the prediction of drug distribution through a tumour more accurate. This model will be further developed in the future and is outlined in Chapter 5. New work that incorporates convection of angiogenic factors and its effect on the overall angiogenic activity of the tumour will also be shown.

The necessary groundwork has been laid out to consider a model of the binding of drug delivery vehicles to the cancer cell membrane and will be considered in future models. Along with these considerations, it is believed that the future of angiogenesis models lies in including the specific structure of tumour blood vessel networks in order to consider the precise flow and perfusion in these vessels. A novel algorithm for generating these blood vessel networks will also briefly presented in future work. Depending on the application, many of these existing tumour growth and angiogenesis models will continue to be relevant to mathematical oncologists. The development of mathematical oncology will continue to provide insight and understanding into the biological processes of cancer and the outcomes of various treatments.

# Chapter 3

# Cancer Modelling with ODEs

A general ODE model for tumour growth and chemotherapy will be coupled with the Hahnfeldt model for incorporating a vasculature-dependent carrying capacity and antiangiogenic treatments. Various treatment scenarios and parameters are evaluated and discussed.

## 3.1 Tumour Growth and Chemotherapy

Letting $n(t)$ denote the mass of cancer cells present in a tumour at time $t$, it is assumed that tumour growth is governed by the differential equation

$$\frac{dn}{dt} = f(n) - g(n,t), \qquad n(t_0) = n_0 (> 0) \tag{3.1}$$

where the function $f$ describes the growth rate of the tumour and $g$ describes the negative effect of the drug on the tumour size. We use a simple case for the chemotherapy effect given by log-kill:

$$g(n,t) = A_n c(t) n,$$

where $A_n > 0$ is the strength of the chemotherapeutic agent being administered and $c$ is the temporal profile of the drug concentration.

First, the tumour growth function $f$ is taken to be logistic as in equation (2.2). Now, solving the equation

$$\frac{dn}{dt} = rn\left(1 - \frac{n}{n_\infty}\right) - A_n c(t) n$$

gives the solution

$$n(t) = \frac{n_0 n_\infty \exp(rt - A_n \int_0^t c(s)ds)}{n_\infty + r n_0 \int_0^t \exp(rq - A_n \int_0^q c(s)ds)dq}. \tag{3.2}$$

Tumour eradication occurs when the average chemotherapy-induced death rate is larger than the proliferation rate. That is, $\lim_{t\to\infty} n(t) = 0$ when the condition

$$\frac{A_n}{T}\int_0^T c(t)\,dt > r$$

is satisfied. Assuming only that the function $c$ is piecewise continuous, this function has been taken to be many different forms in various scenarios. In some applications $c$ has been taken to be a periodic function, a constant value or in our case the sum of exponentially decaying functions; this will be described shortly.

If the model is complicated slightly by taking tumour growth to be generalized logistic, the expected curve for $n$,

$$n(t) = \frac{n_0 n_\infty \exp(\frac{rt}{\nu} - A_n \int_0^t c(s)ds)}{(n_\infty^\nu + r n_0^\nu \int_0^t \exp(rq - \nu A_n \int_0^q c(s)ds)dq)^{1/\nu}}$$

is found. A similar condition for tumour eradication can be easily observed to be

$$\frac{A_n}{T}\int_0^T c(t)\,dt > \frac{r}{\nu}.$$

The final scenario considered is tumour growth in the Gompertz regime. This leads to the following solution:

$$n(t) = n_\infty \exp\left[e^{-rt}\left(\ln\frac{n_0}{n_\infty} - A_n\int_0^t c(s)e^{rs}ds\right)\right].$$

Without knowledge of the analysis to follow, it should be noted now that with log-kill chemotherapy, the quantity $\int_0^t c(s)ds$ occurs in the solution for generalized logistic tumour growth while $\int_0^t c(s)e^{rs}ds$ appears in the solution for Gompertz. This will be important later, since for treatment comparisons a positive normalization constant $C$ is chosen so that $\int_0^{t_f} c(s)ds = C$ where $t_f$ is the final time considered for the simulations, so that fair treatment comparisons are made.

| Parameter | Value | Units |
|---|---|---|
| $r$ | 1 | $\text{day}^{-1}$ |
| $b$ | 0.25 | $\text{day}^{-1}$ |
| $d$ | $3.63 \times 10^{-4}$ | $\text{day}^{-1}\text{mm}^{-2}$ |
| $k$ | 0.001 | $\text{day}^{-1}$ |

Table 3.1: Parameters for the biological model based on those from [36].

## 3.2 The Effect of Angiogenesis

While tumour growth was originally taken to be Gompertz growth in [36], we will heed the advice given in [38] on the grounds of cell doubling time and assume the tumour growth to be logistic, thus,

$$\frac{dn}{dt} = rn\left(1 - \frac{n}{m(t)}\right) - A_n c(t) n. \tag{3.3}$$

It is important to note that while the form of the above equation is 'logistic', tumour growth is now highly dependent on the dynamics of tumour angiogenesis and is bounded only by the vasculature support present at the time. If the endothelial cells were to proliferate exponentially, then the tumour would similarly exhibit this type of growth. However, this situation will not arise, since the original equation suggested in [36] is used where $d > 0$, ensuring that the tumour size will saturate:

$$\frac{dm}{dt} = bn - dmn^{2/3} - km - A_m m a(t). \tag{3.4}$$

The suggested replacement of $n$ with $m$ in the growth term [37] (or any other alterations [38]) is not performed since the effect of chemotherapy would be proangiogenic due to the fact that tumour cell density would be present only in the angiogenic inhibition term.

For our treatment simulations, the parameters in Table 3.2 are used. A schematic of the biological model with treatments included as defined by (3.3) and (3.4) is given in Figure 3.1. While growth factor concentrations are not explicitly modelled, their contribution comes as the inhibitory and stimulatory terms in the ODE for

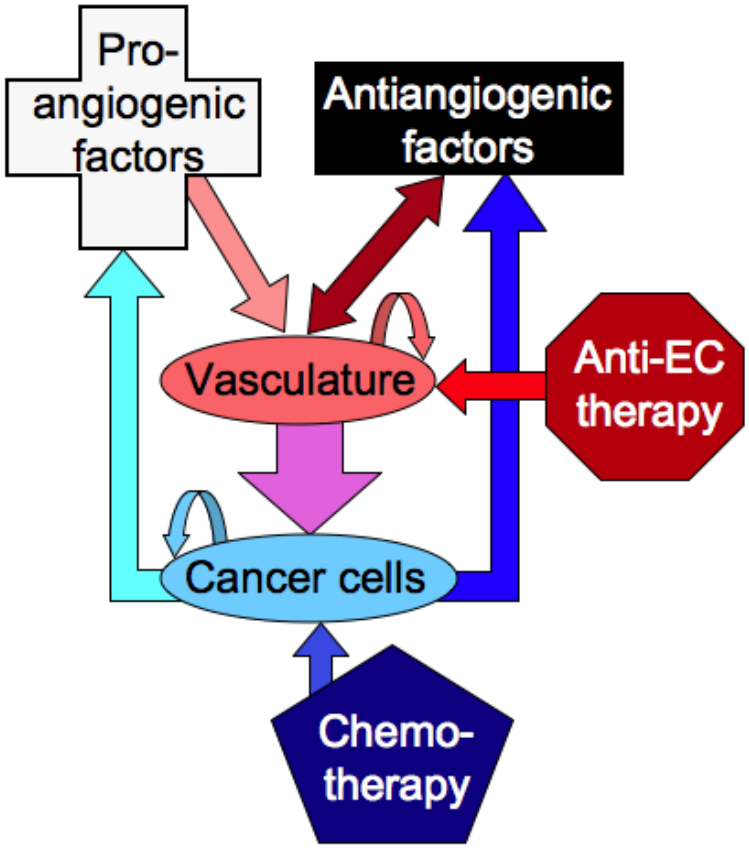


Figure 3.1: Schematic diagram of the ODE model showing interactions between the model variables and treatments.

the carrying capacity. The thickest arrow pointing from vasculature to tumour cells represents the primary interaction in the model.

## 3.3 Drug Dosages

The equations used for drug delivery equations will be outlined here and applied to describe the concentrations of chemotherapy and antiangiogenic agents in and around the tumour.

### 3.3.1 Free Agents

To describe the release of drugs not encapsulated in a delivery vehicle (or assuming that one does not exist), a purely exponential release is typically used. That is, for a single drug administration at time $t = t_i$ the dosage contribution is given by

$$c_i(t) = H(t - t_i)e^{-(t-t_i)/\tau}, \tag{3.5}$$

where $H(t)$ denotes the Heaviside function defined by

$$H(t) = \begin{cases} 0 & t < 0, \\ 1 & t \geq 0, \end{cases}$$

and $\tau$ is the time constant of the exponential decay process of the drug. This $\tau$ is related to the commonly measured values of decay rate $\lambda$ and drug half-life $t_{1/2}$ by the equations

$$\tau = \frac{1}{\lambda} = \frac{t_{1/2}}{\ln(2)}.$$

The main drawback to the exponential decay model is that $c_i(t)$ achieves its maximum at $t = t_i$, the time of administration. More realistically, this maximum is not reached until some later time $t > t_i$. This is usually due to two factors, the first being that it takes some time for the drug to circulate through the bloodstream and end up in the tumour vicinity. The second is that if the drug is in a delivery vehicle, it does not release its load of drug immediately and typically takes some time to erode. It should be noted that the amount of drug administered and the amount that enters the tumour depends on many factors including the immune system avoidance and tumour targeting of the delivery vehicle along with the tumour vasculature network (specifically the extent of perfusion and fenestration). If we wanted to capture these phenomena in a simple way and move the maximum of the drug release equation to some time later than immediately after administration, the purely exponential equation could be modified by multiplying by a factor of $(t - t_i)^p$ where $p \geq 0$ giving

$$c_i(t) = H(t - t_i)(t - t_i)^p e^{-(t-t_i)/\tau}, \tag{3.6}$$

where clearly now $c_i(t_i) = 0$ and $p = 0$ gives the usual exponential decay case. This shifts the maximum from $t = t_i$ to $t = \tau p$, allowing us to choose $p$ based on this criteria assuming knowledge of when this maximum occurs and a measurement of $\tau$ (or $\lambda$ or $t_{1/2}$). To describe the drug dosage on a treatment schedule where treatments are administered at times $(t_1, t_2, \ldots, t_N)$, we use the equation

$$c(t) = \frac{1}{C}\sum_{i=1}^{N} c_i(t) = \frac{1}{C}\sum_{i=1}^{N} H(t-t_i)(t-t_i)^p e^{-(t-t_i)/\tau}, \tag{3.7}$$

where $C$ is an appropriately chosen constant that will discussed later.

It is assumed that the antiangiogenic agent concentration $a(t)$ has the same form as (3.7) with altered constants ($\tau$,$N$,$C$,$p$) and schedule ($t_i$) having a subscript $a$ (and now denote the constants for cytotoxic drugs with a subscript $c$).

### 3.3.2 Dosage Normalization

Considering the tumour size at some time $t_f$ of interest, after the treatment schedule has finished, we wish to compare the tumour response to that of other schedules.

In order to compare the effectiveness of different treatment schedules of combined antiangiogenic and cytotoxic therapies, the dosages involved with the different treatment techniques are normalized by setting the integrals of the different dosages to some appropriate constant. Assuming treatment starts at $t_0 = 0$, we will require the entire treatment regime to take place over a period of $t_f (> t_N)$ days (or other time unit) and hence we impose

$$\frac{1}{C_c^{(1)}}\int_0^{t_f} c^{(1)}(t)\,dt = \cdots = \frac{1}{C_c^{(k)}}\int_0^{t_f} c^{(k)}(t)\,dt = I_c,$$

and

$$\frac{1}{C_a^{(1)}}\int_0^{t_f} a^{(1)}(t)\,dt = \cdots = \frac{1}{C_a^{(k)}}\int_0^{t_f} a^{(k)}(t)\,dt = I_a,$$

where $\{c^{(1)}, a^{(1)}\}, \ldots, \{c^{(k)}, a^{(k)}\}$ are the $k$ different treatment regimes that we will consider. Typically we will set $I_c = I_a = 1$ since we independently control the strength of the drug by the log-kill parameters $A_c$ and $A_m$. This allows us to simply take $C$ equal to the dosage integral.

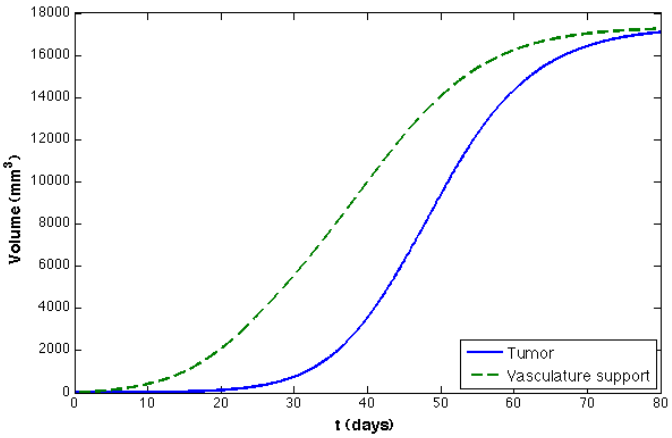


Figure 3.2: Control case of the ODE model based on the model by Hahnfeldt et al. [36].

If the dosage is of the form given in equation (3.5) and $t_i = iT$ (and $t_f = (N+1)T$) where $T$ is the constant time between treatments, then by taking

$$C = \tau \left( N + \frac{1 - \exp(-NT/\tau)}{1 - \exp(T/\tau)} \right)^{-1},$$

we achieve normalization. However, for a more complicated form, such as the one given in (3.6), we would simply need to approximate the dosage integrals with a numerical integration scheme and take

$$C_c \approx \int_0^{t_f} c(t)\, dt, \qquad C_a \approx \int_0^{t_f} a(t)\, dt.$$

## 3.4 Model Simulations

The control case using initial conditions of $n_0 = m_0 = 3\text{mm}^3$, represents a primitive tumour preparing to throw the angiogenic switch and recruit its own blood supply. While $m_0 > 0$, initially there is no vasculature present, this is simply representing that there is adequate resources to maintain the tumour's current size. At this point it will now have to rely on more than the diffusion of oxygen. For the control case (see Figure 3.2), it is observed that just before day 33, the tumour reaches

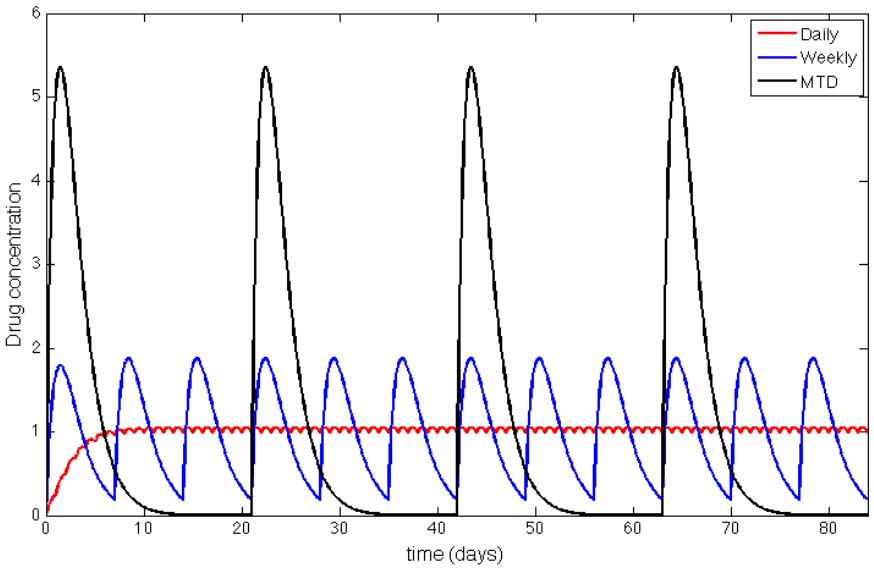


Figure 3.3: Comparison of normalized dosages (normalization constant $C = t_f$ so that average dosage is 1) for 12-week schedules with drug half-life of 1 day and a delay constant of $p = 1$.

a size of $1\text{cm}^3$ and it is at this point in time that we assume that the tumour is detected in the patient and (while unrealistic in most cases) when treatment begins. It should be noted that the growth dynamics are fast, reaching its maximum size in less than 3 months, and assumedly leading to death in around 2 months, this would be considered an extremely aggressive tumour.

### 3.4.1 MTD vs. Metronomic Therapy

These treatment scheduling regimes are two different methodologies employed widely by oncologists depending on the type of cancer, whether the cancer has metastasized along with other factors. There is a spectrum of treatment strategies in between these two depending on the frequency and size of the individual doses. Using equation (3.7) for these schedules, the difference between giving frequent administrations and giving the MTD is shown in Figure 3.3.

In Figure 3.4, the results of the three chemotherapy schedules are shown. The MTD scheme shows the typically observed initial cell-kill success of the treatment, followed by the rapid regeneration of the tumour between administrations. The enforced delay between successive treatments allows the body to recover, specifically the damage done to normal cells, but unfortunately this also gives the tumour a chance to proliferate uncontrollably after the initial anti-tumoural effects of the drug wear off. With each large dosage a significant portion of the tumour cells are killed but due to the breaks the population always recovers. It should be noted that we have also assumed that there is no chemo-resistance, whereby certain tumour subpopulations are immune to the treatment or the tumour develops a resistance to specific agents as the treatment progresses meaning these results are mostly likely a best-case scenario. As this MTD schedule progresses, the tumour growth between treatments is such that critical life-threatening tumour sizes are still reached which could lead to patient death mid-schedule. In addition to the negative outcome, this treatment regime is also associated with increased severity of side effects.

The tumour growth pattern exhibited by metronomic schedules with weekly and daily administrations exhibit similar behaviour with the weekly treatments showing less tumour size variation than the MTD schedule but still fluctuating more than the consistent daily schedule. Using these therapies eradication is not achieved, but the tumour size is controlled within a fixed nonlethal range for an extended period of time. Simply controlling the cancer is a valid strategy in some cancer cases but it still leaves the door open for metastases to form in other parts of the body. It should be noted that these simulations are slightly biased toward a favourable outcome of the MTD schedule since the dosage integrals are normalized, ignoring the fact that these metronomic schedules could in practice use slightly larger individual dosages without encountering the severe side effects of the MTD.

Indeed, while employing the MTD is most likely not beneficial for outcome, it remains very likely that at some time a high dose would be the optimal strategy. Since the dosages are assumed to be equal with constant-sized breaks between these

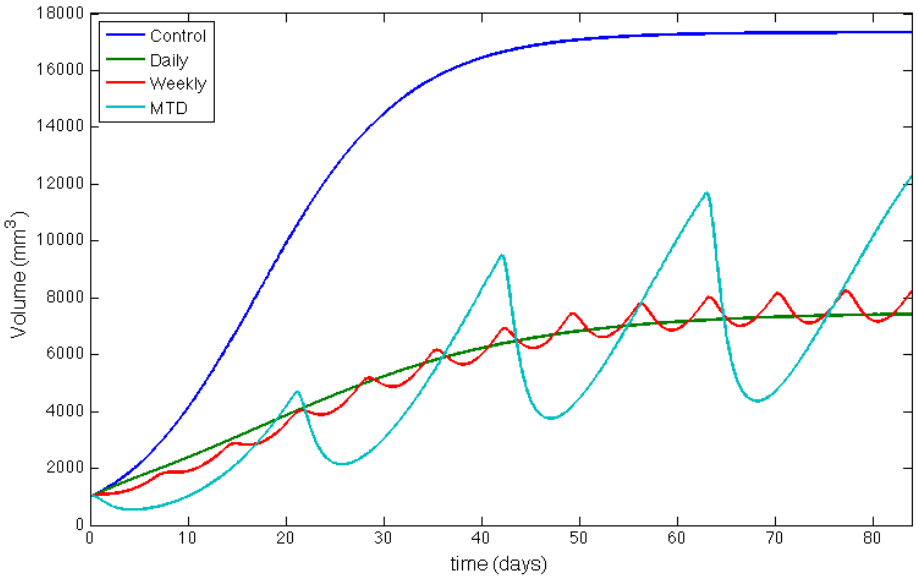


Figure 3.4: Tumour volume subject to the drug schedules depicted in Figure 3.3. For these simulations the chemotherapy log-kill $A_n = 0.08$.

dosages, the upside of a strategic MTD is not encountered in this model. With these schedule-limiting assumptions, the optimal schedule will continue to lay somewhere closer to constant continuous treatment rather than the MTD.

### 3.4.2 Drug Release

We will now look at the effect of altering $\tau$ in our dosage equations (Figure 3.5). For these simulations it should be noted that for longer release times, less of the drug is actually administered since it will stay in the tumour or circulate in the blood for longer periods of time. This is due to dosage normalization even though the dosage schedules will be identical.

These results align with our intuition that a longer circulating agent will yield better results. However, we must remember that the drugs that decay faster are administered in larger doses. Thus, it remains surprising that even after dosage normalization, this model predicts that quickly cleared agents will be less effective

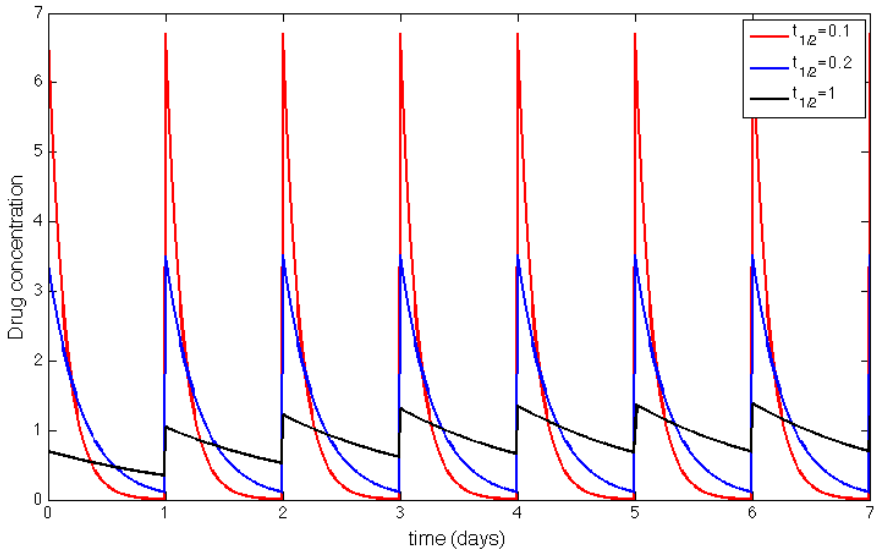


Figure 3.5: Daily administration schedule normalized over 84 days but only one week shown to display the effect of modifying the release profile.

than those with staying power; see Figure 3.6.

### 3.4.3 Combination Therapy

Of the greatest relevance to potential applicability in clinical settings is the effective modelling of treatments that include more than one form of therapy, specifically those that combine chemotherapy agents with antiangiogenic agents. Since the effects of both of these agents are incorporated into the model, any given combination schedule can be evaluated. Combining these therapies has been widely touted in the literature as superior to either on their own. Whether the result of increased chemotherapy toxicity due to tumour vasculature normalization or (as in the model) by the deprivation of nutrients due to antiangiogenic agents, the tumour response has been shown to be significant in clinical settings.

Now considering Figure 3.7, using a daily schedule of chemotherapy alone, the tumour size is suppressed to approximately 40% of the size of the control case. While not eradicated this tumour is controlled at a specific level. The angiogenic-

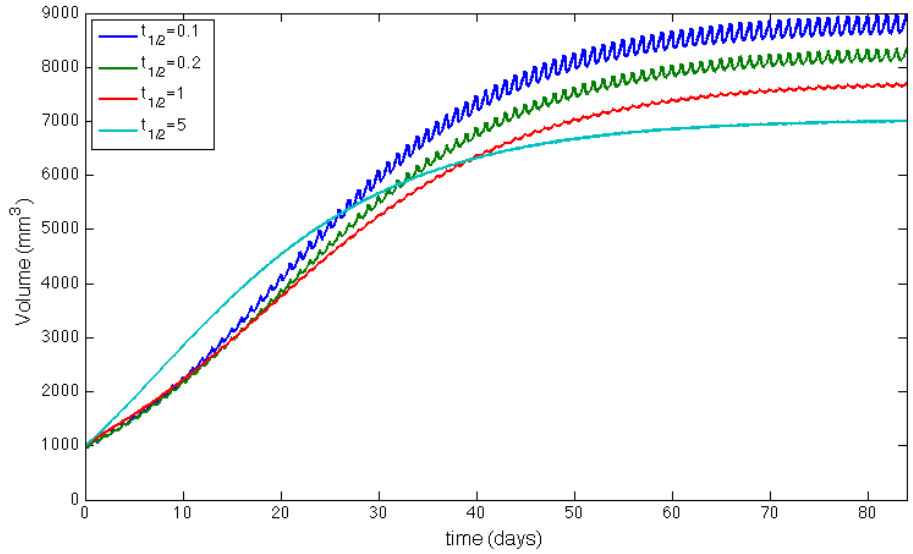


Figure 3.6: Even though the dosages have been normalized, a longer release results in a smaller tumour.

based carrying capacity has also decreased but in this case by only 25%. This is a result of the lack of proangiogenic factors being produced by the smaller tumour. In reality chemotherapeutic agents that act predominantly against rapidly dividing cells would also kill a substantial amount of cells that comprise the tumour vasculature. While this is not explicitly addressed in the model, it is evident that metronomic chemotherapy regimes do have antiangiogenic effects (as suggested in [15]).

For an antiangiogenic agent acting alone, the effect is assumed to be against the carrying capacity of the tumour since the specific mechanism that is targeted (endothelial cells , angiogenic factors, etc.) is not included in this ODE model. The antiangiogenic agents still reduce the carrying capacity, by the same amount as the chemotherapy agent did, but since the tumour cells are not directly targeted, the tumour is still able to grow all the way to this reduced carrying capacity instead of being forced to an even lower value.

When the combination of these two therapies are administered, the above effects

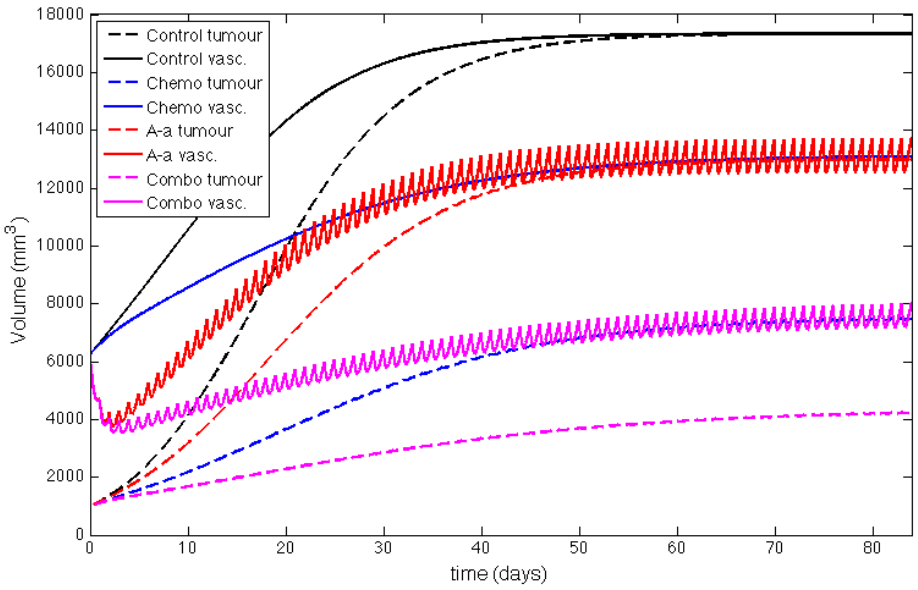


Figure 3.7: Improved tumour response to combination therapy due to cytotoxic and antiangiogenic agents working in tandem.

compound to be extremely effective. The tumour size is suppressed by chemotherapy while antiangiogenic agents force down the carrying capacity, resulting in the tumour being reduced to less than 25% of the control tumour volume. As in the previous cases, the tumour is not eradicated and if therapy were stopped, the model would still predict a rapid increase to the carrying capacity. However, if treatment continued to be administered the tumour would be controlled at a size that is theoretically nonlethal. However, there is still a chance that the primary tumour could metastasize to a different region of the body.

It may be obvious that both agents working together will work more effectively than either on its own, however the question of optimal scheduling and dosage remains. While this has been treated as an optimal control problem, our attention will be turned to including spacial inhomogeneity into the model before detailed analysis is resumed.

## 3.5 Model Evaluation

In Equation (2.7), the assumptions on the production of angiogenic factors will lead to inaccuracies since these factors are produced at some constant rate outside the tumour, while inside the tumour this production rate depends on a number of factors, most importantly the tumour size and local levels of hypoxia.

The inaccuracy that arises from the assumption of radial symmetry is made in practically all ODE models, in order to make the model non-spatial. While this assumption could be viewed as some sort of average or homogenization of the tumour, angiogenic signalling and tumour growth are generally highly heterogeneous processes. In the early stages of tumour growth, they can be observed to form spheroids, but once angiogenesis begins tumours form highly irregular shapes based on the local oxygen and nutrient supply along with spatial constraints and surrounding host tissue type. Hypoxic regions within a tumour are also characterized by temporal and spatial irregularity. Due to these concerns, we will turn to spatial models in order to capture the more complex interactions that occur in the growth of cancer cell populations.

# Chapter 4

# Cancer Modelling with PDEs

To facilitate the incorporation of the spatial heterogeneities present in tumours, a two-dimensional PDE model that does not assume radial symmetry will be considered. Proangiogenic and antiangiogenic factor equations will be linked to tumour growth, while their imbalances will be included in the equation for vasculature development. The presence of vasculature will then be assumed to positively influence tumour cell proliferation. Extensions to this model will be considered and the results of treatment schedules will be given.

## 4.1 Angiogenic Factors

The production of angiogenic factors is modelled using an equation similar to (2.10). Instead of assuming that the production, degradation and diffusion parameters are different outside and inside the tumour, a term is added that corresponds to the upregulation of these factors which is dependent on the tumour cell density $n$ (due to this the superscript $e$ indicating the environment is discarded). A phenomenological term is also added to capture the observation that these factors are typically pushed out of the tumour. While this is due primarily to outward convection as a result of high interstitial fluid pressure inside the tumour, pressure will be omitted in this simple model. In the next chapter effects of including pressure will be considered,

but for now it is assumed that these angiogenic factors slide along the tumour cell density gradient toward the periphery. The equation for these factors is given by

$$\frac{\partial f_j}{\partial t} = D_j \nabla^2 f_j - k_j f_j + g_j + \beta_j n + \gamma_j \nabla \cdot (f_j \nabla n), \tag{4.1}$$

where $j = a, p$ (antiangiogenic, proangiogenic). The constant production rates $g_i$ are typically taken to be the rates in normal tissue. However, locally around the tumour, many normal cells have also upregulated their production due to stimuli from the tumour cells. Due to this phenomena, the base production rates will be taken to be slightly higher than that of host tissue to account for this.

The balance between these factors, represented by $\alpha_{\mathrm{GF}} = f_p/f_a - 1$ is taken to be an indicator of angiogenesis stimulation as in [39]. Negative values indicate antiangiogenic activity, most likely induced by antiangiogenic agents while positive values indicate tumour angiogenesis, the formation of new vasculature due to angiogenic factor imbalance.

## 4.2 Angiogenesis

The endothelial cell density will now be dependent on growth factor balance $\alpha_{\mathrm{GF}}$ via a PDE instead of the previously formulated dependence given in the empirical formula (2.13). To model the vascularization of our tumour the equation (2.18) is used but to this the contribution of the growth factor balance $\alpha_{\mathrm{GF}}$ is added giving

$$\frac{\partial m}{\partial t} = D_m \nabla^2 m + m(-1 + 3m - 2m^2) + \alpha_m m \alpha_{\mathrm{GF}}.$$

The growth factors will have the desired effect of increasing the upper fixed point when $\alpha_{\mathrm{GF}} > 0$ or pushing it down when $\alpha_{\mathrm{GF}} < 0$.

In essence, an additional step has been inserted into our modelling instead of the tumour cells and endothelial cells directly influencing each other, they interact through the action of proangiogenic and antiangiogenic factors. It must be kept in mind that while this is an improvement, it still does not model specific

factor concentrations. It simply categorizes them into these two broad categories of proangiogenic and antiangiogenic factors. However, many molecules do act in both of these roles concurrently or depending on the microenvironment (or do so indirectly), so these factor concentrations must only be considered as a means of measuring heterogeneous angiogenic activity.

## 4.3 Tumour Growth

Incorporating spatial effects into the tumour equation (3.1) was performed in [45]. Regular logistic growth is retained and can be interpreted as the maximum cell density attainable before the angiogenic switch is thrown. The effect of increased proliferation of tumour cells near nutrient-providing blood vessels is added, replacing the previous assumption of the vasculature increasing the tumour carrying capacity. Tumour growth is coupled to tumour vasculature by assuming they are positively and linearly related with coefficient $\alpha_n > 0$. The invasive random walks of individual tumour cells are approximated by assuming that the tumour cells diffuse with diffusion coefficient $D_n$. The PDE for tumour vasculature will be presented shortly, for now note that the vasculature distribution is denoted by $m$. This gives the following equation for tumour growth

$$\frac{\partial n}{\partial t} = D_n \nabla^2 n + rn\left(1 - \frac{n}{n_\infty}\right) + \alpha_n m(x,t) n. \tag{4.2}$$

It should be noted that in the presence of vasculature, there is exponential tumour growth present in that area. While most likely this growth would eventually reach a maximum possible value, the exponential growth is justified since times of interest to treat the tumour occur while it is experiencing this growth rather than after it reaches the carrying capacity since the patient will most likely not live until the point when the tumour approaches the carrying capacity.

## 4.4 Directed Cell Movements

Not considered in detail in this model, but a potentially important further consideration is the directed cell movements in response to stimuli in their environment. In [45] these movements were modelled using a term similar to one used in the equation for growth factor concentrations to move out of the tumour. The following terms were added to the equations indicated:

$$\left.\frac{\partial n}{\partial t}\right|_{\text{DCM}} = \gamma_n \nabla \cdot (n \nabla m(x,t)),$$
$$\left.\frac{\partial m}{\partial t}\right|_{\text{DCM}} = \gamma_m \nabla \cdot (m \nabla n(x,t)),$$

where the vertical line with subscript indicates the directed cell movements (DCM) contribution to their respective PDEs. With the addition of angiogenic factors to the model, these cell movements can be in reaction to their stimuli instead of the more general observation that endothelial cells and tumour cells tend to move toward each other. Instead, endothelial cells could move toward areas of high angiogenic activity ($\alpha_{\text{GF}} > 0$) and tumour cells (assuming the omission of oxygen or nutrient profile from the model) would remain attracted to areas of increased vascularization. This would result in an altered term in the PDE for blood vessel distribution given by,

$$\left.\frac{\partial m}{\partial t}\right|_{\text{dcm}} = \beta_m \nabla (m \cdot \nabla \alpha_{\text{GF}}(x,t)).$$

These directed cell movements are an interaction term that could be considered as a measure of tissue invasion capabilities in the case of tumour cells or as a measure of the speed of angiogenesis in the case of endothelial cells. For the sake of simplicity, we do not include thes terms in the model to follow.

## 4.5 Drug Distributions

Treatment dosages will be briefly outlined and are similar to the equations used in the previous chapter. However, we now add spatial effects on the drug distribution.

### 4.5.1 Dosages

Let us consider a drug treatment consisting of $N$ administrations of a specific drug. Denoting the amount of the drug administered to the patient by the $i$th treatment at time $t_i$ by $d_i(t)$, $i = 0, \ldots, N$, then the amount of drug entering the patient's tumour at time $t$, would be given by the dosage rate function

$$\Gamma(t) = \frac{1}{C} \sum_{i=0}^{N} H(t - t_i) d_i(t), \tag{4.3}$$

where $C > 0$ is the appropriately chosen normalization constant. The normalization procedure for the temporal release function is identical to that given in Section 3.3.2. The simplest form for $d_i(t)$ would assume that the drug delivery is purely exponential and hence

$$d_i(t) = e^{-(t-t_i)/\tau}, \tag{4.4}$$

where $\tau$ is the rate of decay of drug delivery. A more accurate form to consider for this function as mentioned before would be

$$d_i(t) = (t - t_i)^p e^{-(t-t_i)/\tau}, \tag{4.5}$$

where the maximal delivery occurs at a time later than administration.

### 4.5.2 Free Agents

Along with the temporal delivery functions, the spatially dependent framework allows for the addition of other processes that effect the distribution of chemotherapy and antiangiogenic therapy concentrations. The first obvious inclusion is the simple diffusion of these agents. A term including the temporal delivery and another with the natural decay of the agent are added. Another important determinant of drug release is drug reabsorption by nearby blood vessels. This is modelled by a usual uptake term with coefficient $\mu_c$. This gives the equation

$$\frac{\partial c}{\partial t} = D_c \nabla^2 c + \lambda_c \Gamma_c(t) m \exp\left( - \left( \frac{m}{m_{\lim}} \right)^2 \right) - k_c c - \mu_c c m,$$

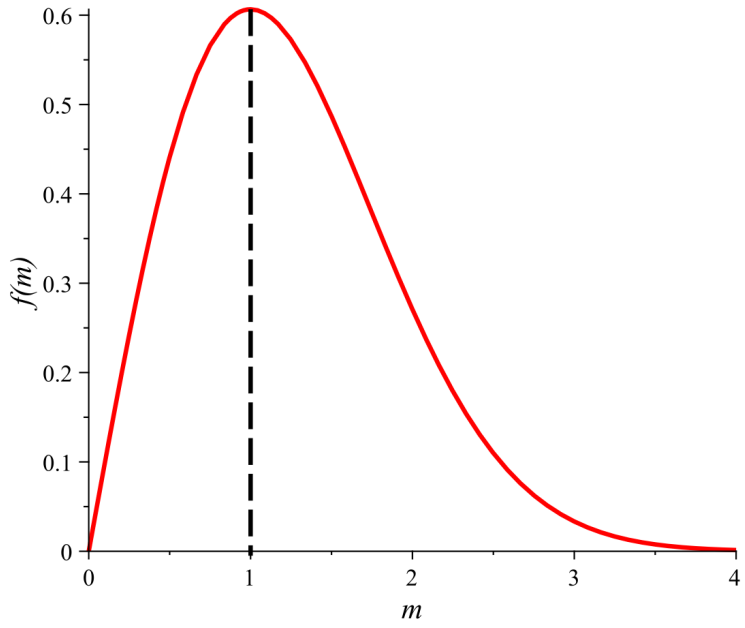


Figure 4.1: The efficiency of drug delivery as a function of vascular density.

where the term $f(m) = m\exp(-(m/m_{\text{lim}})^2)$ plays the role of delivery efficiency. This function has the form shown in Figure 4.1 with a maximum occurring at $m = 1$ corresponding to normal vasculature. For values of $m > 1$, this corresponds to tumour vasculature and leads to decreased delivery efficiency of the drug. This decreased delivery efficiency is predominantly due to a lack of perfusion of tumour blood vessels and inconsistent flow along with the other characteristics of tumour vasculature such as elevated IFP. Similarly for $m < 1$ representing immature or degrading vessels, less drug is delivered in this situation as well.

### 4.5.3 Delivery Vehicles

For delivery vehicles, we will consider their size to be such that their diffusion and reabsorption are negligible and take

$$\frac{\partial S_i}{\partial t} = \lambda_s d_i(t) m \exp\left(-\left(\frac{m}{m_{\text{lim}}}\right)^2\right) - k_s S_i, \qquad i = 1, \ldots, N,$$

where $d_i$ has the form of (4.4). The release of the free agents would be modified (for example the chemotherapy dosage) so that their evolution is given by

$$\frac{\partial c}{\partial t} = D_c \nabla^2 c + \lambda_c \Gamma_c(t) - k_c c - \mu_c c m,$$

where now

$$\Gamma_c(t) = \frac{1}{C} \sum_{i=0}^{N} c_i(t) S_i,$$

and $c_i$ has the form of (4.5).

Note that while only the equations for chemotherapy concentration $c$ has been given, similar equations are employed for anti-endothelial cell treatments $a_m$ and proangiogenic factor inhibitors $a_f$. Typically when considering nanocell treatments, the value of $p$ in (4.5) for the antiangiogenic treatment is smaller than that for chemotherapy indicating it is released faster than chemotherapy.

The effect of different forms of therapy are incorporated by adding a treatment term to the appropriate equations. For example, in (4.2) the term would have the form: $-A_c n c(x,t)$. Other treatment terms could be added to the PDEs describing proangiogenic factor concentration for antiangiogenic treatments which block or inactivate these factors and endothelial cell density for drugs which attack endothelial cells. Complicated combination therapies could then be tested using the full set of equations. Also the effects of nanocells which carry more than one type of drug could be studied. A schematic of the primary interactions in the full PDE model is given in Figure 4.2; note that arrows connecting vasculature to the antiangiogenic treatments are omitted along with the arrow from cancer cells to antiangiogenic factors since this production is relatively small.

## 4.6 Model Simulation

The initial condition for cancer cell density will be a Gaussian distribution centered at (0,0) representing a tumour about to transition out of a diffusion-limited pseudo-steady state. While the tumour is considered to be in a pseudo steady-state while

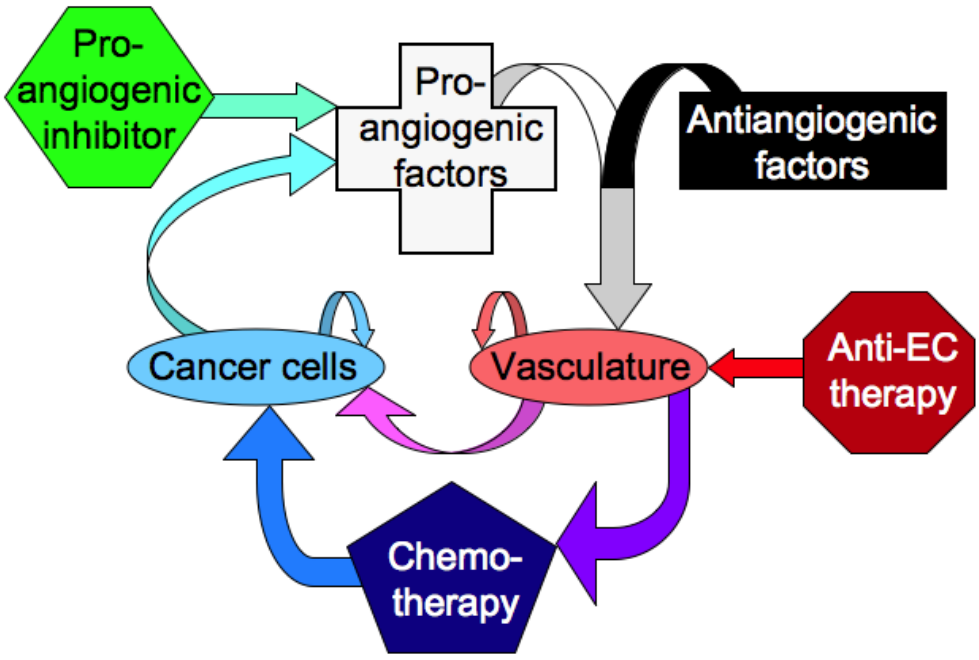


Figure 4.2: Schematic of the biological interactions and treatments of the PDE model. Notice the balance between the factors and the various treatment mechanisms.

the tumour is small, this assumption must be discarded at later times. Hence, the equations (2.10) are used to evolve the pro- and antiangiogenic factor concentrations through time. These concentrations will have an initial condition of a constant value corresponding to their concentration in the hose tissue.

For the endothelial cell density some random initial condition is set and then evolved through time for some pre-determined amount of time until a steady state is reached. These non-symmetric and random initial conditions will lead to heterogeneous tumours. However, even though the assumption of radial symmetry is not used, symmetric initial conditions for tumour and endothelial cell density along with antiangiogenic and proangiogenic factors will lead to strictly symmetric tumour growth.

### 4.6.1 Parameters

Tumour growth:

| Parameter | Value | Source |
|---|---|---|
| $D_n$ | 0.035 mm$^2$/day | [45] |
| $r$ | 0.16/day | [45] |
| $n_\infty$ | $2 \times 10^6$ cells/mm$^2$ | [45] |
| $\alpha_n$ | 0.1-0.3 cells/mm$^2$/day | this work |

Table 4.1: Dimensional parameters for the tumour growth equation.

The parameters in this table were primarily given in [45] and based on experimental data for glioma from [71].

Angiogenesis:

| Parameter | Value | Source |
|---|---|---|
| $D_m$ | 0.005 | [45] |
| $\alpha$ | -1 | [45] |
| $\beta$ | 3 | [45] |
| $\gamma$ | -2 | [45] |
| $\alpha_m$ | 0.5-1 | this work |

Table 4.2: Nondimensional parameters for the vasculature equation.

The nondimensional parameters for angiogenesis (see A.4) are also based on values from [45] with $\alpha$, $\beta$ and $\gamma$ being selected for specific fixed point behaviour. The range of reasonable values for the interaction term $\alpha_m$ is based on the speed of tumour growth/regression from areas of angiogenic activity/suppression.

Angiogenic factors:

These angiogenic factor parameters are predominantly from [39] and assumed due to a distinct lack of experimental data. The upregulation coefficient is based on approximated upregulation parameters from [39] as well. The convection parame-

| Parameter | Pro | Anti | Source |
|---|---|---|---|
| $D$ | 2 | 1.5 | [39] |
| $k$ | 1.3 | 1.5 | [39] |
| $g$ | 0.3 | 0.3 | [39] |
| $\beta$ | 0.15 | 0.01 | this work |
| $\gamma$ | 2.5-15 | 3.5-21 | this work |

Table 4.3: Nondimensional parameters for the angiogenic factor equations.

ters are assumed, the range representing the possible speeds at which the factors approach the tumour rim.

Treatment parameters depend not only on the form of treatment (chemotherapy, anti-endothelial or proangiogenic inhibitor) but also the specific agent that is being used. The relationship between diffusion coefficient and molecular size, shape, weight, etc. is not an exact science and is typically found from experiments. Degradation rate, reabsorption rate and treatment strength also vary from drug to drug. For example for a typical antibody, such as Immunoglobin G (IgG), a diffusion coeffcient of $D = 0.11\text{mm}^2/\text{day}$ is reasonable [60]. For antiangiogenic agents decay rates have been found to range from $\tau = 2.6/\text{day}$ for angiostatin to $\tau = 0.6/\text{day}$ for endostatin [36]. Due to a lack of experimentation on drug reabsorption rates of cancer treatments, we will uses values ranging from 1-10$\text{mg}/\text{mm}^2/\text{day}$.

It should be noted that the constants for tumour growth correspond to those in the full system of equations, whereas all simulations were performed using nondimensionalized equations (see A.4 for details) and the scaled parameters found in the other tables above.

## 4.7 Results

First, some qualitative results from the model will be shown displaying the effect on the biological system due to specific treatments. In Figure 4.3, the tumour is

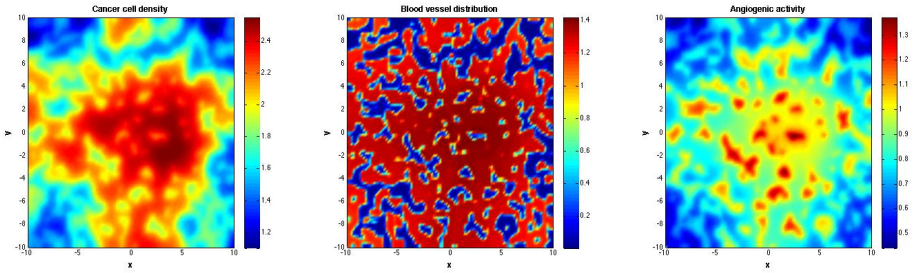


Figure 4.3: Control case for the PDE model.

shown after 3 months of unperturbed growth as well as the areas of vascularization and angiogenic activity. As can be seen, the tumour has invaded nearby tissues and displays typical invasive 'fingering' behaviour along with irregular density and shape. The vasculature shows higher than normal concentration in the tumour in a large area of vascularization along with areas that are non-vascularized (and presumedly hypoxic) shown in blue. The angiogenic imbalance is evident since the entire domain of consideration has a positive measure of angiogenic activity $\alpha_{\mathrm{GF}}$. Those areas directly outside of the tumour have the highest levels of angiogenic activity representing areas that will be vascularized next, leading to additional tumour growth around the tumour rim.

This control case will be contrasted with a couple of treatment possibilities. Applying a free agent proangiogenic inhibitor on a metronomic daily schedule will decrease the angiogenic activity throughout the tumour microenvironment, see Figure 4.4. The areas of highest angiogenic activity continue to reside in the tumour periphery but have decreased approximately twenty-fold. Regarding the vasculature, the vasculature structure is now seen to be somewhat normalized leading to improved chemotherapy delivery. Mathematically, this is achieved via the delivery efficiency term since values of $m$ closer to 1 leads to improved delivery of all agents. While these antiangiogenic agents do have an anti-tumoural effects, decreasing the tumour density significantly, the tumour can rarely be eradicated using this method alone.

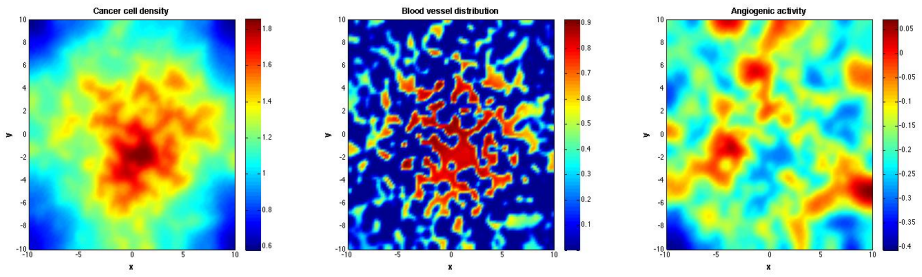


Figure 4.4: The effect of antiangiogenic treatment on the model.

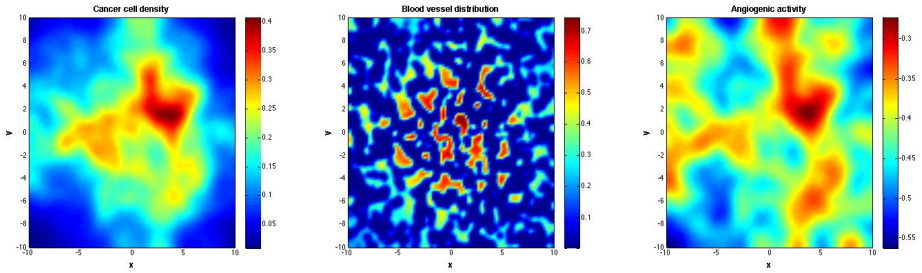


Figure 4.5: The effect of combination treatment on the model.

A diagram of chemotherapy alone is omitted since its temporal performance will be considered later but the combination of these agents will be considered (see Figure 4.5), utilizing the power of vascular normalization to apply a more potent chemotherapeutic payload. This improved performance leads to a significant reduction in tumour volume and controls its spatial spread, potentially blocking attempts at metastasis. In this case the vasculature is reduced to a further extent than antiangiogenic agents alone since the tumour reduction leads to decreased levels of angiogenic factor production and hence greater vessel regression. It can be seen that the temporal sequence of these combinations is very important since destroying too much of the tumour vasculature before applying sufficient chemotherapy would lead to suboptimal treatment outcome and unnecessary toxicity. This suggests that at some point in time the antiangiogenic agents should be stopped or the dosages tapered back.

Before taking a look at the temporal evolution of the tumour size, we will look

| Case | Percentage Vascular Area |
|---|---|
| Control | 29.2% |
| Chemotherapy | 21.0% |
| Anti-endothelial | 9.7% |
| Proangiogenic inhibitor | 13.5% |
| Combination (C+A-E) | 6.1% |
| Combination (C+P.I.) | 8.1% |

Table 4.4: Comparison of the effect of individual treatments and combination treatments of chemotherapy and antiangiogenic agents.

briefly at a measure of tumour vascularization that is commonly measured experimentally. The tumour area will be considered to be the area of the grid that has a tumour cell density above a (nondimensional) threshold of 0.2 which is assumed to correspond to the detectable boundary of a tumour. Within this area of the grid, we consider those parts of the tumour with $m > 0.5$ as vascularized. Using this methodology to calculate percentage vascular area, we can compare the vascular effect of various treatments and combination treatments. See Table 4.7 for a summary of these values after three weeks of daily administrations of drug. As expected, the compounded anti-vascualr effect of chemotherapy with anti-endothelial cell treatment provides the largest decrease in vascular area. With many of the anti-angiogenic treatments, this percentage would eventually decrease to 0 if the schedule was continued. This highlights the importance of the temporal scheduling of combinations to ensure that chemotherapy is applied before all vasculature is destroyed (preferably during the normalization window) and that anti-angiogenic treatments are halted before this occurs.

Figure 4.6 shows that chemotherapy remains the most effective single free agent, outperforming both forms of antiangiogenic therapies. These two therapies have very similar results with the proangiogenic inhibitor slightly outperforming the anti-endothelial cell treatment as time passes.

In Figure 4.7, a similar conclusion to one from the ODE model is reached. Specif-

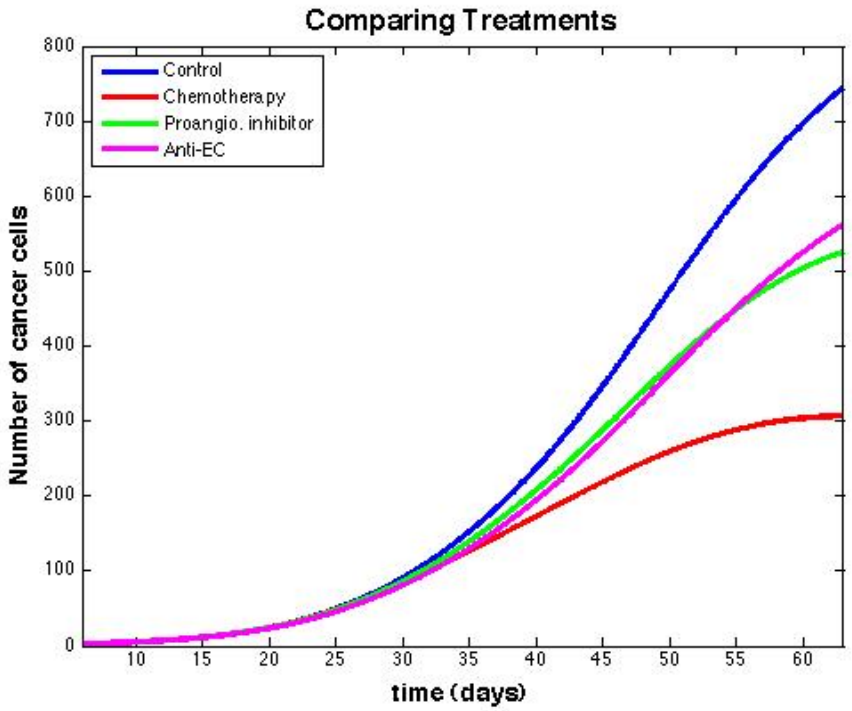


Figure 4.6: Free agent results.

ically the conclusion that suggests longer release vehicles improve treatment efficacy despite dosage normalization. However, in this case, the combinations considered include chemotherapy with one of two agents that target different antiangiogenic mechanisms. Once again, it is observed that the anti-endothelial cell agent has greater initial success followed by the proangiogenic inhibitor working better down the stretch. This is thought to be a result of the anti-endothelial cell killing initially returning the vasculature to a normalized state but during the course of treatment it destroys too much of the tumour vasculature leading to decreased chemotherapy being delivered to the tumour. In the case of proangiogenic inhibitors the normalization process happens indirectly through the action of angiogenic repression and does not destroy as much of the vasculature as those that directly target endothelial cells leading to prolonged tumour normalization.

Now considering a shorter time frame, rather than the 3 months schedules, we will see the effect of a high-dose administration of combination therapy given ev-

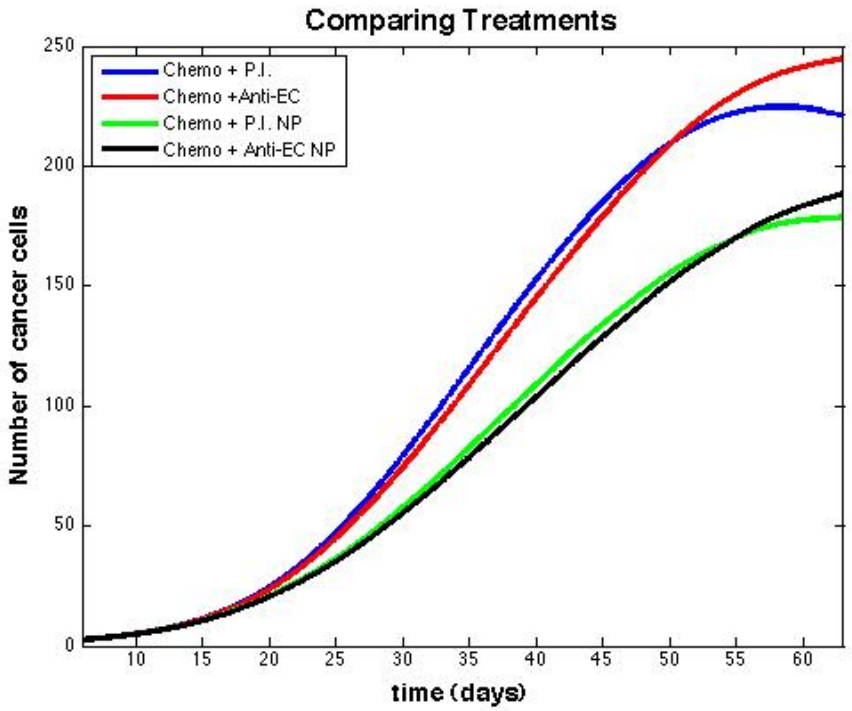


Figure 4.7: Combining chemotherapy and anti-angiogenic agents as free agents and in a nanoparticle.

ery other day over a 2 week period. In Figure 4.8, the results of a few treatment possibilities are shown. Since combination therapies are typically delivered with an initial antiangiogenic therapy, followed by a chemotherapy agent in order to facilitate normalization, we will first consider single agent administrations of both antiangiogenic forms in liposomal delivery vehicles (faster release) and chemotherapy in a polymer nanoparticle (slower release). Over this short time period, the chemotherapy does perform better, and this improvement would become more evident over time. These were simply for comparison's sake in order to contrast them to delivery vehicles that contain both types of agents. In the liposomal carrier, both agents are released simultaneously over a fast timescale, resulting in the best results initially. The staggered release from a nanocell shows better results leading to potential tumour eradication within months (assuming no chemo-resistance). This is due to the tumour vasculature normalization performed before the chemotherapy

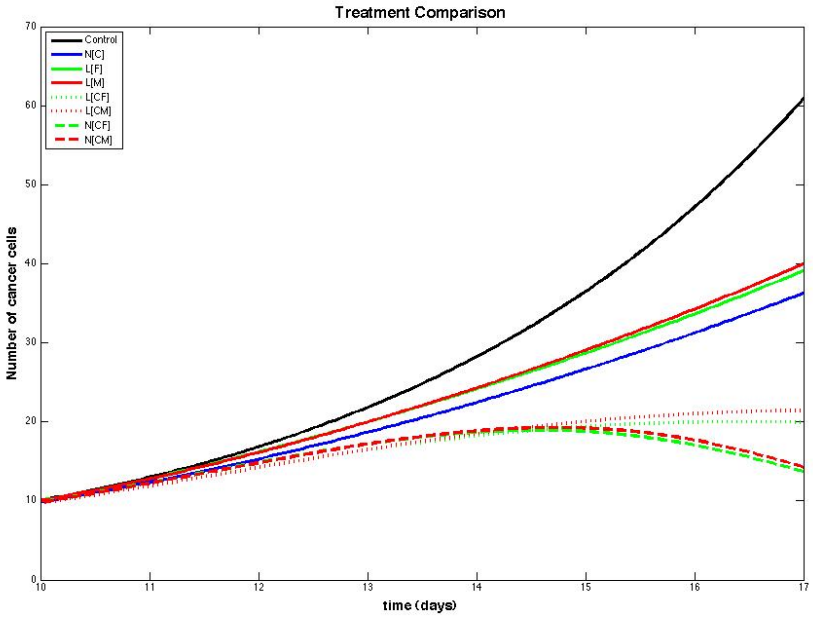


Figure 4.8: Combining treatments in a nanocell shows improvement over simultaneous release from a liposome.

is applied.

## 4.8 Model Evaluation

This model proves to be a useful empirical method of analyzing the results of various treatment regimes on the spatial distribution of the tumour, the tumour vasculature and the angiogenic activity in this system. By integrating over the domain a meaningful quantitative comparison of treatment schedules can also be acquired and results similar to those from the ODE model can be reached. While this model incorporates the spatial distribution of drugs, handicapping the delivery of those found in the tumour vasculature, it does not capture the full extent of the poor delivery of drugs to the tumour cells. Another key player is interstitial fluid pressure, a factor that wreaks havoc on the efficient delivery of drugs. The outward convection caused by the IFP will have an effect on both the distribution of drugs

as well as the angiogenic factor concentrations.

# Chapter 5

# Interstitial Fluid Pressure in Solid Tumours

Elevated interstitial fluid pressure is a tumour phenomenon resulting primarily from highly fenestrated tumour vasculature leaking large volumes of fluid into the tumour bulk. Without functional lymphatics, the tumour does not have the capability to dispose of this excess fluid leading to the outward convection of molecules and highly compromised drug delivery. Including pressure into the drug delivery equations could make simulations more realistic in future models. Here, we will look at the effect of IFP on proangiogenic and antiangiogenic factors, with a focus on their balance.

## 5.1 IFP Modelling in a Tumour

We will model the interstitial fluid pressure $p_i$ using the equation (2.22), given below in its general form

$$\nabla^2 p_i = -\frac{\alpha^2}{R^2}(p_v - \sigma_T(\pi_v - \pi_i) - p_i) \tag{5.1}$$

where $\alpha = R\sqrt{L_p S/KV}$ is a nondimensional parameter. For details of the derivation, see Section 2.3. The various parameters are the hydraulic conductivity of

| Parameter | Units | Normal | Tumour |
|---|---|---|---|
| $R$ | cm | 0.4 | 0.4 |
| $K$ | $\text{cm}^2$/s/mm Hg | $2.5\times10^{-7}$ | $2.5\times10^{-7}$ |
| $L_p$ | cm/s/mm Hg | $3.6 \times 10^{-8}$ | $1.86\times10^{-7}$ |
| $S/V$ | $\text{cm}^2/\text{cm}^3$ | 50–250 | 50–250 |
| $p_v$ | mm Hg | 15-25 | 5.5-34 |
| $\sigma_T(\pi_v - \pi_i)$ | mm Hg | 9.1 | $2.2\times10^{-4}$ |

Table 5.1: Parameters for the pressure model [72].

microvascular wall $L_p$, the surface area of vessel wall per volume of tumour $S/V$, the vascular pressure $p_v$, the average osmotic reflection coefficient for plasma proteins $\sigma_T$ and the plasma (interstitial) osmotic pressure $\pi_{p(i)}$. Typical parameters for normal and tumour tissues are given in Table 5.1.

This equation can be nondimensionalized by scaling the length scale with $R$ and setting $p_i = p_e\tilde{p}_i$ with the effective pressure $p_e = p_v - \sigma_T(\pi_v - \pi_i)$, giving

$$\nabla^2\tilde{p}_i = \alpha^2(\tilde{p}_i - 1). \tag{5.2}$$

We can solve for $p_i$ (dropping tildes) analytically by assuming radial symmetry and a fixed value at the tumour rim. The boundary conditions at the tumour core and the tumour boundary are respectively

$$\left.\frac{\partial p_i}{\partial r}\right|_{r=0} = 0, \qquad p_i(1) = 0,$$

and using these analytical solutions can be found; see A.3 for details. In Figure 5.1 the solutions of (5.2) corresponding to a reasonable range of $\alpha$ values are shown. These solutions show the highest pressure present in the center of the tumour along with the typical sharp drop-off in pressure moving toward the tumour periphery. Larger values of $\alpha$ show sharper declines and higher pressures at the core.

It may be observed that these solutions are obvious given the nature of the boundary conditions imposed, however, only the one ensuring symmetry at the core is natural. The other is forced and can only be justified if the tumour is isolated

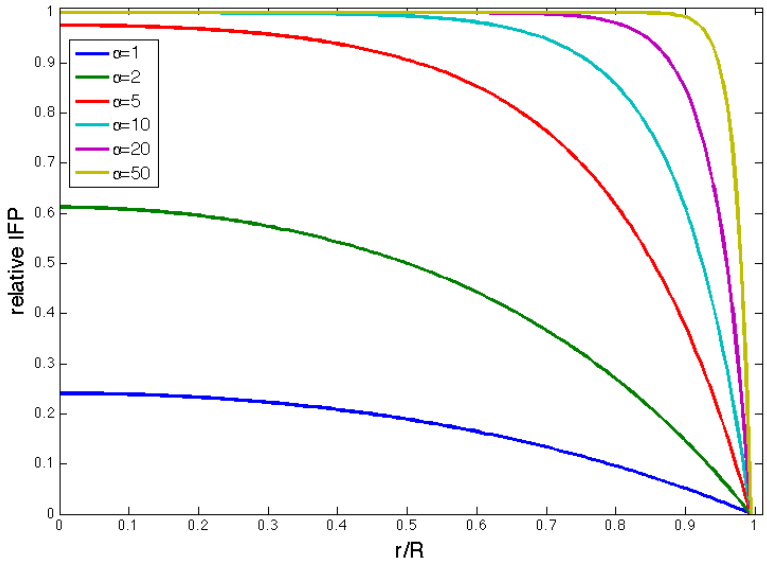


Figure 5.1: Radial solutions of the interstitial fluid pressure in a tumour.

in a medium that would ensure zero pressure at the tumour boundary. More likely the pressure slowly decreases as you move away from the tumour. Due to this, we will now consider a tumour to be present in some host tissue. To account for this, the normal tissue outside the tumour will be considered to have a different value of $\alpha$. Once again analytical solutions are presented in A.3. For the simulations, the value in the normal tissue ($r > 1$) is $\alpha = 2$. In Figure 5.2, the same values of $\alpha$ as Figure 5.1 are used but now instead of enforcing Dirichlet boundary conditions at the boundary, we have imposed continuity and smoothness conditions

$$p_i|_{r=1^-} = p_i|_{r=1^+} \qquad \text{and} \qquad \left.\frac{\partial p_i}{\partial r}\right|_{r=1^-} = \left.\frac{\partial p_i}{\partial r}\right|_{r=1^+}.$$

Along with these, it is a requirement that

$$\lim_{r\to\infty} p_i(r) = 0,$$

a weaker condition than $p_i(1) = 0$. These solutions show a steep decline approaching the tumour boundary but then slowly level off to normal values.

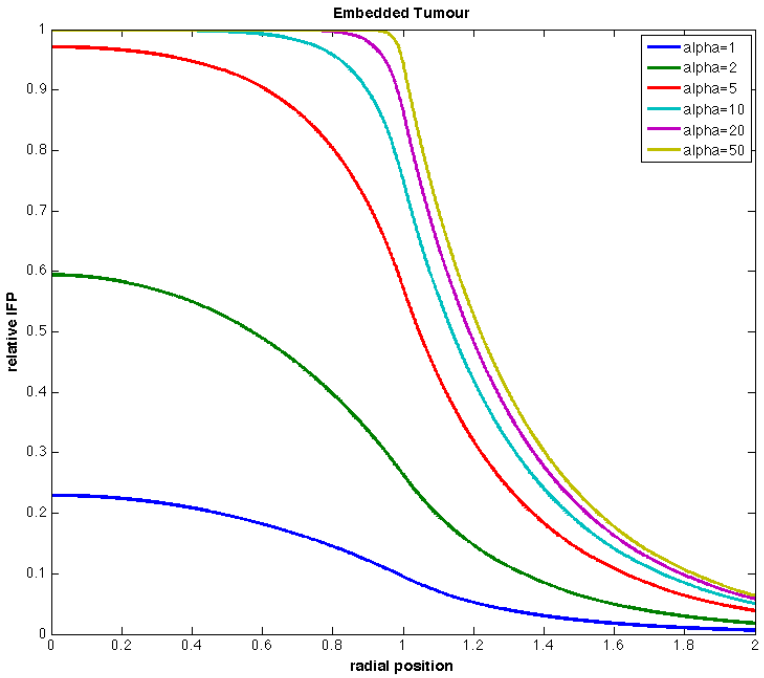


Figure 5.2: Radial solutions of the interstitial fluid pressure in a tumour.

## 5.2 IFP and Angiogenic Factors

When including interstitial fluid pressure, it is natural to consider the effect on drug concentration in the tumour. However, its effect on the concentrations of other entities in the model should also be considered. While interstitial fluid pressure may also directly effect the proliferation of tumour cells or tumour endothelial cells, these processes (in most cases) occur on a much longer time scale than those of interstitial fluid pressure, drug distribution and growth factor production and diffusion. Due to this, we should consider a pressure-dependent equation for the concentrations of proangiogenic and antiangiogenic factors. To facilitate this, we will identify interstitial convection as an important transport mechanism for these molecules and add a convection term to (2.10) giving

$$\frac{\partial f_j}{\partial t} = D_j \nabla^2 f_j + K \nabla \cdot (f_j \nabla p_i) + g_j - k_j f_j \tag{5.3}$$

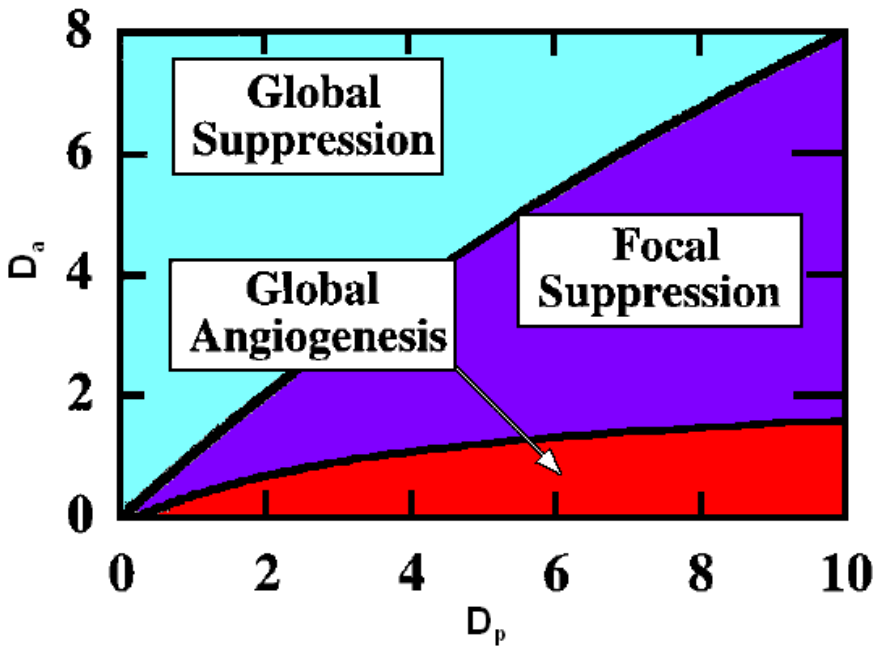


Figure 5.3: Sensitivity of the angiogenic activity behaviour due to the diffusion coefficient of proangiogenic and antiangiogenic factors. Image from [39].

for $j = a, p$. In fact, in [39], it is mentioned that, "Interstitial convection is not addressed independently but is lumped together with diffusion, characterized by an effective diffusion coefficient," indicating that convection was considered but absolved by a simplifying assumption. We simply seek to treat this convection as a separate process from diffusion.

Considering just the interior of the tumour, with the noted motivation of incorporating interstitial fluid pressure into the behaviour of angiogenic factor concentrations, the parameters from [39] will be used for proangiogenic and antiangiogenic factor diffusion, production and degradation inside the tumour. The boundary condition of $f_i(R) = g_i/(k_i)^2$ (the host tissue factor concentration) will be imposed along the boundaries of the grid.

Radially symmetric solutions to (5.3) can be found numerically by solving the related inverse matrix problem. Setting $K = 0$, a sensitivity analysis originally performed in [39] is reproduced in Figures 5.3 and 5.4. As can be seen, only

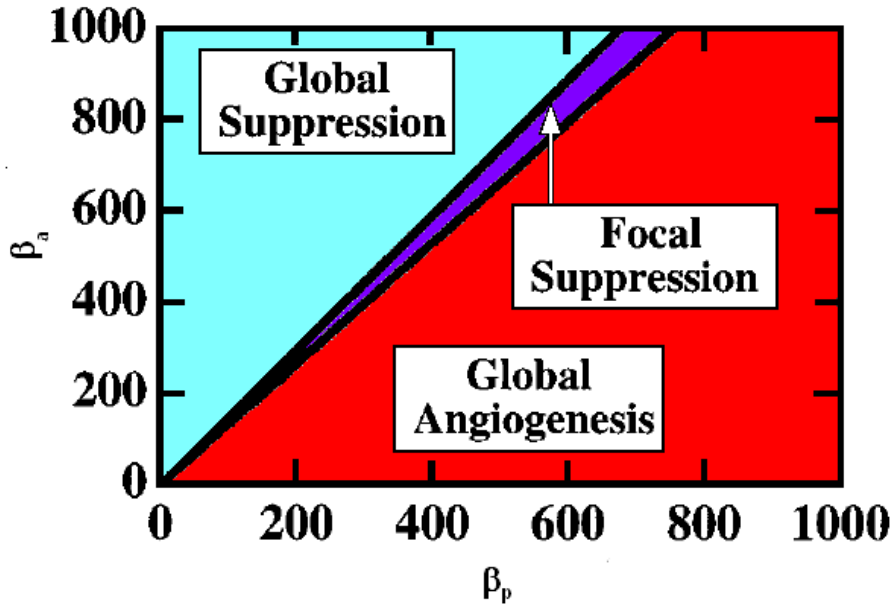


Figure 5.4: Sensitivity to the tumour cell production rates. Image from [39].

specific parameters will give the focally suppressive behaviour, that is for some value $r_0 \in [0,1]$ we have $\alpha_{\mathrm{GF}}(r) \leq 0$ for $r \in [0, r_0]$ and $\alpha_{\mathrm{GF}}(r) \geq 0$ for $r \in [r_0, 1]$. The other reasonable possibilities for angiogenic behaviour are global suppression ($\alpha_{\mathrm{GF}}(r) \leq 0, \forall r$) and global angiogenesis ($\alpha_{\mathrm{GF}}(x) \geq 0, \forall r$) which can also be found in this model. These two possibilities do happen in some cases where tumours are either thoroughly vascularized or on the other hand, unable to grow due to a global suppression of angiogenic activity (potentially due to antiangiogenic therapies). In the case of the tumour production parameter, it is interesting to note that focal necrosis is observed only for a narrow sliver of the parameter space. This is realistic since one would assume that the behaviour is extremely sensitive to the the balance of these factors production.

As can be seen in Figure 5.6, this model suggests that the convection of these factors could also lead to very different angiogenic behaviours in the tumour. The sensitivity to the convection parameters (hydraulic conductivities) is a more complicated relationship than those for the other angiogenic factor parameters. Depending on the pressure gradient, we can see that for low values of $\alpha$ the region of angiogenic

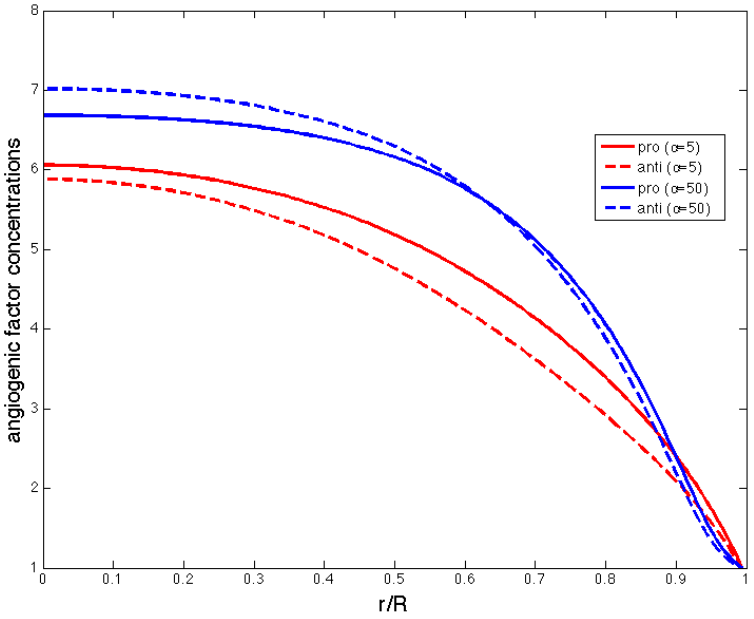


Figure 5.5: Concentrations of proangiogenic and antiangiogenic factors in an isolated tumour.

suppression (RAS) is conserved while for mid-values of $\alpha$ the core of the tumour is seen to be an area of angiogenic activity as well, although to a lesser degree than the rim. For high values of $\alpha$ the core once again becomes a RAS with the high levels of angiogenic activity occurring closest to the tumour rim.

The switch from suppression to stimulation of angiogenesis (when $\alpha_{\mathrm{GF}}$ changes from a negative value to a positive value) or vice versa occurs when the angiogenic factor concentrations intersect each other as shown in Figure 5.5. As observed above, a change in any of the parameters from the base case given in Table 4.6.1 can elicit a change in the global behaviour of the solution. An analytical determination of what parameter conditions, specifically for the convection parameters, would elicit an intersection of the factor concentrations would be a worthwhile endeavour.

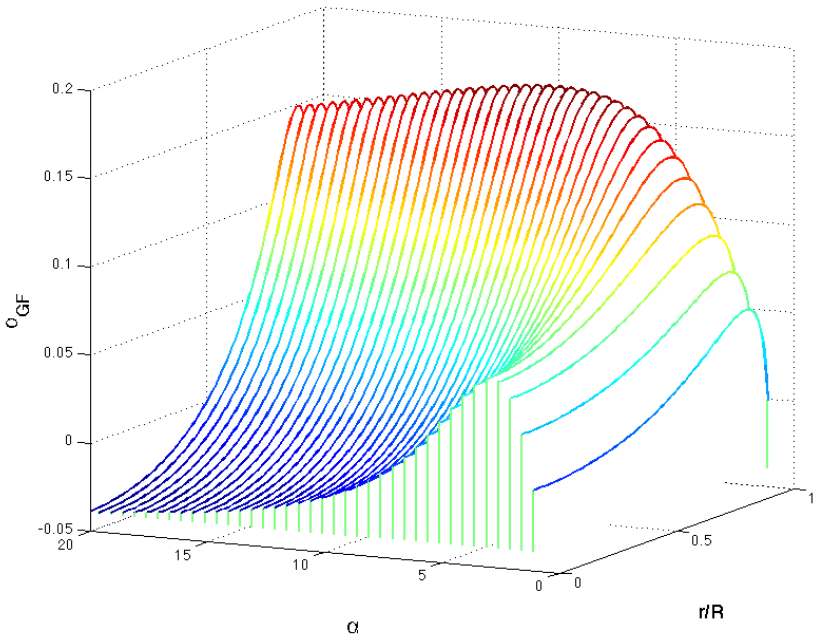


Figure 5.6: Angiogenic activity of an isolated tumour.

## 5.3 Model Evaluation

Once again, we are assuming radial symmetry for the pressure-related models just presented. Due to this, we are not able to observe a number of phenomena including the heterogeneous production of angiogenic factors and multiple areas of angiogenic suppression. While tumour cells are not explicitly modelled, typically angiogenic suppression is correlated with cell death. A fairly global phenomenon is that tumours exhibit necrosis at the core, however, this area is usually irregular in shape and potentially disconnected.

A goal for the future remains to incorporate these pressure equations and effects into a three-dimensional model that includes clinically relevant distributions of tumour cell density and tumour vasculature networks.

# Chapter 6

# Conclusions

## 6.1 Summary and Implications of Findings

The ODE model used to analyze the results of combination therapies comprising chemotherapy and antiangiogenic therapies has given some insight into the relationship between the mechanisms of the two drug types working in tandem. The central assumption to this model is that the vasculature is the growth-limiting factor and is used to represent the carrying capacity of the tumour size [36]. The resulting explanation of the success of combination therapies is the compounding effects of the carrying capacity decrease associated with antiangiogenic agents and the tumour suppression granted by the chemotherapy agent. While either alone has a significant impact on tumour size, the combination of both results in a greater potentiality for treatment success. Also briefly considered are the benefits of metronomic treatment schedules and the advantage of longer release drugs, touting the advantages of longer circulation delivery vehicles.

The PDE model allows the addition of specific antiangiogenic mechanisms due to the inclusion of angiogenic factors. These factors can be inhibited or the endothelial cells can be directly attacked. Due to a delivery efficiency term added to the chemotherapy and antiangiogenic therapy dosages, the inefficiency of the irregular tumour vasculature is represented while the vasculature that has been

normalized by antiangiogenic agents allows the successful delivery of chemotherapy drugs. The antiangiogenic agents still have some anti-tumoural effects since the presence of vasculature is coupled to tumour growth. Qualitatively, the two-dimensional simulations show reasonable representations of the spatial distributions of tumour cells and vasculature before and after treatment. Considering specific treatment schedules shows that comparable levels of both types of antiangiogenic agents with chemotherapy give similar results. However, those combinations delivered in longer (and staggered) release nanoparticles shows improved results, a more general result than the one obtained in the ODE chapter.

The final chapter of results shows the beginnings of incorporating pressure into a drug distribution model and some preliminary simulations show how the pressure gradient induced convection effects the behaviour of angiogenic activity. The specific relationship between the relevant convection parameters and the possible behaviours of focal suppression, global suppression and global stimulation remains unknown but all of these can be observed by altering the convection parameters alone.

These models can be expanded on many fronts and many of these will be incorporated in the future; a few possibilities are outlined now.

## 6.2 Possible Extensions and Open Problems

### 6.2.1 Tumour Growth

When it was realized that tumour growth was more accurately modelled when spatial effects were included, we expanded our mathematical framework from ordinary to partial differential equations. However, we only considered logistic growth for the tumour cell proliferation when we outlined a number of alternatives in the ODE section, not to mention the countless additional extensions to these basic models which exist in the literature to describe the growth of numerous forms of

cancers. The merits of each model have been debated extensively in the literature, but for illustrative purposes logistic growth is sufficient since it is an accurate enough approximation based on a simple assumption. To model this process more convincingly, we must choose a model which more accurately describes the increase in tumour cell density over time while not introducing additional complexity or parameters. Creating a more biologically sound and more realistic tumour growth equation would still be a worthwhile area of further research.

### 6.2.2 Vasculature Modelling

The area of three-dimensional vasculature modelling, with specific emphasis on tumour vasculature, has been widely reported in the literature with many viable models recently coming to the forefront, incorporating many biological considerations across many scales. Going forward, a model must be developed that is comprehensive enough for spatially dependent heterogeneous tumour growth and drug distributions that can be compared to and reconciled with experimental data. We have developed a couple of possibilities for simulating vasculature networks.

Inspired by the work in [46], we attempt to improve the vessel structures while omitting their considerations of the underlying cellular network. We propose the following steps:

1. A random point $(x_0, y_0)$ is generated on a $N \times N$ grid and a random angle $\theta_0 \in [0, \pi]$ is generated.

2. The vessel extends from $(x_0, y_0)$ at the angle $\theta$ and in the other direction at the angle $\theta_0 + \pi$ until the boundary of the grid is reached.

3. A point $(x, y)$ is chosen on the pre-existing vessel(s) at which a vessel will extend unless a vessel already has sprouted from this vessel within a distance $\Delta$ of this point.

4. A vessel extends at a random angle $\theta \in [0, 2\pi)$ from the point $(x, y)$ until one of the following occurs

   (a) The vessel reaches the boundary of the grid.

   (b) The vessel intersects a pre-existing vessel.

   (c) The vessel comes within a distance $\Delta$ of a previous vessel intersection.

5. We repeat steps 3-4 until the occupancy of our grid reaches a certain threshold.

The above algorithm prevents intersections of vessels that create a four-way junction, a consideration that corresponds to the branching typically observed in nature.

Random walk techniques have been widely employed with an example in [44] whereas random tripod placement was used in [52]. We derive inspiration for the initial conditions from [54] to simulate the vasculature for our model. We dismiss the hexagonal lattice used since this is not easily extended to 3-D and simply use a standard rectangular lattice. First we simulate a number of initial source and sink vessels (that come from one of the boundaries of our domain) to establish some sort of basic structure; we distinguish between them by using the colours red and blue respectively. After these are in place, we randomly choose a node with exactly two edges connected to it. Again, this prevents nodes from having four edges radiating from them (unlike in [46]). Once a node is selected we randomly walk under the following conditions:

1. The vessel can not intersect a vessel of the same colour. Note that we do not terminate the vessel if a direction that would cause an intersection is chosen in the random walk, we simply choose from the admissible directions.

2. When a vessel intersects a vessel of the other colour, it terminates at the node of their intersection.

3. A vessel is not allowed to form a $1 \times 1$ square on the lattice (preventing small loops in the vasculature).

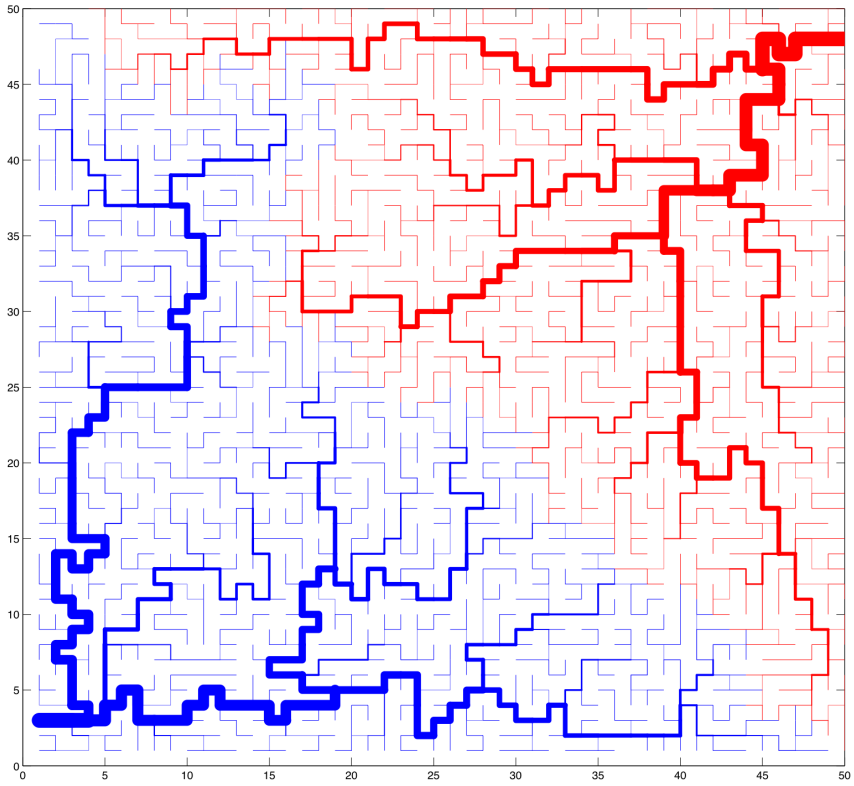


Figure 6.1: A blood vessel network developed using the random walk algorithm with a length restriction of 5 steps..

The above conditions imply that a vessel terminates when all four possible directions would lead to a violation of one of the rules. This process does not require the additional step of capillary formation (as in [52]) since we add random walk vessels instead of discrete elements (such as tripods). The simulation ends when every node on the lattice has at least one edge connected to it (unless this is impossible), corresponding to a fully vascularized tissue. A slight alteration allows walks of a specific length or less; in Figure 6.1 a maximum walk length of 5 grid spaces is imposed.

### 6.2.3 Receptor-Ligand Binding

As outlined in Section 2.4, receptor-ligand binding between nanoparticles or nanocells and cancer cells would be a worthwhile research topic. Specifically, the spatial distribution of conjugated ligands that would optimize the binding of delivery vehicles to cancer cell receptors. The concentration of polymer chains that prevent removal from the blood vessels by the immune system would have to be considered when examining this problem.

### 6.2.4 Optimal Scheduling

Many of these models have been treated as control problems in the literature in order to uncover the 'optimal' treatment based on the model equations and dosage possibilities subject to some constraints. Our model has not undergone such a process but it would be a worthy endeavour to better quantify the relationships that exist between changes in the biological parameters and their effect on the best treatment schedule.

### 6.2.5 Parameter Estimation

The parameters used in the simulations and studies come from a variety of studies and some correspond to observations made on more than one form of cancer while others are set to values dependent on a crude sensitivity analysis alone. Clearly, the initial conditions and some key parameters must be altered in order to differentiate the tumour behaviour in varying tissues with specific mutations. For instance, the invasiveness of a tumour could be measured on some scale and associated with the parameter responsible for incorporating the speed of directed cell movements ($\beta_n$).

While treatment parameters have been chosen to correspond to specific drugs, certain parameters such as diffusion coefficient are not as widely available as the more commonly used decay constant. The parameters associated with proangio-

genic and antiangiogenic factors from [39] are all assumed due to a lack of experimental data. Since these concentration do not correspond to specific molecules, we must take this a a qualitative model only.

### 6.2.6 Interstitial Fluid Pressure

As mentioned in the previous chapter, the effect of IFP should be included in future drug distribution models. As in the model developed for macromolecule extravasation from tumour vasculature [59] (see Section 2.3), the following equation describes the concentration of drug delivery vehicles $C_i$ in the interstitium of the tumour

$$\frac{\partial C_i}{\partial t} = D\nabla^2 C_i - \nabla \cdot (r_f u_i C_i) + \frac{J_s}{V} \tag{6.1}$$

where $u_i = -K\nabla p_i$ is the interstitial fluid velocity and $J_s$ is the flux across the vessel given by

$$J_s = J_v(1-\sigma)C_p + PS(C_p - C_i)\frac{\mathrm{Pe}}{e^{\mathrm{Pe}}-1} \tag{6.2}$$

where $J_v$ is the volume flux through vessel wall given by

$$J_v = L_p S(p_e - p_i), \tag{6.3}$$

$C_p$ is the concentration of delivery vehicles present in the blood plasma, $P$ is the permeability of the vessel and Pe$= J_v(1-\sigma)/PS$ is the Peclet number. To model this concentration, we would use the typical dosage equations exponential decay (3.5) or delayed exponential (3.6).

Rewriting equation (6.1) in its full form, we get

$$\frac{\partial C_i}{\partial t} = D\nabla^2 C_i + K\nabla p_i \cdot \nabla C_i + \frac{L_p S}{V}(p_e - p_i)(1-\sigma)C_p + \frac{PS}{V}(C_p - C_i)\frac{\mathrm{Pe}}{e^{\mathrm{Pe}}-1}. \tag{6.4}$$

While this full equation will be useful for macromolecules of a specific size, for some molecule sizes only some of interstitial/vessel diffusion/convection are important processes in their transport. For large liposomes containing cytotoxic agents, evidence suggests that the most important transport mechanism is interstitial convection.

While simulations have been performed for a angiogenic factor concentration model that incorporates interstitial convection, these should be extended to include the embedded tumour case and more accurate angiogenic factor parameters should be sought out.

# APPENDICES

# Appendix A

# Calculations

## A.1 Nondimensionalization of ODEs

For logistic growth (see equation 2.2), we can easily nondimensionalize the tumour cell density by setting $\tilde{n} = n/n_\infty$ which (dropping tildes) reduces the ODE to

$$\frac{dn}{dt} = rn(1-n).$$

By further scaling of the time $\tilde{t} = t/r$, we get $dn/dt = n(1-n)$, a first-order non-linear parameter-free ordinary differential equation.

For generalized logistic growth, given in (2.4), we can nondimensionalize in a very similar fashion, the only difference being the time nondimensionalization is now $\tilde{t} = \nu t/r$, giving

$$\frac{dn}{dt} = n(1-n^\nu),$$

while Gompertz growth equation is nondimensionalized in exactly the same manner as logistic growth giving

$$\frac{dn}{dt} = n\ln(1/n).$$

Note how in each case we were able to eliminate the two key parameters: $n_\infty$ and $r$. The solutions of these basic equations are easily found by plugging in $r = 1$ and $n_\infty = 1$ into the dimensional solutions.

## A.2 Growth factor solutions

In section 2.2.1, solutions to the moving boundary problem governed by the equation,

$$D_j^e \frac{1}{r^2}\frac{\partial}{\partial r}\left(r^2 \frac{\partial f_j^e}{\partial r}\right) - k_j^e f_j^e + g_j^e = 0 \tag{A.1}$$

were not presented or derived. Here we show some further details of the solution since it differs slightly from the solution originally given in [39] where this model was initially proposed.

Non-dimensionalization of (A.1) can be achieved by setting $r = R\tilde{r}$, $f_j^e = L_j \tilde{f}_j^e$ and by defining the rescaled parameters $\kappa_j^e = \sqrt{k_j^e R^2/D_j^e}$ and $\gamma_j^e = g_j^e R^2/D_j^e L_j$ where

$$L_j := \lim_{r\to\infty} f_j^h(r) = \frac{g_j^h}{k_j^h}.$$

Dropping tildes, this gives the equation

$$\frac{1}{r^2}\frac{\partial}{\partial r}\left(r^2 \frac{\partial f_j^e}{\partial r}\right) - (\kappa_j^e)^2 f_j^e + \gamma_j^e = 0. \tag{A.2}$$

Solutions to equation (A.2) are of the form

$$f_j^m(r) = A_j^m \frac{\sinh(\kappa_j^m r)}{r} + B_j^m \frac{\cosh(\kappa_j^m r)}{r} + \Omega_j, \qquad 0 \le r \le 1 \tag{A.3}$$

$$f_j^h(r) = A_j^h \frac{\sinh(\kappa_j^h r)}{r} + B_j^h \frac{\cosh(\kappa_j^h r)}{r} + 1, \qquad 1 < r < \infty. \tag{A.4}$$

where $\Omega_j = \gamma_j^m/(\kappa_j^m)^2$. Considering boundary conditions, we require the concentration to approach the steady state value as we move into the host tissue and this can occur if and only if $A_j^h + B_j^h = 0$. At the center of the tumour, we will enforce symmetry and so $\partial f_j^m/\partial t|_{r=0} = 0$ leading to $B_j^m = 0$. This gives $f_j^m(0) = A_j^m \kappa_j^m + \Omega_j$ at the tumour core. To ensure that the solutions in each environment smoothly match up at the boundary of the tumour we must also have $f_j^m(1) = f_j^h(1)$ and $\partial f_j^m(r)/\partial r\big|_{r=1} = \partial f_j^h(r)/\partial r\big|_{r=1}$. These two equations along with our previous observations allow us to solve for the remaining constants,

$$A_j^m = \omega_j \frac{1+\kappa_j^h}{\sinh(\kappa_j^m)}, \tag{A.5}$$

$$A_j^h = -B_j^h = \omega_j \frac{1-\kappa_j^m \coth(\kappa_j^m)}{\sinh(\kappa_j^h) - \cosh(\kappa_j^h)}, \tag{A.6}$$

where $\omega_j = (1-\Omega_j)/(\kappa_j^h + \kappa_j^m \coth \kappa_j^m)$. Thus, the final solution is given by

$$f_j^m = \omega_j \frac{1+\kappa_j^h}{\sinh(\kappa_j^m)} \frac{\sinh(\kappa_j^m r)}{r} + \Omega_j, \qquad 0 \leq r \leq 1 \tag{A.7}$$

$$f_j^h = \omega_j \frac{1-\kappa_j^m \coth(\kappa_j^m)}{\sinh(\kappa_j^h) - \cosh(\kappa_j^h)} \left( \frac{\sinh(\kappa_j^h r) - \cosh(\kappa_j^h r)}{r} \right) + 1, \qquad 1 < r < \infty. \tag{A.8}$$

## A.3 Pressure solutions

Performing similar calculations as the ones performed above, we will derive the solutions to the non-dimensional pressure equation

$$\nabla^2 p = \alpha^2 (p-1), \tag{A.9}$$

as done in the supplementary material in [72]. The general solution is of the form

$$p(r) = A \frac{\sinh(\alpha r)}{r} + B \frac{\cosh(\alpha r)}{r} + 1.$$

Considering the case of an isolated tumour, we enforce the boundary condition

$$\left. \frac{\partial p}{\partial r} \right|_{r=0} = 0$$

by taking $B = 0$. At the tumour boundary, the pressure is zero and hence take $p(1) = 0$. This gives $A = -1/\sinh(\alpha)$ and so the solution is

$$p(r) = 1 - \frac{\sinh(\alpha r)}{r \sinh(\alpha)}.$$

The more realistic boundary conditions associated with the embedded tumour case are:

$$p|_{r=1^-} = p|_{r=1^+} \qquad \text{and} \qquad \left. \frac{\partial p}{\partial r} \right|_{r=1^-} = \left. \frac{\partial p}{\partial r} \right|_{r=1^+}.$$

Enforcing these conditions gives the analytical solution and denoting tumour tissue parameters with a subscript $t$ and host tissue parameters with a subscript $h$

$$p(r) = 1 - \frac{(1+\alpha_h)\sinh(\alpha_t r)}{r(\phi+\theta)}, \qquad r \leq 1$$

$$p(r) = \frac{\theta e^{\alpha_t (1-r)}}{r(\phi+\theta)}, \qquad r > 1,$$

where $\theta = K[\alpha_t \cosh(\alpha_t) - \sinh(\alpha_t)]$ and $\phi = (1 + \alpha_h)\sinh(\alpha_t)$. The relative hydraulic permeability $K$ is given by $K_t/K_h$ (and is typically greater than one).

## A.4 Nondimensionalization of PDEs

To nondimensionalize (4.2), we set $t = \tilde{t}/r$, $x = \sqrt{D_n/r}\tilde{x}$ and $n = n_\infty \tilde{n}$ , we get

$$\frac{\partial \tilde{n}}{\partial \tilde{t}} = \nabla^2 \tilde{n} + \tilde{n}(1 - \tilde{n}) + \tilde{\alpha_n} m \tilde{n}, \tag{A.10}$$

where $\tilde{\alpha_n} = \alpha_n/r$.

Substituting these rescaled variables into (2.10) and setting $f_j = (g_j/r)\tilde{f_j}$ $(j = p, a)$ gives

$$\frac{\partial \tilde{f_j}}{\partial t} = \tilde{D}_j \nabla^2 \tilde{f}_j - \tilde{k}_j f_j + 1 + \tilde{\beta}_j \tilde{n} + \tilde{\gamma}_j \nabla \cdot (f_j \nabla n), \tag{A.11}$$

where $\tilde{D}_j = D_j/D_n$, $\tilde{k}_j = k_j/r$, $\tilde{\beta}_j = \beta_j n_\infty/g_j$ and $\tilde{\gamma}_j = \gamma_j n_\infty/D_n$.

Since $m$ is already a nondimensional variable, we have

$$\frac{\partial m}{\partial t} = \tilde{D_m} \nabla^2 m + \tilde{g}(m) + \tilde{\alpha_m} m \tilde{\alpha}_{\mathrm{GF}}, \tag{A.12}$$

where $\tilde{D}_m$ is scaled with $D_n$, $\tilde{g}$ and $\tilde{\alpha_m}$ with $r$ and $\tilde{\alpha}_{\mathrm{GF}} = g_p f_p/g_a f_a - 1$. These four dimensionless PDEs give all the equations for a basic biological model for tumour growth.

We can similarly nondimensionalize the equations that model the behaviour of chemotherapy and antiangiogenic therapies in a tumour along with their delivery vehicles allowing the inclusion of treatments.

# References


[1] D. Hanahan and R. A. Weinberg. The hallmarks of cancer. *Cell*, 100:57–70, 2000. 2

[2] J. W. Shay and S. Bacchetti. A survey of telomerase activity in human cancer. *Eur. J. Cancer*, 33:787–791, Apr 1997. 2

[3] Judah Folkman. Tumor angiogenesis: therapeutic implications. *N. Engl. J. Med.*, 285:1182–1186, 1971. 4, 5

[4] D. Hanahan and J. Folkman. Patterns and emerging mechanisms of the angiogenic switch during tumorigenesis. *Cell*, 86:353–364, 1996. 4

[5] G. M. Tozer. Measuring tumour vascular response to antivascular and antiangiogenic drugs. *Br. J. Radiol.*, 76 Spec No 1:23–35, 2003. 7

[6] R.K. Jain. Normalizing tumor vasculature: an emerging concept in antiangiogenic treatment. *Science*, 307:58–62, 2005. 7

[7] Judah Folkman. Angiogenesis and apoptosis. *Seminars in Cancer Biology*, 13(2):159 – 167, 2003. 8

[8] G. M. Tozer, C. Kanthou, C. S. Parkins, and S. A. Hill. The biology of the combretastatins as tumour vascular targeting agents. *Int. J. Exp. Pathol.*, 83:21–38, 2002. 8

[9] H. Hurwitz et. al. Bevacizumab plus irinotecan, fluorouracil, and leucovorin for metastatic colorectal cencer. *N. Engl. J. Med.*, 350:2335–2342, 2004. 8

[10] S. Pennacchietti, P. Michieli, M. Galluzzo, M. Mazzone, S. Giordano, and P. M. Comoglio. Hypoxia promotes invasive growth by transcriptional activation of the met protooncogene. *Cancer Cell*, 3:347–361, 2003. 9

[11] E. K. Rofstad, H. Rasmussen, K. Galappathi, B. Mathiesen, K. Nilsen, and B. A. Graff. Hypoxia promotes lymph node metastasis in human melanoma xenografts by up-regulating the urokinase-type plasminogen activator receptor. *Cancer Res.*, 62:1847–1853, 2002. 9

[12] F. Mac Gabhann and A.S. Popel. Targeting neuropilin-1 to inhibit VEGF signaling in cancer; comparison of therapeutic approaches. *PLoS Comput. Biol.*, 2, 2006. 9

[13] A. V. Rao, G. Akabani, and D. A. Rizzieri. Radioimmunotherapy for non-Hodgkin's lymphoma. *Clin. Med. Res.*, 3:157–165, 2005. 10

[14] D. Hanahan, G. Bergers, and E. Bergsland. Less is more, regularly: metronomic dosing of cytotoxic drugs can target tumor angiogenesis in mice. *J. Clin. Invest.*, 105:1045–1047, 2000. 11

[15] Robert S. Kerbel and Barton A. Kamen. The anti-angiogenic basis of metronomic chemotherapy. *Cancer Rev.*, 4:423–436, 2004. 11, 60

[16] S. Man, G. Bocci, G. Francia, S. K. Green, S. Jothy, D. Hanahan, P. Bohlen, D. J. Hicklin, G. Bergers, and R. S. Kerbel. Antitumor effects in mice of low-dose (metronomic) cyclophosphamide administered continuously through the drinking water. *Cancer Research*, 62:2731–2735, 2002. 11

[17] F. Bertolini et. al. Maximum tolerable dose and low-dose metronomic chemotherapy have opposite effects on the mobilization and viability of circulating endothelial progenitor cells. *Cancer Res.*, 63:4342–4346, 2003. 11

[18] R. A. Gatenby. A change of strategy in the war on cancer. *Nature*, 459:508–509, 2009. 11

[19] S. M. Moghimi, A. C. Hunter, and J. C. Murray. Long-circulating and target-specific nanoparticles: theory to practice. *Pharmacol. Rev.*, 53:283–318, 2001. 12

[20] Y. Matsamura and H. Maeda. A new concept for macromolecular therapeutics in cancer chemotherapy: mechanisms of tumoritropic accumulation of protein and the antitumor agent smancs. *Cancer Res.*, 46:6387–6392, 1986. 12

[21] Y. Lu and P. S. Low. Folate-mediated delivery of macromolecular anticancer therapeutic agents. *Adv. Drug Deliv. Rev.*, 54:675–693, 2002. 15

[22] J. F. Ross, P. K. Chaudhuri, and M. Ratnam. Differential regulation of folate receptor isoforms in normal and malignant tissues in vivo and in established cell lines. Physiologic and clinical implications. *Cancer*, 73:2432–2443, 1994. 15

[23] R. J. Lee and P. S. Low. Folate-mediated tumor cell targeting of liposome-entrapped doxorubicin in vitro. *Biochim. Biophys. Acta*, 1233:134–144, 1995. 14

[24] J. Sudimack and R. J. Lee. Targeted drug delivery via the folate receptor. *Adv. Drug Deliv. Rev.*, 41:147–162, 2000. 14

[25] D. Goren, A. T. Horowitz, D. Tzemach, M. Tarshish, S. Zalipsky, and A. Gabizon. Nuclear delivery of doxorubicin via folate-targeted liposomes with bypass of multidrug-resistance efflux pump. *Clin. Cancer Res.*, 6:1949–1957, 2000. 14

[26] P. C. Brooks, A. M. Montgomery, M. Rosenfeld, R. A. Reisfeld, T. Hu, G. Klier, and D. A. Cheresh. Integrin alpha v beta 3 antagonists promote tumor regression by inducing apoptosis of angiogenic blood vessels. *Cell*, 79:1157–1164, 1994. 15, 16

[27] P. C. Patel, D. A. Giljohann, D. S. Seferos, and C. A. Mirkin. Peptide antisense nanoparticles. *Proc. Natl. Acad. Sci. U.S.A.*, 105:17222–17226, 2008. 17

[28] S. Sengupta, D. Eavarone, I. Capila, G. Zhao, N. Watson, T. Kiziltepe, and R. Sasisekharan. Temporal targeting of tumour cells and neovasculature with a nanoscale delivery system. *Nature*, 436:568–572, 2005. 17, 18

[29] S. Awasthi. A dendrimer-based prodrug for use in an anti-cancer nanocell. Master's thesis, Massachusetts Institute of Technology, 2007. 17

[30] Benjamin Gompertz. On the nature of the function expressive of the law of human mortality, and on a new mode of determining the value of life contingencies. *Philos. Trans. R. Soc. Lond.*, 115:513–585, 1825. 22

[31] F.J. Richards. A flexible growth function for empirical use. *J. Exp. Bot.*, 10:290–300, 1959. 22

[32] A. d'Onofrio. A general framework for modeling tumor-immune system competition and immunotherapy: Mathematical analysis and biomedical inferences. *Physica D*, 208:220–235, 2005. 23

[33] T. E. Wheldon. *Mathematical Models in Cancer Research*. Taylor & Francis, 1988. 24

[34] H. E. Skipper, F. M. Schabel, and W. S. Wilcox. Experimental evaluation of potential anticancer agents. XIII. On the criteria and kinetics associated with curability of experimental leukemia. *Cancer Chemother. Rep.*, 35:1–111, 1964. 25

[35] L. Norton and R. Simon. Tumor size, sensitivity to therapy, and design of treatment schedules. *Cancer Treat. Rep.*, 61:1307–1317, 1977. 25

[36] P. Hahnfeldt, D. Panigrahy, J. Folkman, and L. Hlatky. Tumor development under angiogenic signaling: A dynamical theory of tumor growth, treatment response and postvascular dormancy. *Cancer Res.*, 59:4770–4775, 1999. ix, 25, 51, 55, 72, 88

[37] A. Ergun, K. Camphausen, and L. M. Wein. Optimal scheduling of radiotherapy and angiogenic inhibitors. *Bull. Math. Biol.*, 65:407–424, 2003. 26, 51

[38] A. d'Onofrio and A. Gandolfi. Tumor eradication by antiangiogenic therapy: analysis and extensions of the model by hahnfeldt et al., (1999). *Math. Biosci.*, 191:159–184, 2004. 27, 51

[39] S. Ramanujan, G.C. Koenig, T.P. Padera, B.R. Stoll, and R.K. Jain. Local imbalance of proangiogenic and antiangiogenic factors: a potential mechanism of focal necrosis and dormancy in tumors. *Cancer Res.*, 60:1442–1448, 2000. x, xi, 28, 29, 64, 71, 72, 84, 85, 94, 98

[40] B.R. Stoll, C. Migliorini, A. Kadambi, L.L. Munn, and R.K. Jain. A mathematical model of the contribution of endothelial progenitor cells to angiogenesis in tumors: implications for antiangiogenic therapy. *Blood*, 102:2555–2561, 2003. 29

[41] B. Endrich, H. S. Reinhold, J. F. Gross, and M. Intaglietta. Tissue perfusion inhomogeneity during early tumor growth in rats. *J. Natl. Cancer Inst.*, 62:387–393, 1979. 29

[42] D.J. Nolan, A. Ciarrocchi, A.S. Mellick, J.S. Jaggi, K. Bambino, S.Gupta, E. Heikamp, M.R. McDevitt, D.A. Scheinberg, R. Benezra, and V. Mittal. Bone marrow-derived endothelial progenitor cells are a major determinant of nascent tumor neovascularization. *Genes & Dev.*, 21:1546–1558, 2007. 30

[43] S. Rafii, D. Lyden, R. Benezra, K. Hattori, and B. Heissig. Vascular and haematopoietic stem cells: novel targets for anti-angiogenesis therapy? *Nature Rev. Cancer*, 2:826–835, 2002. 30

[44] A.R.A. Anderson and M.A.J. Chaplain. Continuous and discrete mathematical models of tumor-induced angiogenesis. *Bull. Math. Biol.*, 60:857–900, 1998. 31, 34, 35, 91

[45] M. Kohandel, M. Kardar, M. Milosevic, and S. Sivaloganathan. Dynamics of tumor growth and combination of anti-angiogenic and cytotoxic therapies. *Phys. Med. Biol.*, 52:3665–3677, 2007. 32, 65, 66, 71

[46] J.L. Gevertz and S. Torquato. Modeling the effects of vasculature evolution on early brain tumor growth. *J. Theor. Biol.*, 243:517–531, 2006. 33, 35, 90, 91

[47] T. W. Secomb, R. Hsu, N. B. Beamer, and B. M. Coull. Theoretical simulation of oxygen transport to brain by networks of microvessels: effects of oxygen supply and demand on tissue hypoxia. *Microcirculation*, 7:237–247, 2000. 33

[48] S. R. McDougall, A. R. Anderson, M. A. Chaplain, and J. A. Sherratt. Mathematical modelling of flow through vascular networks: implications for tumour-induced angiogenesis and chemotherapy strategies. *Bull. Math. Biol.*, 64:673–702, 2002. 35

[49] S. R. McDougall, A. R. Anderson, and M. A. Chaplain. Mathematical modelling of dynamic adaptive tumour-induced angiogenesis: clinical implications and therapeutic targeting strategies. *J. Theor. Biol.*, 241:564–589, Aug 2006. 35

[50] J. Wu, Q. Long, S. Xu, and A. R. Padhani. Study of tumor blood perfusion and its variation due to vascular normalization by anti-angiogenic therapy based on 3D angiogenic microvasculature. *J. Biomech.*, 42:712–721, 2009. 35

[51] J. W. Baish, Y. Gazit, D. A. Berk, M. Nozue, L. T. Baxter, and R. K. Jain. Role of tumor vascular architecture in nutrient and drug delivery: an invasion percolation-based network model. *Microvasc. Res.*, 51:327–346, 1996. 36

[52] R. Gdde and H. Kurz. Structural and biophysical simulation of angiogenesis and vascular remodeling. *Dev. Dyn.*, 220:387–401, 2001. x, 36, 37, 91, 92

[53] K. Sandau and H. Kurz. Modelling of vascular growth processes: a stochastic biophysical approach to embryonic angiogenesis. *J. Microsc.*, 175:205–213, 1994. 36

[54] M. Welter, K. Bartha, and H. Rieger. Emergent vascular network inhomogeneities and resulting blood flow patterns in a growing tumor. *J. Theor. Biol.*, 250:257–280, 2008. 36, 91

[55] M. Welter, K. Bartha, and H. Rieger. Vascular remodelling of an arteriovenous blood vessel network during solid tumour growth. *J. Theor. Biol.*, 2009. x, 36, 37, 38

[56] C. D. Murray. The physiological principle of minimum work: I. The vascular system and the cost of blood volume. *Proc. Natl. Acad. Sci. U.S.A.*, 12:207–214, 1926. 37

[57] K. Sandau and H. Kurz. Measuring fractal dimension and complexity–an alternative approach with an application. *J. Microsc.*, 186:164–176, 1997. 37

[58] N. V. Mantzaris, S. Webb, and H. G. Othmer. Mathematical modeling of tumor-induced angiogenesis. *J. Math. Biol.*, 49:111–187, 2004. 38

[59] R. K. Jain. Transport of molecules across tumor vasculature. *Cancer Metastasis Rev.*, 6:559–593, 1987. 38, 94

[60] R. K. Jain and L. T. Baxter. Mechanisms of heterogeneous distribution of monoclonal antibodies and other macromolecules in tumors: Significance of elevated interstitial pressure. *Cancer Res.*, 48:7022–7032, 1988. 38, 72

[61] L. T. Baxter and R. K. Jain. Transport of fluid and macromolecules in tumors. I. Role of interstitial pressure and convection. *Microvasc. Res.*, 37:77–104, 1989. 39

[62] T. P. Butler, F. H. Grantham, and P. M. Gullino. Bulk transfer of fluid in the interstitial compartment of mammary tumors. *Cancer Res.*, 35:3084–3088, 1975. 39

[63] E. M. Sevick and R. K. Jain. Blood flow and efferent blood ph of tissue-isolated walker 256 carcinmoa during hyperglycemia. *Cancer Res.*, 48:1201–1207, 1988. 39

[64] P. Vaupel, H. P. Fortmeyer, S. Runkel, and F. Kallinowski. Blood flow, oxygen consumption, and tissue oxygenation in human breast cancer xenografts in nude rats. *Cancer Res.*, 47:3496–3503, 1987. 39

[65] G. I. Bell. Models for the specific adhesion of cells to cells. *Science*, 200:618–627, 1978. x, 41, 44

[66] M. Eigen. Diffusion control in biochemical reactions. *Quant. Stat. Mech. Nat. Sci.*, pages 37–61, 1974. 42

[67] S. N. Zhurkov. *Int. J. Fract. Mech.*, 1:311–323, 1965. 43

[68] John P. Sinek, Hermann B. Frieboes, B. Sivaraman, S. Sanga, and V. Cristini. Mathematical and computational modeling: Toward the development and application of nanodevices for drug delivery. In Challa S. S. R. Kumar, editor, *Nanodevices for the life sciences Vol. 4*, chapter 2, pages 29–66. WILEY-VCH Verlag GmbH & Co. KGaA, Weinheim, 2006. 44

[69] S. K. Bhatia, M. R. King, and D. A. Hammer. The state diagram for cell adhesion mediated by two receptors. *Biophys. J.*, 84:2671–2690, 2003. 46

[70] G. I. Bell, M. Dembo, and P. Bongrand. Cell adhesion. Competition between nonspecific repulsion and specific bonding. *Biophys. J.*, 45:1051–1064, 1984. 46

[71] F. Winkler, S. V. Kozin, R. T. Tong, S. S. Chae, M. F. Booth, I. Garkavtsev, L. Xu, D. J. Hicklin, D. Fukumura, E. di Tomaso, L. L. Munn, and R. K. Jain. Kinetics of vascular normalization by VEGFR2 blockade governs brain tumor response to radiation: role of oxygenation, angiopoietin-1, and matrix metalloproteinases. *Cancer Cell*, 6:553–563, 2004. 71

[72] R. K. Jain, R. T. Tong, and L. L. Munn. Effect of vascular normalization by antiangiogenic therapy on interstitial hypertension, peritumor edema, and lymphatic metastasis: insights from a mathematical model. *Cancer Res.*, 67:2729–2735, 2007. ix, 81, 99

[73] C. Phipps, G. Powathil, S. Speziale, and M. Kohandel. Effects of combination treatments on tumor microenvironment: a mathematical approach. *In preparation.*

[74] M. Kohandel, S. Sivaloganathan, and A. Oza. Mathematical modeling of ovarian cancer treatments: Sequencing of surgery and chemotherapy. *J. Theor. Biol.*, 242:62–68, 2006.

[75] S. Takano, Y. Yoshii, S. Kondo, H. Suzuki, T. Maruno, S. Shiral, and T. Nose. Concentration of vascular endothelial growth factor in the serum and tumor tissue of brain tumor patients. *Cancer Res.*, 56:2185–2190, 1996.

[76] A. Obermair, E. Kucera, K. Mayerhofer, P. Speiser, M. Seifert, K. Czerwenka, A. Kaider, S. Leodolter, C. Kainz, and R. Zeillinger. Vascular endothelial growth factor (VEGF) in human breast cancer: correlation with disease-free survival. *Int. J. Cancer (Pred. Oncol.)*, 74:455–458, 1997.

[77] N. H. Holford and L. B. Sheiner. Pharmacokinetic and pharmacodynamic modeling in vivo. *Crit. Rev. Bioeng.*, 5:273–322, 1981.

[78] M. O. Stefanini, F. T. H. Wu, F. Mac Gabhan, and A. S. Popel. A compartment model of VEGF distribution in blood, healthy and diseased tissues. *BMC Systems Biology*, 2, 2008.

[79] G. A. Truskey, F. Yuan, and D. F. Katz. *Transport phenomena in biological systems.* Pearson Prentice Hall, 2004.

[80] F. Mac Gabhann and A.S. Popel. Interactions of VEGF isoforms with VEGFR-1 and VEGFR-2, and neuropilin in vivo: a computational model of human skeletal muscle. *Am. J. Physiol. Heart Circ. Physiol.*, 292:459–474, 2007.

[81] F. Mac Gabhann, J.W. Ji, and A.S. Popel. Multi-scale computational models of pro-angiogenic treatments in peripheral arterial disease. *PLoS Comput. Biol.*, 35:982–994, 2006.

[82] C. S. Patlak, D. A. Goldstein, and J. F. Hoffman. The flow of solute and solvent across a two-membrane system. *J. Theor. Biol.*, 5:426–442, 1963.